UNIVERSITY OF CALIFORNIA SAN DIEGO

Convenient Approaches for Measuring the Glass Transition and Fracture Behavior of Semiconducting Polymers

A Thesis submitted in partial satisfaction of the requirements for the degree of Master of Science

in

Chemical Engineering

by

Mohammad Ayman Alkhadra

Committee in charge:

Professor Darren J. Lipomi, Chair
Professor Vlado A. Lubarda
Professor David P. Fenning

2018

This Thesis of Mohammad Ayman Alkhadra is approved, and it is acceptable in quality and form for publication on microfilm and electronically:

Chair

University of California San Diego

2018

DEDICATION

This Thesis is dedicated to my parents, Hanan and Ayman, and to my brother, Omar.

EPIGRAPH

"*I have no special talents. I am only passionately curious*."

TABLE OF CONTENTS

LIST OF FIGURES

LIST OF TABLES

LIST OF IMAGES

ACKNOWLEDGEMENTS

Thank you. I have been blessed my entire life with kind, loving, and supporting people. My parents, brother, extended family, friends, co-workers, teachers, and mentors have all been an integral part of my intellectual and emotional development. Without them, I would not have been able to accomplish what I have thus far.

Parents. In a sense, I completed my first residency (a stage of graduate medical training) by the age of one. My parents, Hanan and Ayman, had me while undertaking rigorous medical training in the US; apparently, I was there with them during every step of the journey. As I was growing up, my parents were rather strict and demanded a high level of discipline, but I believe that they truly succeeded at inspiring me to become an independent, thoughtful, and open-minded human being. My mother is a hardworking physician who motivates me in her tireless effort to promote women's rights and to inspire women to pursue careers that have long been dominated by men. From my mother, I derived an incredible work ethic that endowed me with a set of values founded upon hard work, rather than material possessions and social status. Just like my mother, my father is a diligent physician who motivates me in his passion to serve others and make a tangible difference in society. My father passed to me his curious and inquisitive spirit, along with an even-handed temperament and relaxed personality. It is without a doubt that my parents have been the most important role models in my life.

During my early years in elementary school (in Saudi Arabia), I paid little attention to my education and focused heavily on catching all sorts of "Pokémon," as well as collecting all kinds of "Yu-Gi-Oh!" cards. A most memorable moment of my childhood

was when I received a yearly cumulative average of 85% in fifth grade and ranked in the bottom half of my classroom (yes, we took exams and received grades in elementary school). This event was memorable not because I cared about my academic performance, but because my parents cared more than I did; frankly, they were distraught with my performance. To rectify the situation, I took it upon myself to never again disappoint my parents about my education. At this point, I can say with certainty that I succeeded at that task, and I aspire to continue to make my beloved parents proud.

Omar. My younger brother, Omar, is intriguing to me; he is very clever and sharp-witted, though he often refrains from letting the world know what he is capable of. Omar is gifted and talented in many ways that he is likely not yet aware of. For example, he is capable of spending incredible amounts of time playing video games with a level of focus unparalleled by most people his age. When I was in high school, I played video games just as much as Omar (perhaps even more than he does!) and realized that I could leverage the skills that I acquired in the process to advance myself towards my career goals. Because of my passion for video games, I developed the abilities to focus intensively on the task at hand, to organize my duties efficiently (which I structured around time to play, of course), and to reach goals and achievements that I set for myself (indeed, I have always set the bar high). I believe that Omar—who will be graduating soon and enrolling in college—can (and will) reach a similar, if not greater, level of focus, organization, and achievement. I argue that it is just a matter of time for him to find his passion, whether it be in science, business, community service, or management. If you are reading this, Omar, *go out there and prove me right*!

Family. Every member of my family means a great deal to me; I love them all. Certain members, however, have had a greater influence than others on my intellectual, emotional, and spiritual growth. Since my childhood, my maternal grandfather, "Jaddi" (Grandpa) Hassan, has been a huge source of my inspiration because of the extraordinary sacrifices that he made for the sake of his education. Jaddi Hassan also taught me to appreciate the intellectual culture of my antecedents and instilled in me an incomparable pleasure in learning. My paternal grandfather, "Jaddo" (Grandpa) Samih, has similarly been a huge source of my inspiration, though for a different reason: Jaddo Samih had to flee Palestine—the country of his ancestors—at only eight years of age. He grew up in Syria and eventually immigrated to Saudi Arabia, where he founded his private laboratories that specialize in pharmaceutical chemistry. His tenacity and devotion to his business allowed him to provide his offspring and grandchildren with a comfortable life. Without my grandmothers, however, my appreciation for grandparents would be incomplete. My maternal grandmother, "Nena" (Grandma) Ruqayya, and paternal grandmother, "Teta" (Grandma) Bushra, were equally important in my emotional and spiritual development as a child. From them I learned valuable lessons in kindness, humility, and respect. I am blessed to have such a wonderful family of intelligent, kind, and hardworking individuals. My gratitude to my parents, brother, and family is without measure.

Friends. Throughout high school and college, I have always been surrounded by a great group of friends, most of whom I do not list below. Among my friends from high school, I am greatly indebted to Ryan Hawkins, Kareem Jaroudi, Ziad Al-Mouhtasseb, Akhil Kallur, Maher Turk, Caterina Raimondi, Sara ElSouri, Sarah Sanbar, and many others. From UC San Diego, I am greatly indebted to Eric Zhao, Adam Klie, Ghanim

Hableel, Ghassan and Omar Farah, Milad Torabi, Khanh Tran, the entire Blake II crew, and very many more.

UC San Diego. As a proud Triton, I had the great privilege of working under the supervision of Professor Darren J. Lipomi (see below). I am grateful to all of my professors, particularly those who instructed me in chemical engineering (Professors Opatkiewicz, Miller, Lubarda, Drews, Fenning, Talbot, Russ, Sanchez, Chen, and Krasheninnikov), physics (Professor Eric Michelsen), mathematics (Dr. Ali Behzadan), and humanities (Professor John Hoon Lee). I am also grateful to all of my wonderful teaching assistants (TAs), especially those who were dedicated to their students and peers. Karcher Morris (engineering TA) deserves special acknowledgement because he motivated me to join a research group as an undergraduate; it was actually at a Starbucks near campus where I decided to join Professor Lipomi's group after having an informal conversation with Karcher.

UC San Diego has definitely been and will always remain my second home (in fact, my first in the US). I moved by myself to sunny San Diego from Riyadh, Saudi Arabia, at the age of 18 as curious and excited to learn as ever. San Diego (La Jolla, to be precise), the University, and the people who make up these places made my experience an absolute pleasure. I have grown intellectually, culturally, emotionally, and physically in ways that I never would have imagined at 18. Moreover, San Diego is where I had many pivotal, first-time experiences including (but not limited to) legitimately cooking my own meals, lifting real weights, signing my first residential lease, receiving my first paycheck, living on my own in an apartment, owning my first car, voting in US elections, eating my first bowl of

Chipotle, renting a car, publishing my first research paper, earning my first academic degree, and meeting my first love, Giahan (pronounced Ya-han) Nguyen. (Giahan and I actually first met in Professor Lipomi's course on polymeric materials; please see below for more details.) With my utmost sincerity, and from the bottom of my heart, I love UC San Diego and all of the people who were a part of my experience there.

Darren Lipomi and Samuel Root. It was as a sophomore when I first heard about Darren and the course on polymeric materials that he teaches yearly. Exactly one year after that, I enrolled in Darren's course in which I performed so well that Darren congratulated me on my achievement: "Great job on the final exam and the course! A+ :)." Unlike many instructors, Darren sought to develop a real connection with one of the highest achieving students in his class, and he quickly won me over. Because of his kind remark, I strongly considered joining Darren's research team, without really knowing (or even caring about) what they worked on. (Karcher advised me to join a group led by a supportive advisor and graduate students who would be willing to take on an inexperienced undergraduate; so, I did exactly that.) Darren told me to contact the TAs from his course to set up a meeting and discuss potential projects; those TAs were Drs. Brandon (ODB) Marin and Samuel (Sam) Root. After a single meeting, Sam agreed to take me on as an undergraduate research assistant. The projects that Sam devised would have been challenging for a student who had only recently completed a first course on polymeric materials and had no prior laboratory experience. Sam and Darren, however, believed that I was up to the challenge. My work ethic, extensive contributions, and overall dedication to our first project earned me co-first authorship in the research article published in *Chem. Mater.* (**2017**, *29*, 2646). Sam and I continued to come up with new projects and work closely in the Lipomi group

to create and disseminate new scientific knowledge. A less obvious but equally important outcome of our collaborative effort has been the formation of a strong personal bond between Sam and I—two young scientists of seemingly conflicting cultural backgrounds. (Sam and I are in fact descendants of the long-standing Israeli-Palestinian conflict, and our families stem from vastly different cultural backgrounds.)

Not only have Darren and Sam empowered me to grow academically and scientifically, these gentlemen have been a source of my cultural, physical, and spiritual enrichment. Darren and I engaged in deep, meaningful conversation on a regular basis. We share many common interests, including the scientific method, physical fitness, classical music, nutrition, and expansion of the human mind. The beauty of our relationship is that we have listened and learned from each other with an open mind. Darren also helped me improve my scientific writing considerably by giving me the opportunity to lead the authorship of a chapter to be published on the mechanical properties of semiconducting polymers (*Handbook of Conducting Polymers*, **2018**). Completing this gargantuan task was no easy feat, and I certainly could not have done it without the assistance of Darren, Sam, and the remaining contributors. I have been (and will continue) paying forward what Darren and Sam had done for me by teaching and inspiring young, passionate individuals. My gratitude to these men is without bounds.

Giahan Nguyen. Meeting this lovely lady was one of the best things that happened to me at UC Diego. Interestingly enough, Giahan (pronounced Ya-han) and I first met in Professor Lipomi's course on polymeric materials after taking his first summative exam. (Giahan and I were actually both in the chemical engineering class of 2017, but we had not

met until the middle of our third year in the program.) I had seen Giahan many times studying at the Biomedical Library but never mustered the courage to approach her because she was always focused and seemingly indifferent. It was not until after Professor Lipomi's first summative exam when Giahan asked me, at BML, about my opinion of the test. I told her that I "killed it," and on that day we became close friends. After a year of friendship, I became interested in knowing Giahan more personally, and so I took her out for dinner at Ki Sushi—a staple of the UC San Diego experience that is also notorious for the so-called "sake bomb" (of course, I never participated in such debauchery; I only drink protein shakes). We bonded well over that dinner, and we both anticipated a second date. After trying with all my might, Giahan accepted to go out with me a second time, and then a third. At that point, our relationship was becoming more serious, and each of us was devoted to the other.

It has been exactly one year (from the time of writing) since I took Giahan out on our first date, and she has succeeded at teaching me what love is. In her own words, "love is kindness, patience, and sacrifice." (I may have very slightly paraphrased that.) Giahan has been my rock, and I could not have gotten through this endeavor without her immeasurable care and support. Fortunately, I managed to convince her to move with me to Boston, MA, where I will be working on my doctorate in chemical engineering at the Massachusetts Institute of Technology and she will be seeking job opportunities, either as a school teacher or in the biotechnology/pharmaceutical industries. I am extremely grateful to have Giahan in my life, and we are both excited to see what the East Coast has to offer.

The Lipomi Group and Collaborators. During my time in the Lipomi Group, I had the opportunity to develop a number of lifelong friendships and professional relationships. When I first joined the Group, Daniel Rodriquez trained me on the fundamental skills needed to study the mechanical properties of semiconducting polymers. I am eternally grateful for his mentorship and commitment to give back to all members of our Group. Sitting just next to Daniel was Julian Ramirez. Although Julian and I collaborated very little scientifically, we developed a strong friendship, mutual respect, and deep interest in each other's work. I look forward to the day Julian defends his PhD; I expect nothing but savagery from you, coach. Also defending his PhD soon is Cody Carpenter, a great friend whom I got to know very well thanks to a collaboration that he led. Cody and I also developed a strong relationship outside of the academic setting by lifting weights at the gym and feasting, together with Dr. Sam Root. Cody has taught me much about myself and about life, in general, for which I am eternally grateful. I eagerly look forward to learning about his success and accomplishments in the future.

When I first joined the Lipomi Group, I often looked up to the senior graduate students for advice and wisdom. These (former) students include Drs. Brandon (ODB) Marin, Aliaksandr Zaretski, and Timothy O'Connor. These gentlemen taught me much about adapting to the (then) new research setting and encouraged my passion for science and learning. I would also like to acknowledge other members of the Group with whom I had interacted a little later into my time there, including Dr. Charles Dhong, Dr. Laure Kayser, Dr. Suchol Savagatrup, Dr. Adam Printz (via email), Mickey Finn III, Andrew Kleinschmidt, Fumitaka Sugiyama, Rory Runser, Liban Jibril, Kristan Hilby, and Armando Urbina. In summary, all members of the Lipomi Group had a largely positive impact on

my research experience and helped shape the optimistic outlook that I have on my future as an aspiring scientist.

I also include the following acknowledgements below as required by the University of California San Diego:

Chapter 1, in full, is currently in press for publication of the material by Mohammad A. Alkhadra, Andrew T. Kleinschmidt, Samuel E. Root, Daniel Rodriquez, Adam D. Printz, Suchol Savagatrup, and Darren J. Lipomi*. The thesis author was the primary investigator and author of this material.

Chapter 2, in full, is a reprint of the material as it appears in *Chemistry of Materials*, 2017, 28, 2646–2654. The American Chemical Society, 2017. Samuel E. Root,‡ Mohammad A. Alkhadra,‡ Daniel Rodriquez, Adam D. Printz, and Darren J. Lipomi* (‡ Equal contribution). The thesis author was a primary investigator and author of this paper.

Chapter 3, in full, is a reprint of the material as it appears in *Chemistry of Materials*, 2017, 29, 10139–10149. The American Chemical Society, 2017. Mohammad A. Alkhadra,‡ Samuel E. Root,‡ Kristan M. Hilby, Daniel Rodriquez, Fumitaka Sugiyama, and Darren J. Lipomi* (‡ Equal contribution). The thesis author was a primary investigator and author of this paper.

VITA

2016–2017	Undergraduate Researcher, University of California San Diego
2017	Bachelor of Science in Chemical Engineering, University of California San Diego
2017–2018	Graduate Researcher, University of California San Diego
2018	Master of Science in Chemical Engineering, University of California San Diego
2019–TBD	Graduate Researcher, Massachusetts Institute of Technology
TBD	Doctor of Philosophy in Chemical Engineering, Massachusetts Institute of Technology

PUBLICATIONS

M.A. Alkhadra, A.T. Kleinschmidt, S.E. Root, D. Rodriquez, A.D. Printz, S. Savagatrup, and D.J. Lipomi. "Mechanical Properties of Semiconducting Polymers," in *Handbook of Conducting Polymers*, 4th ed., T.A. Skotheim, J.R. Reynolds, and B.C. Thompson, Eds. Invited book chapter, in press.

F. Sugiyama, A.T. Kleinschmidt, **M.A. Alkhadra**, J.M-H. Wan, A.S-C. Chiang, D. Rodriquez, S.E. Root, and D.J. Lipomi. "Stretchable and Degradable Semiconducting Multi-Block Copolymers." Submitted.

D. Rodriquez, J.G. Kohl, P. Morel, K. Burrows, G. Favaro, S.E. Root, J. Ramírez, **M.A. Alkhadra**, Z. Fei, P. Boufflet, M. Heeney, and D.J. Lipomi. "Measurement of Cohesion and Adhesion of Semiconducting Polymers by Scratch Testing: Effect of Side-Chain Length and Degree of Polymerization." Submitted.

C.W. Carpenter, C. Dhong, N.B. Root, D. Rodriquez, E.E. Abdo, K. Skelil, **M.A. Alkhadra**, J. Ramírez, V.S. Ramachandran, and D.J. Lipomi. "Human ability to discriminate surface chemistry by touch." *Mater. Horiz.* **2018**, *5*, 70–77.

M.A. Alkhadra,‡ S.E. Root,‡ K.M. Hilby, D. Rodriquez, F. Sugiyama, and D.J. Lipomi. "Quantifying the Fracture Behavior of Brittle and Ductile Thin Films of Semiconducting Polymers." *Chem. Mater.* **2017**, *29* (23), 10139–10149. ‡Equal contribution. ***Lectureship and Best Paper Award from *Chem. Mater.*, 2017**.

S.E. Root,‡ **M.A. Alkhadra**,‡ D. Rodriquez, A.D. Printz, and D.J. Lipomi. "Measuring the Glass Transition Temperature of Conjugated Polymer Films with Ultraviolet–Visible Spectroscopy." *Chem. Mater.* **2017**, *29* (7), 2646–2654. ‡Equal contribution.

ABSTRACT OF THE THESIS

Convenient Approaches for Measuring the Glass Transition and Fracture Behavior of Semiconducting Polymers

by

Mohammad Ayman Alkhadra

Master of Science in Chemical Engineering

University of California San Diego, 2018

Professor Darren J. Lipomi, Chair

Semiconducting polymers—typically fabricated as thin films (~100 nm)—have always been associated with flexible applications, such as solar cells, active-matrix displays, and biomedical sensors. Mechanical flexibility of these materials, however, is not automatic. The thermal and mechanical properties of semiconducting polymers must be

engineered by tuning the chemical structure, molecular weight, processing conditions, and interactions with other materials in the device stack. The thermal transition of semiconducting polymers that perhaps most greatly influences the mechanical response is the glass transition, and the temperature (T_g) at which it occurs. We develop a new technique that leverages the unique aggregation behavior of semiconducting polymers to measure the T_g. With ultraviolet−visible (UV−vis) spectroscopy, we measure changes in the absorption spectrum due to rearrangement of chains at the molecular scale and formation of photophysical aggregates on heating above the T_g.

Thermal transitions are not the only properties of semiconducting polymers that are challenging to measure; the mechanical properties, too, of these materials are difficult to characterize due to the diverse range of fracture behavior that thin polymer films exhibit. In addition, the mechanics that govern ductile fracture—compared to brittle fracture—are underexplored. Understanding the mechanics of ductile fracture is crucial for the improved design and fabrication of mechanically robust organic electronics. For this mechanism of fracture, we find that diamond-shaped microvoids, which originate at pinholes and defects within the film, propagate with an aspect ratio that increases linearly with applied strain. We define the rate of change of the aspect ratio of a microvoid with respect to applied strain as the "microvoid-propagation number." This dimensionless film parameter, previously unreported, is a useful measure of ductility in thin films supported by an elastomer.

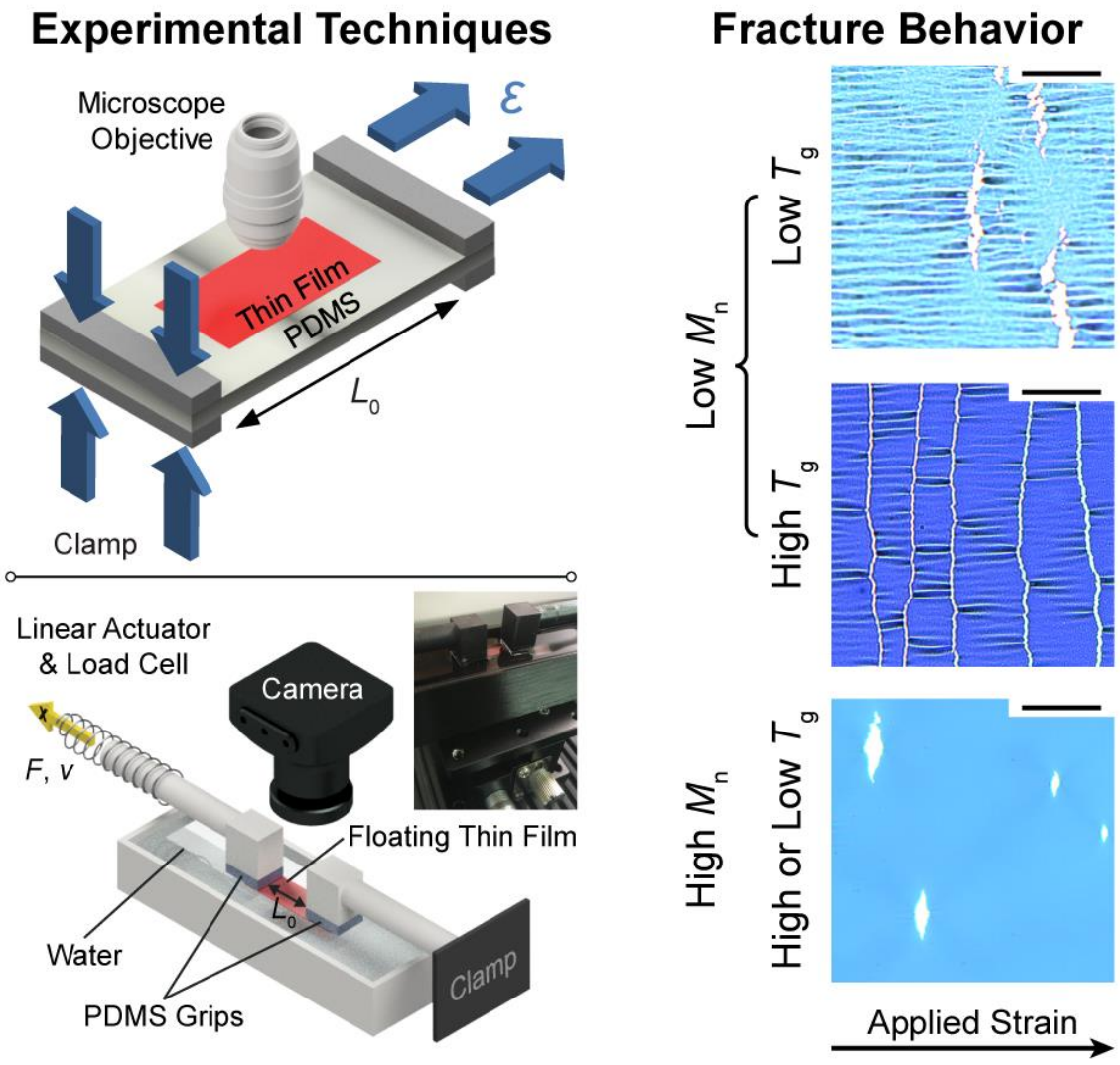

Image 1. Convenient approaches for quantifying the fracture behavior of both brittle and ductile thin films of semiconducting polymers.

Chapter 1

Mechanical Properties of Semiconducting Polymers

Mohammad A. Alkhadra, Andrew T. Kleinschmidt, Samuel E. Root, Daniel Rodriquez, Adam D. Printz, Suchol Savagatrup, and Darren J. Lipomi*

Department of NanoEngineering, University of California, San Diego

9500 Gilman Drive, Mail Code 0448, La Jolla, CA 92093-0448

Abstract

The mechanical properties of conjugated polymers are central to their use in flexible electronic devices and to their processing by roll-to-roll coating. Moreover, applications in wearable bioelectronics demand knowledge of these properties. The mechanical properties are influenced by aspects of the molecular structure and the ways that these structures pack in the solid state, as mediated by processing conditions. Parameters such as the glass transition and entanglement density are emphasized in this chapter, as are their influence on elasticity, plasticity, and fracture. The fragility of thin films poses a challenge for measurement. Metrologies include the buckling test for elastic modulus, along with pull testing of thin films suspended on water. Methods of predicting the mechanical properties include simple semi-empirical models, along with molecular dynamics simulations. A recurring theme is the perceived competition between charge transport and deformability, and how this competition can be balanced.

1.1 Introduction and Background

Semiconducting polymers have always been associated with flexible applications, such as solar cells, active-matrix displays, and biomedical sensors.[1,2] Mechanical flexibility of these materials, however, is not automatic. The mechanical properties of semiconducting polymers must be engineered by tuning the chemical structure, molecular weight, processing conditions, and interactions with other materials in the device stack.[3,4] Despite the importance of mechanical deformability in essentially all applications of semiconducting polymers, mechanical properties have, until recently, been an afterthought. For example, the mechanical stability of organic solar cells has often been overlooked in

favor of improving power conversion efficiencies. However, the development of semiconducting polymers that can endure the rigors of roll-to-roll coating, survive long term against mechanical deformations in the outdoor environment, and withstand packing and transportation in portable devices demands an understanding of their mechanical properties. These properties—including elasticity, extensibility, strength, and toughness—are critically dependent not only on the molecular structure of the materials, but on the ways these structures pack in the solid state, which are, in turn, mediated by the conditions of processing. Prediction of the mechanical behavior of materials in a device is confounded by the fact that the properties of materials measured in the laboratory can depend on testing conditions, such as temperature, strain rate, and choice of substrate.

The mechanical properties of polymers, at the most basic level, can be usefully classified according to their response to applied loads (glassy or rubbery) and the corresponding mechanism of fracture (brittle or ductile). The mechanical response and fracture mechanism of any polymer under deformation can be captured in a stress–strain curve, an idealized example of which is shown in **Figure 1.1**. For a given material, a stress–strain curve reveals mechanical properties such as the elastic modulus, yield point, and toughness. The mechanical property to be optimized depends on the application. For example, bonding a device to a nonplanar surface such as a lens or windshield may require large extensibility that need not be reversible (i.e., plastic as opposed to elastic), while incorporating such a material into a device to be worn on the skin, which is reversibly deformable, requires the opposite. Applications that will be subject to twisting and shear deformations require high cohesive and adhesive energies within and between the layers in the device stack. The mechanisms by which semiconducting polymers store or dissipate

mechanical energy depend on many of the same characteristics that influence the mechanical behavior of commodity polymers and engineering plastics: e.g., the barriers to molecular rotation, degree of crystallinity, glass transition temperature. The ways in which semiconducting polymers mediate mechanical energy also depend, however, on characteristics that are rarely found in conventional polymers: e.g., stiffness of the π-conjugated backbone, the flattened, anisotropic shape of a polymer chain, and the ubiquitous presence of side chains.

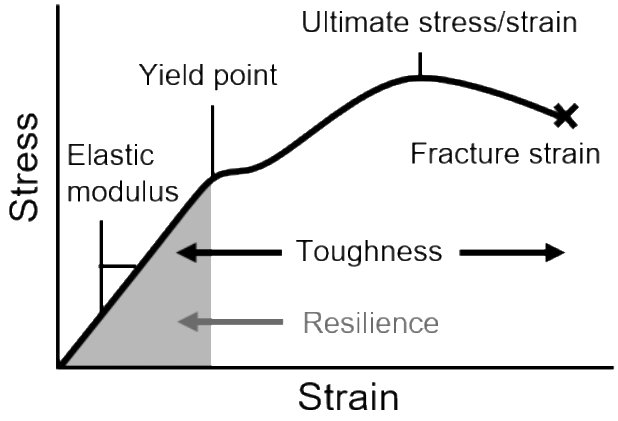

Figure 1.1. A hypothetical stress–strain curve illustrating its most important features.

1.1.1 Semiconducting Polymers as a Subset of All Solid Polymers

The presence of solubilizing pendant groups in semiconducting polymers is required for solution processing, as the unsubstituted main chain of a π-conjugated polymer is generally insoluble.[4] Semiconducting polymers are rendered soluble by the attachment of alkyl side chains, which afford solubility by weakening strong van der Waals interactions between main chains and by conferring greater entropic freedom of the polymer in solution.[5] These side chains also strongly affect the thermomechanical properties and solid-state packing. Among these "comb-like" polymers, the side chains in the solid state can point end-to-end or they can interdigitate. A polymer whose side chains

interdigitate is often stiffer and more brittle because of increased crystallinity. Improved molecular packing in crystalline regions also results in an anisotropic elastic modulus due to unequal densities of van der Waals interactions in orthogonal directions (e.g., π–π stacking vs interactions between interdigitated side chains).

Analysis of the mechanical properties of commodity polymers and engineering plastics is a well-established discipline. Semiconducting polymers, however, differ from conventional, non-conjugated plastics in a number of ways. These differences include obvious dissimilarities in chemical structure—namely, increased stiffness of the backbone due to π-conjugation—and practical considerations such as the availability of materials for mechanical testing. Conventional pull-testing of a solid polymer to obtain a stress–strain curve often requires large quantities of the material. Pilot-scale syntheses of semiconducting polymers, however, typically produce materials in quantities sufficient to fabricate only thin films (~100 nm).[4] While the thin film is the only geometry of these materials used in devices, it is inconvenient to measure the mechanical response of a thin film. Methods have thus been developed specifically to determine the mechanical properties of thin films of semiconducting polymers, though the choice of method often has an effect on the mechanical response. Conveniently, the mechanical properties of semiconducting polymers are intrinsically coupled to their thermal properties and phase transitions, and these transitions—in particular the glass transition temperature, assuming it too can be measured—may be used to predict at least some of the mechanical behavior.

The thermal transition of semiconducting polymers which perhaps most greatly influences the mechanical response is the glass transition, and the temperature at which it occurs (T_g). Traversing the T_g corresponds to a second-order phase transition from a glass

to a rubbery solid. The transition is also characterized by an increase in heat capacity, specific volume, and deformability.[6–8] While the T_g of conventional plastics is usually determined calorimetrically, the small change in heat capacity of semiconducting polymers around the T_g is often difficult to detect, though several methods have been developed to circumvent this difficulty.[7,9]

Experimental methods developed to understand the thermomechanical properties of semiconducting polymers—especially the aspects of semiconducting polymers that differ from conventional polymers—have been supplemented by computation.[8,10] When semiconducting polymers are processed from solution, the morphology that forms upon evaporation of the solvent is often difficult to predict. Theoretical models have thus been developed to investigate the nanoscale structural characteristics and conformational behavior that control the mechanical properties of semiconducting polymers and—as are required for organic solar cells—their composites with soluble fullerenes.[11]

Effects of molecular mixing on the thermomechanical behavior of polymer–fullerene composites, such as stiffening and embrittling of the polymer, are the result of molecular recognition (i.e., intercalation of fullerenes between side chains) and corresponding changes in microstructural order. Indeed, the solid-state packing structure, as it is determined by molecular structure and solid-state microstructure, greatly influences the mechanical properties of semiconducting polymers.[12] The following sections discuss the elementary principles that govern the mechanical properties of semiconducting polymers and the ways in which these materials mediate mechanical energy.

1.2 Deformation in Solid Polymers

Depending on the type of material, geometry of the specimen, and conditions of the applied forces, different modes of deformation may occur on the application of tension, compression, shear, or twisting. As these different forces are applied to an object, intermolecular forces arise in the deformed body to resist or minimize deformation. On the application of sufficiently large loads, however, the deformed body may break to dissipate mechanical energy. Deformation may also occur as a result of changes in temperature; in this case, thermal energy induces change in the shape and size of an object (e.g., expansion or contraction).

1.2.1 Mediation of Mechanical Energy

The mechanical response of a solid polymer is governed principally by two structures which are characterized by different length scales: the molecular structure (~1 Å – 10 nm) and the solid-state microstructure (~10 nm – 100 nm). The molecular structure controls the mechanical response by bonding topology, molecular weight, and other parameters at the scale of individual chains. The microstructure determines the mechanical response based on the degree of crystallinity, the glassy state, and the allowance of slip in the crystalline domains. The evolution in the structure of a solid polymer at various size scales upon deformation—i.e., from the bending, stretching, and breaking of covalent bonds to the deformation of entire crystallites—serves to either store or dissipate mechanical energy. The ways in which a solid polymer stores or dissipates this energy can be classified by its modes of deformation: elastic deformation, plastic deformation, and fracture.

At small strains, glassy polymers, in which little molecular motion is allowed, exhibit linear elastic behavior that is driven by an enthalpic response to mechanical

deformation, as polymer chains are displaced from local minima in potential energy. Further elongation of glassy samples causes non-reversible deformations due to sliding and alignment of chains in response to tensile stress. These deformations may occur at constant volume (i.e., shear yielding) or they may be dilatational (i.e., crazing) depending on the degree of entanglement of chains. On the other hand, in rubbery polymers (elastomers), in which considerable molecular motion is allowed, the polymer chains behave as entropic springs: upon elongation, a reduction in the number of conformations available to chains decreases the entropy of the system. This decrease in entropy generates a restoring force that causes chains to relax to their equilibrium states upon releasing the applied strain.

When the applied strain is sufficiently large, solid polymers fracture by either cohesive failure—which occurs when the cohesive energy of the material is overcome—or adhesive failure—which occurs as a result of debonding at the interface between a polymer and the underlying substrate. These modes of deformation in any solid polymer—from linear elasticity to fracture—are all, in turn, affected by the thermomechanical properties of the material and thus the phase of the solid polymer.

1.2.2 Elasticity and Plasticity

For semicrystalline polymers below T_g, elasticity is mediated by van der Waals forces and deformation of covalent bonds. On experimentally relevant time scales, relaxation of polymer chains in such materials is prohibited, which reduces the rotational and translational mobility that these chains can exhibit. Conversely, for semicrystalline polymers above the glass transition temperature, chains are allowed to reorganize and align along the axis of applied tensile strain due to a reduction in viscosity. The resulting decrease in internal, or entropic, degrees of freedom upon deformation and concomitant restoring

force is the basis of linear elasticity in solid polymers. This elastic behavior terminates either with brittle fracture or with plastic deformation followed by ductile fracture.

The yield point marks the onset of plastic deformation, at which point the mechanical energy stored during elastic behavior is dissipated plastically. In other words, polymers chains adopt new configurations at mechanical equilibrium once the elastic strain energy exceeds intermolecular and entropic forces in the elastic regime. This plastic deformation is generally non-reversible and occurs due to sliding and alignment of chains in response to tensile stress. Such mobility of polymer chains is facilitated by a low T_g but may be hindered due to the existence of strong intermolecular forces uniformly in a polymer crystal. For example, interdigitation between side chains in the crystalline domains of semicrystalline semiconducting polymers causes these materials to exhibit brittle behavior, instead of plastic deformation, to dissipate mechanical energy.

1.2.3 Fracture

The total energy per unit volume that a material can absorb before fracture is known as its toughness. Cyclic or intermittent loading can lower the elasticity and toughness by the accumulation of chain scission and microstructural rearrangement produced by strain and local heating. For samples with low molecular weight and therefore low densities of entanglements, pullout of polymer chains can become a dominant mechanism of fracture. Fracture in a real sample is also triggered by the presence of defects in solid films. That is, mechanical energy is concentrated in the vicinity of small inhomogeneities, such that fracture occurs due to the enlargement of these regions.[13] Under tensile elongation, the mechanism of fracture may be determined by the shape of the stress–strain curve (**Figure 1.1**). Moreover, the nature of the fracture surface differs considerably[14] between cracked

thin films of brittle and ductile polymers. In contrast to brittle solids, plasticity contributes to the fracture of ductile solids. A plastic zone develops at the tips of cracks in ductile materials, and energy is dissipated primarily due to plastic flow in the material near these crack tips, rather than due to the creation of new surfaces. In either brittle or ductile materials, fracture produces a new surface, the formation of which is balanced by the dissipation of elastically stored energy.

The cohesion of a semiconducting polymer determines in large part its mechanical reliability and resistance to fracture necessary for deformable applications. The criterion that best portends the fracture of a solid material or interface is the strain-energy release rate, G (in J m^{-2}), which is defined as the energy available for unit increase in crack length, $2c$:

$$G = \frac{dW}{dA} - \frac{dU}{dA} = \frac{1}{h}\left(\frac{dW}{dc} - \frac{dU}{dc}\right) \quad (1)$$

where W is the external work being done on the system, U is the elastically stored energy, A is the surface area of the crack, and h is the thickness of the specimen. It is assumed that fracture occurs when G exceeds the critical value G_c, known as the cohesive fracture energy.[13] This energy is the combined energy of various dissipative processes, which include molecular deformations, plastic flow in fracture process zones (i.e., regions of damage around crack tips), and scission of chemical bonds. The cohesive energy, which may be determined using double-cantilever beam or four-point bending tests,[4] depends on van der Waals interactions, chemical bonding, and the degree of entanglement.

An entanglement is defined as a physical linkage between two polymer chains whereby molecules can slide past but not through each other. Greater degrees of

entanglement correspond to larger values of the cohesive energy. The density of entanglements in a polymer scales with its molecular weight and directly controls the mechanisms of energy dissipation in the fracture process zone. Increasing the molecular weight of a semiconducting polymer results in more extensive plastic deformation and frictional pullout of chains prior to cohesive failure. Eventually, sufficient entanglement entails scission of chemical bonds upon fracture. The cohesion thus strongly influences the mechanical properties and mechanisms of fracture.[15]

1.3 Mechanical Properties and Measurement Techniques

It is generally challenging to measure the mechanical properties of thin films for two reasons. First, handling these films for a conventional pull test is difficult. Second, pilot-scale syntheses typically do not produce material in quantities large enough for testing more than a few films. These challenges have been met by the development of different methods that facilitate the handling of thin films to determine their mechanical response to tensile strain.

1.3.1 Overview of Mechanical Properties

The classical way to obtain the mechanical response of a material is through a stress–strain curve (**Figure 1.1**). The slope of the linear region gives the elastic modulus of a material. This parameter is a measure of the capacity of a material to reversibly store mechanical energy—and thus its resistance to elastic deformation. The area under the linear region is the resilience, which is the maximum energy density that a material can store before exhibiting irreversible plastic deformation. The yield stress corresponds to the stress at which the material deforms plastically and permanently (i.e., when the mechanical response becomes driven by sliding and alignment of chains). Graphically, the yield stress

is represented by the point past which the stress–strain curve becomes nonlinear. The highest point reached on the vertical axis of a stress–strain curve corresponds to the ultimate stress (or strength) and ultimate strain. The strain (stress) at which the material ruptures is known as the fracture strain (stress). Finally, the area under the entire curve is the toughness, which is the maximum energy density that a material can absorb before mechanical failure.

1.3.2 Common Measurement Techniques

There are two common approaches for measuring the mechanical properties of thin films of semiconducting polymers. The first approach (**Figure 1.2a**) is referred to as the film-on-water technique: a thin film is supported on the surface of water and subjected to a uniaxial pull test. A stress–strain curve is then produced by measuring the force required to elongate the film by a set distance. The second approach (**Figure 1.2b**) is a suite of methods referred to as film-on-elastomer techniques. To approximate the mechanical response of semiconducting polymers to tensile strain, the film-on-elastomer method consists of three separate experiments in which a thin film is supported by an elastomer such as poly(dimethylsiloxane) (PDMS).

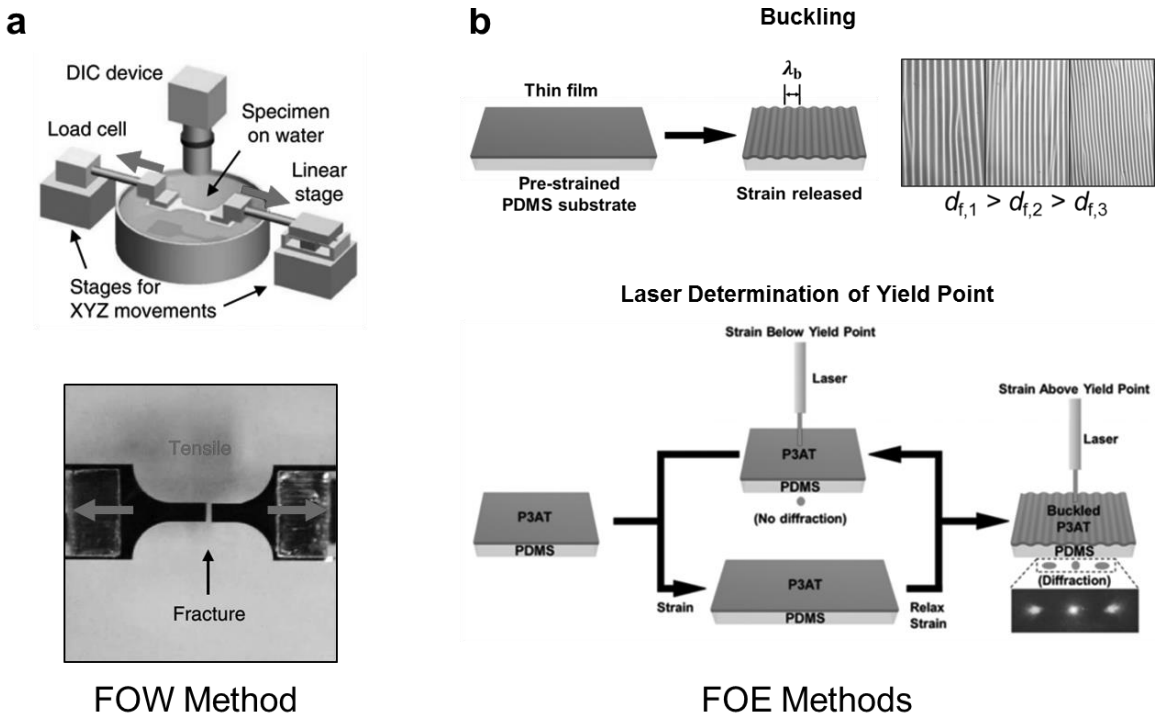

Figure 1.2. Common methods used to determine the mechanical properties of thin films of semiconducting polymers. (a) Diagram of the film-on-water testing procedure; the system for tensile testing consists of a linear stage, a load cell, and a digital image correlation (DIC) camera. Reproduced with permission from ref 16. Copyright 2013, Nature Publishing Group. (b) Diagrams of the film-on-elastomer testing procedures, namely buckling and laser determination of the yield point (LADYP). Reproduced with permission from ref 17. Copyright 2015, American Chemical Society.

The film-on-water method is a pseudo freestanding tensile test.[16,18] This method leverages the high surface tension and low viscosity of water to provide an almost frictionless support for thin films. The film-on-water method works well for a range of semiconducting polymers so long as the materials do not interact with water, particularly through dissolution or swelling. Soft, elastomeric grips are used to make contact between the fragile thin films, linear actuator, and force-sensing equipment. One of the primary advantages of the film-on-water method is that it allows acquisition of a complete trace of force as a function of displacement that, along with the dimensions of the sample, can be

used to generate a stress–strain curve. The mechanical properties of solid polymers, however, depend on the rate of applied strain: higher strain rates generally lead to greater elastic moduli when testing viscoelastic materials such as semiconducting polymers. A more complete description of the effects of strain rate on the mechanical properties of polymers is given in **Section 1.4.3**.

The film-on-elastomer method consists of a buckling-based metrology,[19] laser determination of the yield point (LADYP),[17] and crack-onset strain measurement.[20] The buckling technique, shown schematically in **Figure 1.2b** (top), is used to determine the elastic modulus of thin films of semiconducting polymers based on well-established buckling mechanics.[21] Mechanical buckling occurs when a relatively stiff and thin film is compressed on a compliant, thick substrate. This compression produces a buckling instability due to the balance between the energy required to deform the soft substrate and the energy required to bend the stiff film. This instability manifests as a sinusoidal wrinkling pattern with a well-defined wavelength. At some critical wavelength, which is a function of the material properties of both the film and the substrate, the total strain energy in the system is minimized. The buckling wavelength, λ_b, may be used to calculate the elastic modulus of the film, E_f, using the relation

$$E_f = 3E_s\left(\frac{1-\nu_f^2}{1-\nu_s^2}\right)\left(\frac{\lambda_b}{2\pi h}\right)^3 \quad (2)$$

where E_s is the elastic modulus of the substrate, h is the film thickness, and ν_f and ν_s are the Poisson ratios of the film and the substrate, respectively.

LADYP, shown in **Figure 1.2b** (bottom), is an film-on-elastomer technique used to determine the yield point of thin films by identifying the termination of their elastic

behavior.[17] To implement the LADYP test, thin films are transferred to an elastomeric substrate and are subjected to cyclic, incremental strain in steps of 1%—i.e., 0% → 1% → 0% → 2% → 0% → 3% → 0%, and so forth. Periodic wrinkles are formed when the yield point, or onset of plastic deformation, of the material is reached. These wrinkles can be visualized either directly using an optical microscope or indirectly through their manifestation of a diffraction pattern when irradiated with a laser beam.

Lastly, measurement of crack-onset strain is the simplest film-on-elastomer technique and is used to estimate the strain at fracture of a thin film supported by an elastomer.[22] For this test, a polymer film is transferred to an elastomeric substrate, uniaxially strained in increments of 1%, and imaged under an optical microscope. The crack-onset strain is then identified as the strain at which cracks or pinholes first appear in the film. This measurement, however, is limited by the resolution of the microscope. Moreover, cracking behavior in supported films is dependent on both adhesion and the mismatch between the elastic moduli of the film and the substrate: a greater elastic mismatch produces lower crack-onset strains (increased effective brittleness).[23–26]

1.4 Effects of Physical Parameters

The mechanical properties of thin films of semiconducting are influenced by a wide range of experimentally controllable parameters that are distinct from molecular structure. These physical parameters include substrate compliance, film thickness—which is directly affected by processing conditions—and strain rate. Changes in these parameters primarily manifest as increases or decreases in the strain-energy release rate upon elongation.[24,25] The thickness of the film may also influence the measured cohesive energy, as the size of the plastic zone may depend on thickness.[15,27] In addition, fracture processes are dominated

by viscoelastic relaxation mechanisms, which correspond to a dependence on the strain rate. It follows that the mechanical properties of thin films of semiconducting polymers (as in a device) can be modulated by parameters other than the chemical structures of these materials.

1.4.1 Effects of Elastic Mismatch and Adhesion

The strain-energy release rate (**eq 1**) is a function of the mismatch between the elastic moduli of the film and the substrate.[24] This dependence is a consequence of stress localization at the interface of a strained bilayer structure, such as a rigid film supported by a compliant substrate, with increasing elastic mismatch. The elastic mismatch may be quantified using Dundurs' parameters α and β:[23,24]

$$\alpha = \frac{\overline{E}_\mathrm{f} - \overline{E}_\mathrm{s}}{\overline{E}_\mathrm{f} + \overline{E}_\mathrm{s}}, \beta = \frac{1}{2}\frac{\mu_\mathrm{f}(1-2\nu_\mathrm{s}) - \mu_\mathrm{s}(1-2\nu_\mathrm{f})}{\mu_\mathrm{f}(1-\nu_\mathrm{s}) + \mu_\mathrm{s}(1-\nu_\mathrm{f})} \quad (3)$$

where $\overline{E} = E/(1-\nu^2)$, ν is the Poisson ratio, $\mu = E/(2(1+\nu))$, and subscripts 'f' and 's' denote the film and the substrate, respectively. For stiff films of semiconducting polymers and relatively compliant substrates of PDMS, $E_\mathrm{f} \gg E_\mathrm{s}$ implies that $\alpha \approx 1$. Furthermore, the dependence of G on β is weak when $\alpha > 0$ and β may be neglected, but G becomes an increasingly strong function of α as α tends to 1; in particular, G increases with increasing α.[24,25] Since α quantifies the mismatch between the elastic moduli of the film and the substrate, G exceeds G_c (**Section 1.2.3**) at comparatively lower strains for systems with greater elastic mismatch. Consequently, the more compliant the substrate, the lower the strain at fracture of the supported polymer film, and vice-versa.[26] This effect of elastic mismatch is shown microscopically in **Figure 1.3a**, where samples of 40 kDa P3HT exhibit greater crack densities at 20% applied strain when supported by more compliant PDMS

substrates.[28] Adhesion between the film and the substrate is also an important consideration regarding substrate effects on the mechanical properties of thin films. For plastically deformable films of metal supported by polymeric foils, an adhesion layer suppresses the formation and propagation of microcracks.[29] Moreover, semiconducting polymer films exhibit a significant increase in extensibility upon encapsulation, which is the result of forced Poisson compression and stress delocalization over the films by the encapsulant.[30]

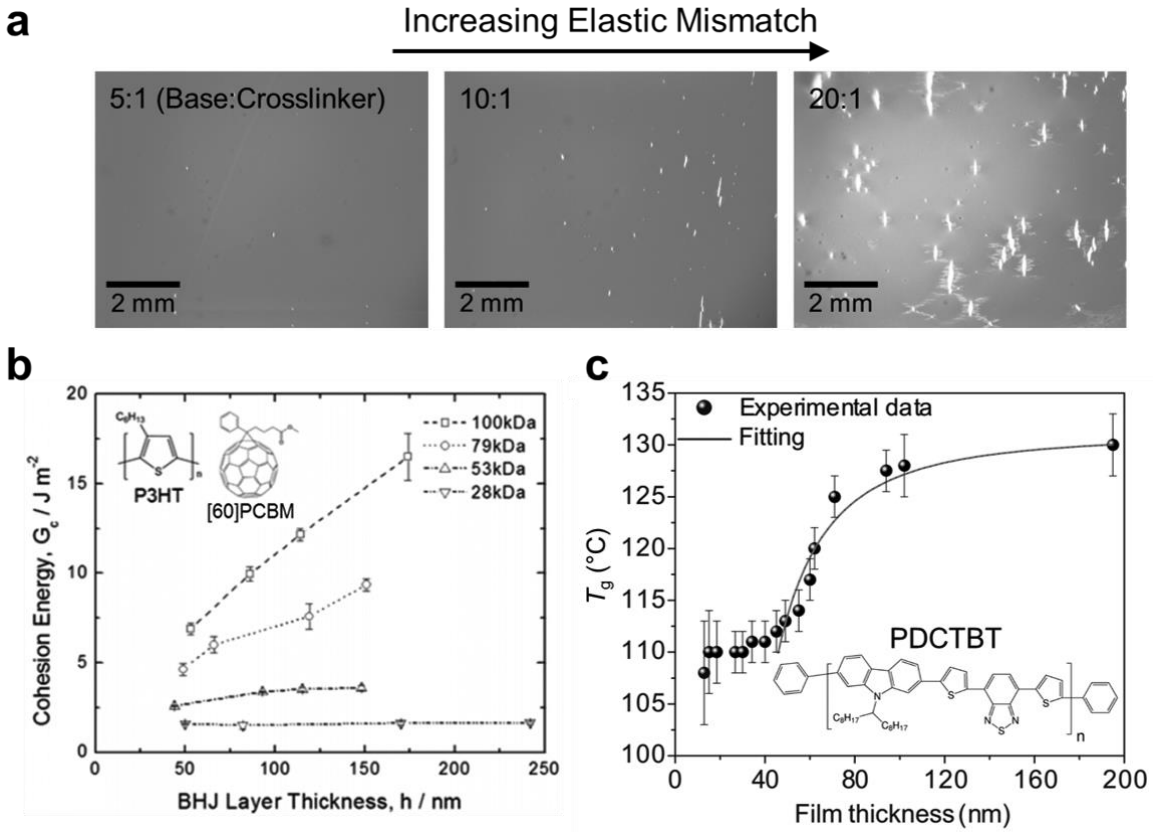

Figure 1.3. Physical parameters affecting the measurement of mechanical properties. (a) Optical micrographs showing samples of 40 kDa P3HT with varying crack densities on PDMS at 20% applied strain; the larger the PDMS curing ratio (base:crosslinker), the more compliant the PDMS, and thus the greater the elastic mismatch. Reproduced with permission from ref 28. Copyright 2017, American Chemical Society. (b) Dependence of the cohesive energy, G_c, of a bulk-heterojunction layer (regioregular P3HT:[60]PCBM) on film thickness, h, and P3HT molecular weight. Reproduced with permission from ref 27. Copyright 2014, American Chemical Society. (c) Glass transition temperature, T_g, of PCDTBT as a function of film thickness; the regression[31] is based on a phenomenological two-layer model. Reproduced with permission from ref 32. Copyright 2012, Springer.

1.4.2 Effects of Film Thickness

Thickness affects virtually all aspects of thin-film behavior, especially for thicknesses below 100 nm (**Figure 1.3b** and **Figure 1.3c**). The dependence of thermomechanical behavior on film thickness is complex. The contribution of a plastic zone that dissipates elastic strain energy at crack tips[14] is appreciable in materials of high molecular weight (**Figure 1.3b**), which exhibit a significant density of entanglements.[15,27] The volume of this plastic zone may be geometrically confined by elastic boundary layers (e.g., adjacent layers in a device stack) as the film is made thinner. A small plastic zone, however, does little to dissipate mechanical stress through plastic flow, and thus the material ruptures more readily in thinner films than for thicker films, at least for polymers of high molecular weight.[15,27] The cohesive energy of polymers of high molecular weight is therefore strongly dependent on thickness, as shown in **Figure 1.3b**, due to significant plastic flow at the tips of cracks that initiate in pre-existing defects.[27] Indeed, thicker films of a particular semiconducting polymer of high molecular weight exhibit greater ductility compared to thinner ones.[14,15] Specifically, there is a marked decrease in the tendency for cracks to propagate in thicker films during tensile loading.

For ultrathin (< 100 nm) films, however, the appearance of cracks may be suppressed for a different reason: namely increased mobility of polymer chains and reduced density of entanglements due to skin-depth effects. The contribution of a mechanically soft, loosely entangled network of chains, which exists near the surface of polymer films, becomes more prominent as the film is thinned below 100 nm.[33–35] This free surface in a geometrically confined polymer film depresses the T_g due to the enhanced dynamics and segmental mobility of polymer chains (see **Figure 1.3c** for the case of

PCDTBT).[32] The loosely entangled network of chains in turn lowers the elastic modulus of the film, reduces its fracture strength, and increases (albeit slightly) its strain at fracture.[36] These skin-depth effects can occur in any polymer film, brittle or ductile, regardless of whether or not a plastic zone exists. Two conclusions can thus be drawn: first, a reduction in intermolecular entanglement density near the free surface of a thinned film enhances segmental mobility and weakens intermolecular forces, both of which soften the material. Second, highly mobile chains at the free surface can effectively relieve mechanical stress induced during elongation.

1.4.3 Effects of Strain Rate

In stress–strain measurements of polymers, higher strain rates generally result in greater apparent elastic moduli.[28] Consistent with previous work on non-conjugated polymers,[37,38] films of 63 kDa P3HT were tested at two strain rates, and the greater strain rate produced a larger apparent elastic modulus (**Figure 1.4**). An increasing strain rate relative to the timescales of chain reptation results in an effective stiffening of the material and thus an increase in its elastic modulus.[38]

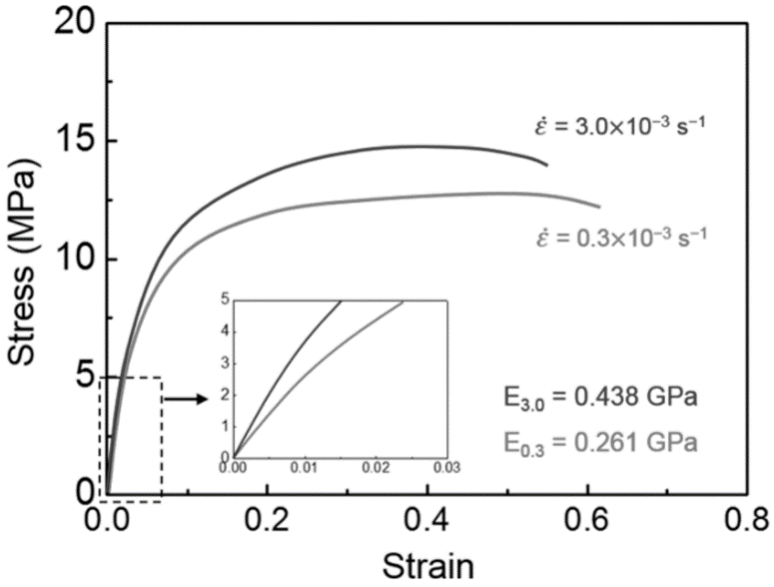

Figure 1.4. Effects of strain rate on the mechanical properties of semiconducting polymers. Stress−strain curves of thin films of 63 kDa P3HT obtained by film-on-water tensile testing at two different strain rates; the pull test performed at the greater strain rate resulted in a larger apparent elastic modulus. Reproduced with permission from ref 28. Copyright 2017, American Chemical Society.

1.5 Effects of Molecular Structure and Microstructure

The molecular weight, length of solubilizing alkyl side chains, and chemical structure of the backbone all influence the plasticity of thin films of semiconducting polymers. The mechanical properties of these materials are also affected by the morphology and packing structure in the solid state, which can be influenced strongly by processing conditions and the kinetics of solidification of films cast from solution.

1.5.1 Role of Molecular Weight

The degree of polymerization of a polymer is quantified by its molecular weight, the distribution of which is reported as either a weight-average, M_w, or a number-average, M_n, molecular weight. Typically, M_w is a more realistic predictor of the mechanical properties of polymers because it is weighted toward the degrees of polymerization that make up the largest weight fraction of the sample. Molecular weight has a large influence

on the cohesion and plasticity of thin films of semiconducting polymers.[28,39] For example, the cohesive energy of P3HT:[60]PCBM bulk heterojunction solar cells increases with increasing molecular weight of P3HT (**Figure 1.3b**) due to plastic dissipation of elastic strain energy.[27] Higher molecular weights can also increase the extensibility of poly(3-alkylthiophene)s (P3ATs), which has been measured in the form of a bulk tape (**Figure 1.5a**)[39] and as a thin film (**Figure 1.5b** and **Figure 1.5c**).[28] The increase in plasticity and cohesion of the films with molecular weight is due to an increase in the density of entanglements. The density of entanglements is proportional to the number of interior kinks (**Figure 1.5d**) in the chains, which increases with degree of polymerization.[40,41] In a theoretical framework, an interior kink occurs at the intersection of the primitive paths of entangled polymer chains. Entanglements raise the energy needed for frictional pullout.[27] In general, semiconducting polymers above a critical molecular weight ($M_c \approx 10$ kDa for P3HT in principle[42]) will exhibit greater viscosity, ultimate strength, toughness, and extensibility due to the entanglement of chains compared to the same material below its M_c.[39]

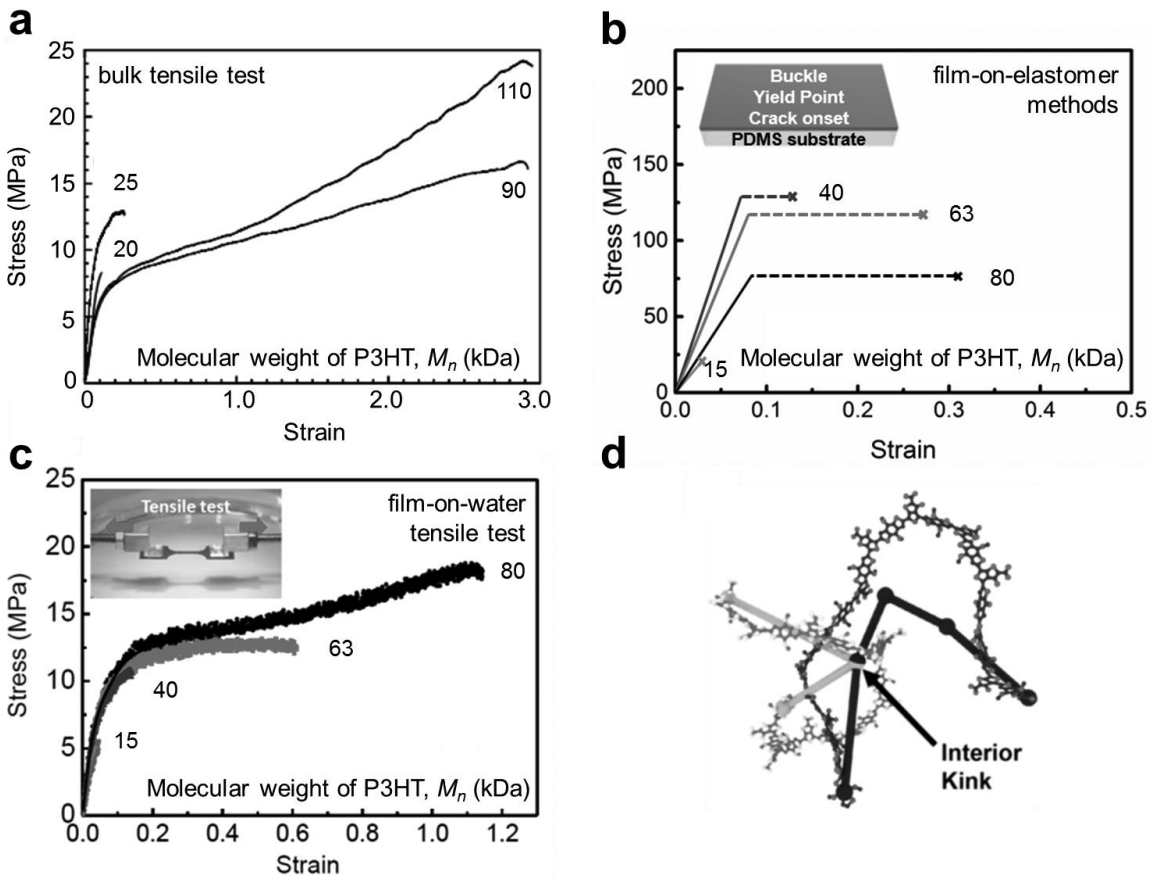

Figure 1.5. Role of molecular weight on the mechanical properties of P3HT. (a) Bulk tensile testing of P3HT tapes with different molecular weights that were solidified from a melt phase. Reproduced with permission from ref 39. Copyright 2013, Elsevier. (b) Film-on-elastomer methods and (c) film-on-water tensile testing of thin films of P3HT with different molecular weights. Reproduced with permission from ref 28. Copyright 2017, American Chemical Society. (d) Representation of an interior kink that results in an entanglement between two polymer chains. Reproduced with permission from ref 8. Copyright 2017, Royal Society of Chemistry.

1.5.2 Role of Alkyl Side Chains

The unsubstituted π-conjugated main chain of semiconducting polymers is not readily soluble. To render these materials soluble, alkyl side chains are typically attached. Side chains confer solubility by interrupting van der Waals interactions between main chains and by permitting greater entropic freedom of the polymer in solution. These side chains also influence the thermomechanical properties. In P3ATs, longer alkyl side chains

increase the crack-onset strain and lower the elastic modulus (**Figure 1.6**).[43,44] In fact, the steepest decrease in modulus with increasing side-chain length, *n*, coincides with the point at which the T_g drops well below room temperature (~25 °C), which occurs between $n = 6$ and $n = 7$ for P3ATs.[43,45] (The T_g of P3HT appears to be a borderline case and has been reported to span a range of temperatures, from approximately –16 °C to 35 °C.[7]) Since the side chains of P3ATs typically do not interdigitate in the solid state,[12,46] increased length of side chains results in weaker van der Waals interactions between chains.[45] This reduction in intermolecular bond strength allows for greater disorder in the system and ability to dissipate mechanical stress. Similarly, branched side chains promote microstructural disorder due to steric hindrance and increased free volume between adjacent main chains,[47] which decreases the correlation lengths of both π–π stacking and lamellar spacing.[48]

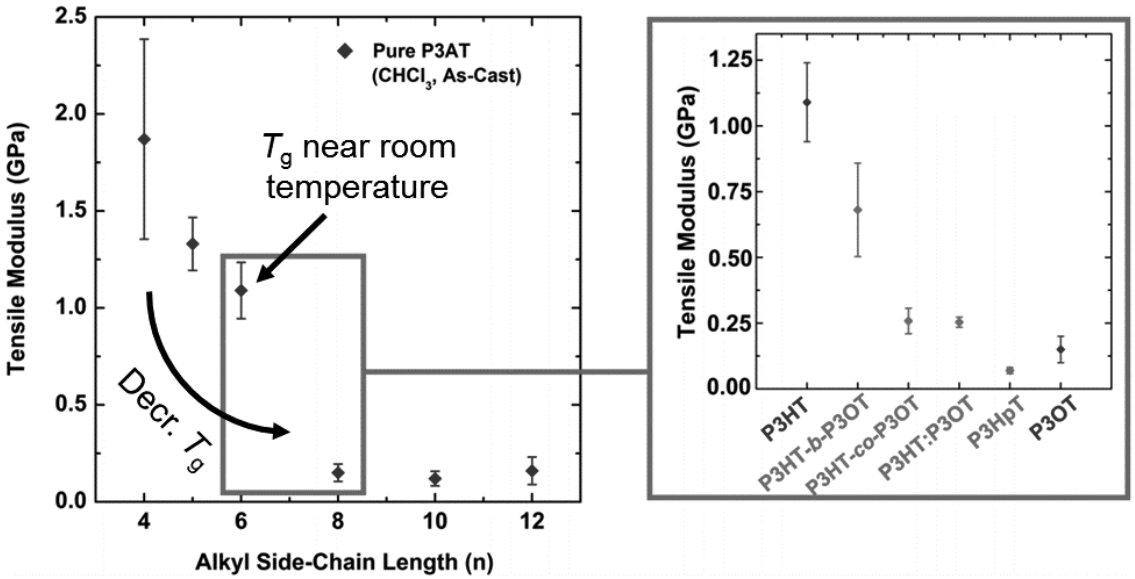

Figure 1.6. Role of the length of alkyl side chains on the tensile modulus of P3ATs. The greatest deviation in modulus occurs when the length of alkyl side chains is increased from $n = 6$ to $n = 7$, which is most likely due to the depression of T_g below room temperature for $n > 6$. Reproduced with permission from ref 43. Copyright 2014, American Chemical Society.

1.5.3 Role of Molecular Structure and Backbone Rigidity

Molecular ordering in semiconducting polymers, particularly intermolecular ordering induced by interdigitation of side chains and crystallization, results in increased elastic moduli and decreased strains at fracture.[46,49] The rigidity of the backbone can affect the mechanical properties of semiconducting polymers;[22] specifically, inflexible backbones may be expected to reduce the flexibility of thin films. Indeed, a correlation between rigid backbones and stiffer films is often observed when incorporating fused rings.[22,50] In contrast, polymer chains can be made more flexible by adding aliphatic spacers to the backbone, which disrupt conjugation and allow for greater exploration of conformational space. Changes in molecular properties by modification of the backbone, however, can altogether change the packing structure. Effects of backbone rigidity are thus often partially or entirely overwhelmed by competing effects of microstructural packing (**Figure 1.7**).[50–52] Because of this interplay of effects, the greatest role that backbone rigidity plays on the mechanical properties of semiconducting polymers is through modulation of the T_g.[7] This role is especially prominent when the glass transition occurs below room temperature.

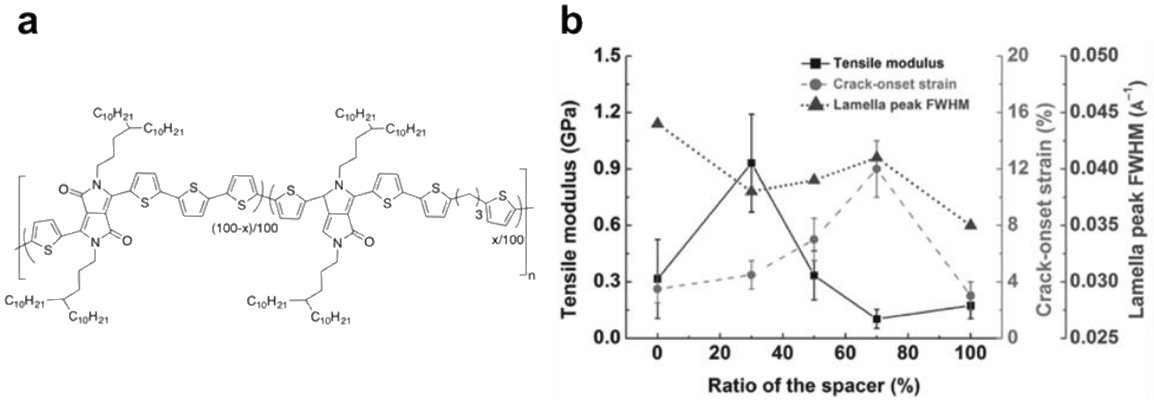

Figure 1.7. Conjugation-break spacer (CBS) in a DPP-based polymer and the impact on the mechanical properties of thin films. (a) Chemical structure of the DPP-*x* polymers bearing a CBS in varying proportions; *x* represents the percentage of the CBS added, with $x = 0$ corresponding to full rigidity and $x = 100$ corresponding to full flexibility along the backbone. (b) Mechanical properties and microstructural data of the DPP-*x* polymers; measurements of tensile moduli and crack-onset strains show no clear trends with increasing percentage of the CBS, as changes in packing structure overshadow decreased backbone rigidity. Reproduced with permission from ref 53. Copyright 2016, Wiley-VCH Verlag, GmbH & Co. KGaA.

1.5.4 Role of Intermolecular Packing

Interdigitation of side chains, and the resulting inhibition of molecular motion, can embrittle semiconducting polymers.[12,22,53] The consequences of interdigitation are seen most clearly in the case of P3HT, the side chains of which can interdigitate upon solvent annealing (called "form II").[46,54] The interdigitated form of P3HT is more brittle than the non-interdigitated form ("form I").[46] Branched side chains generally inhibit interdigitation, and non-interdigitated microstructures exhibit decreased elastic modulus and increased crack-onset strain.[22] The effect of order in a film, especially as a result of increased regioregularity (as in P3ATs), is generally to stiffen and embrittle.[49]

1.6 Glass Transition Temperature and Measurement Techniques

The viscosity of a solid polymer controls the time scales that are required for reorganization of chains in the amorphous domains. These time scales decrease

exponentially with increasing temperature, particularly as the sample passes through the glass transition, characterized by T_g (generally a small range of temperatures), for which several measurement techniques exist.

1.6.1 The Glass Transition in Semiconducting Polymers

As temperature is increased, polymers can reversibly pass to a progressively more fluid and rubbery state, which results in changes in density, viscosity, and refractive index. These changes occur due to relaxation of the main chain (thermally activated translational and rotational modes of motion).[7,55] The nominal temperature that marks the onset of this second-order, non-isothermal phase transition is defined as T_g. At operating temperatures well below the T_g, segmental relaxation is prohibited on experimental time scales, such that existing chain conformations are frozen in metastable states.[7,56] The mechanical degradation of thin films (e.g., during tensile deformation) can be mitigated by decreasing the T_g,[57,58] which is achieved by increasing the length of side chains (see **Section 1.5.2**).[44] In **Figure 1.8**, strains of 10% were applied to films of poly(3-hexylthiophene) (P3HT) and poly(3-dodecylthiophene) (P3DDT) blended with [6,6]-phenyl C_{61} butyric acid methyl ester ([60]PCBM). Upon visual inspection, major cracks on the surface of the P3HT:[60]PCBM film, though not on the surface of the P3DDT:[60]PCBM film, can be observed.[44] Increased ductility in the latter film is due to a reduced T_g and thus improved resistance to decohesion through viscoelastic dissipation of mechanical energy.[43,59]

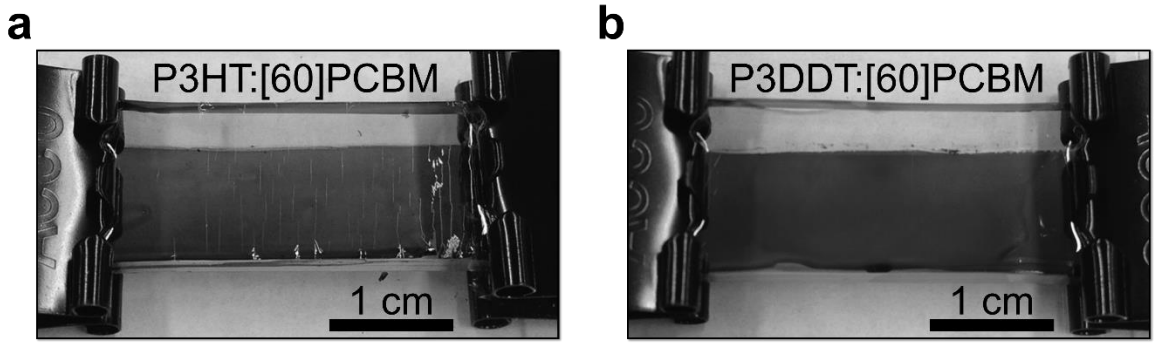

Figure 1.8. Variation in the mechanical response of films of polymer–fullerene composites with T_g. Optical micrographs of thin films of (a) P3HT:[60]PCBM and (b) P3DDT:[60]PCBM on PDMS under an applied strain of 10%. Reproduced with permission from ref 44. Copyright 2014, Wiley-VCH Verlag, GmbH & Co. KGaA.

At operating temperatures well above the T_g, segmental relaxation processes and the associated rate of intermolecular rearrangement can occur on experimentally relevant time scales that decrease exponentially with increasing temperature according to the Vogel–Fulcher law.[55] The resulting decrease in viscosity above the T_g allows polymer chains to reorganize and chain segments to relax towards thermodynamic equilibrium.[56,60] Above the T_g, thin films of semiconducting polymers can exhibit plastic deformation, which aids in accommodating mechanical stresses and dissipating elastic strain energy.[7,59] Furthermore, temperature-dependent phenomena in polymeric materials, such as viscoelastic stress relaxation, phase separation, and crystallization, occur more readily above the T_g.

1.6.2 Techniques to Measure the T_g of Semiconducting Polymers

The T_g is a critical property of materials that is difficult to determine for thin films of semiconducting polymers, despite its importance in predicting the thermal and mechanical stabilities of these materials. There are several techniques to measure the T_g of semiconducting polymers, including differential scanning calorimetry (DSC),[61] dynamic

mechanical analysis (DMA),[62] variable-temperature ellipsometry (VTE),[63] and ultraviolet–visible (UV–vis) spectroscopy.[9] DSC is performed by heating (or cooling) a sample along with an inert reference and measuring the difference in heat flow (**Figure 1.9a**, left). This difference, typically recorded as a function of temperature (**Figure 1.9a**, right), arises due to the release or absorption of heat during phase transitions such as crystallization (release) or melting (absorption).[7] As shown in **Figure 1.9a**, the glass transition corresponds to a change in heat capacity of the sample,[64] i.e., a change in the slope of its DSC thermogram. The sensitivity of a DSC measurement could be amplified by increasing the scan rate, for instance to detect indistinct signals of weak thermal transitions. Conventional DSC setups, however, are limited to bulk samples and cannot be used to study thin films and their thermal properties, which exhibit a non-trivial dependence on thickness below a critical threshold (**Figure 1.3c**) due to geometric confinement and interfacial effects.[32,65]

Alternatively, VTE may be used to determine the T_g of a thin film by examining the dependence of the film's refractive index, n, and thickness, h, on temperature. Ellipsometry involves measuring the change in polarization—quantified by the amplitude ratio and phase shift—of elliptically polarized electromagnetic radiation reflected from the surface of a sample (**Figure 1.9b**, left). Ellipsometry is also used to noninvasively characterize the refractive indices and thicknesses of thin films of polymers. The thermal transitions of these materials can be quantified using an ellipsometer in conjunction with a temperature-controlled stage. For this measurement, the amplitude ratio (or ellipsometric angle), $\tan \Psi$, is evaluated as a function of temperature,[66] which then allows determination of the refractive index and thickness as functions of temperature. The T_g can be approximated as a change in the slope of a graph of refractive index or thickness versus

temperature,[67] which is related to the expansion of free volume above the T_g and, concurrently, an abrupt change in the volumetric coefficient of thermal expansion α_v:

$$\alpha_v = -\frac{1}{\rho}\left(\frac{d\rho}{dT}\right) = -\frac{V}{m}\left(\frac{d(m/V)}{dT}\right) \quad (4)$$

where ρ is density and m is the mass of a thin film of volume V.[63] Assuming that a laterally constrained film of a given area has a fixed mass of polymer, **eq 4** may rewritten as

$$\alpha_v \approx -h\left(\frac{d(1/h)}{dT}\right) = \frac{1}{h}\left(\frac{dh}{dT}\right) \quad (5)$$

using the chain rule. Therefore, an abrupt change in α_v at the T_g corresponds to a distinct variation in the rate of change of h with T, as shown in **Figure 1.9b** (right). Although the T_g of thin films of semiconducting polymers can be extracted from the raw data, ellipsometric systems equipped with temperature-controlled stages are often expensive and not widely available.

A more widely available measurement technique that allows for the determination of the T_g uses a hot plate in an N_2-atmosphere glovebox and a UV–vis spectrometer. UV–vis spectroscopy normally involves radiation with wavelengths between 200 and 800 nm. Irradiated molecules containing π- or non-bonding electrons can absorb the energy to promote electronic transitions: the smaller the bandgap, the less energy is needed to excite electrons, and thus the longer the wavelength of radiation they absorb. Thermal annealing of thin films of semiconducting polymers in the solid state can result in self-assembly and aggregation into densely packed morphologies.[68] The formation of such strong interactions between chains can result in large redshifts[9,69] (i.e., an increase in wavelength) in the UV–vis absorption spectrum because of a reduction in the optical bandgap. The magnitude of the redshift, however, depends on the degree of order imposed on the polymer.[69]

Measurement of the T_g with UV–vis spectroscopy, therefore, works best for materials with a strong propensity to form ordered photophysical aggregates upon thermal annealing. The T_g of a thin film of semiconducting polymer could be measured by quantifying the change in the absorption spectrum that results from a systematic protocol of thermal annealing (**Figure 1.9c**, left and center).[9] A deviation metric, DM_T, may then be defined as the sum of the squared deviations in the absorbance between as-cast films (at room temperature, T_R) and annealed films (at annealing temperature, T):

$$\mathrm{DM_T} \equiv \sum_{\lambda_{min}}^{\lambda_{max}} [I_{\mathrm{T_R}}(\lambda) - I_{\mathrm{T}}(\lambda)]^2 \quad (6)$$

where λ is the wavelength, λ_{min} and λ_{max} are the lower and upper bounds of the optical sweep, respectively, and $I_{\mathrm{T_R}}(\lambda)$ and $I_{\mathrm{T}}(\lambda)$ are the normalized absorption intensities of the as-cast and annealed films, respectively. Approaching the T_g, a sharp increase in the slope of the DM_T when plotted against T occurs because of the activation of chain motion in the solid state.[9] **Figure 1.9c** (right) illustrates the evolution of the deviation metric as a function of annealing temperature for a thin film of poly(3-butylthiophene) (P3BT)—the deviation metric shows a distinct increase near the T_g. Rigorous bilinear regression analysis based on a custom R^2-maximization algorithm is recommended to accurately estimate the T_g (such an algorithm is available in an open-sourced format).[9]

Figure 1.9. Experimental techniques to measure the T_g of a semiconducting polymer. (a, left) Schematic illustrating the main constituents of an original power compensation DSC; PRT stands for platinum resistance thermometer. Reproduced with permission from ref 70. Copyright 2016, Royal Society of Chemistry. (a, right) Second DSC heating and cooling scans of a liquid–crystalline polyfluorene derivative (APFO-3) performed in an N_2 atmosphere at different scan rates. Reproduced with permission from ref 7. Copyright 2015, American Chemical Society. (b, left) A typical ellipsometer comprises a polarizer, compensator, sample, and analyzer; a planar sample is assumed, and the angle of incidence is denoted by φ. Reproduced with permission from ref 71. Copyright 2005, Springer. (b, right) Temperature dependence of the tan Ψ and h of a thin film of APFO-3 measured with VTE; the tan Ψ was measured at a wavelength of 800 nm, near which APFO-3 is optically transparent. Reproduced with permission from ref 72. Copyright 2011, Royal Society of Chemistry. (c) Measuring the T_g with UV−vis absorption spectroscopy involves (left) subjecting a thin film to a thermal cycling protocol, (center) recording the UV−vis spectrum of the film at ambient temperature between successive cycles, and (right) processing the spectra as a plot of the DM_T versus annealing temperature using **eq 6**, the graph of which shows a distinct increase near the T_g. Reproduced with permission from ref 9. Copyright 2017, American Chemical Society.

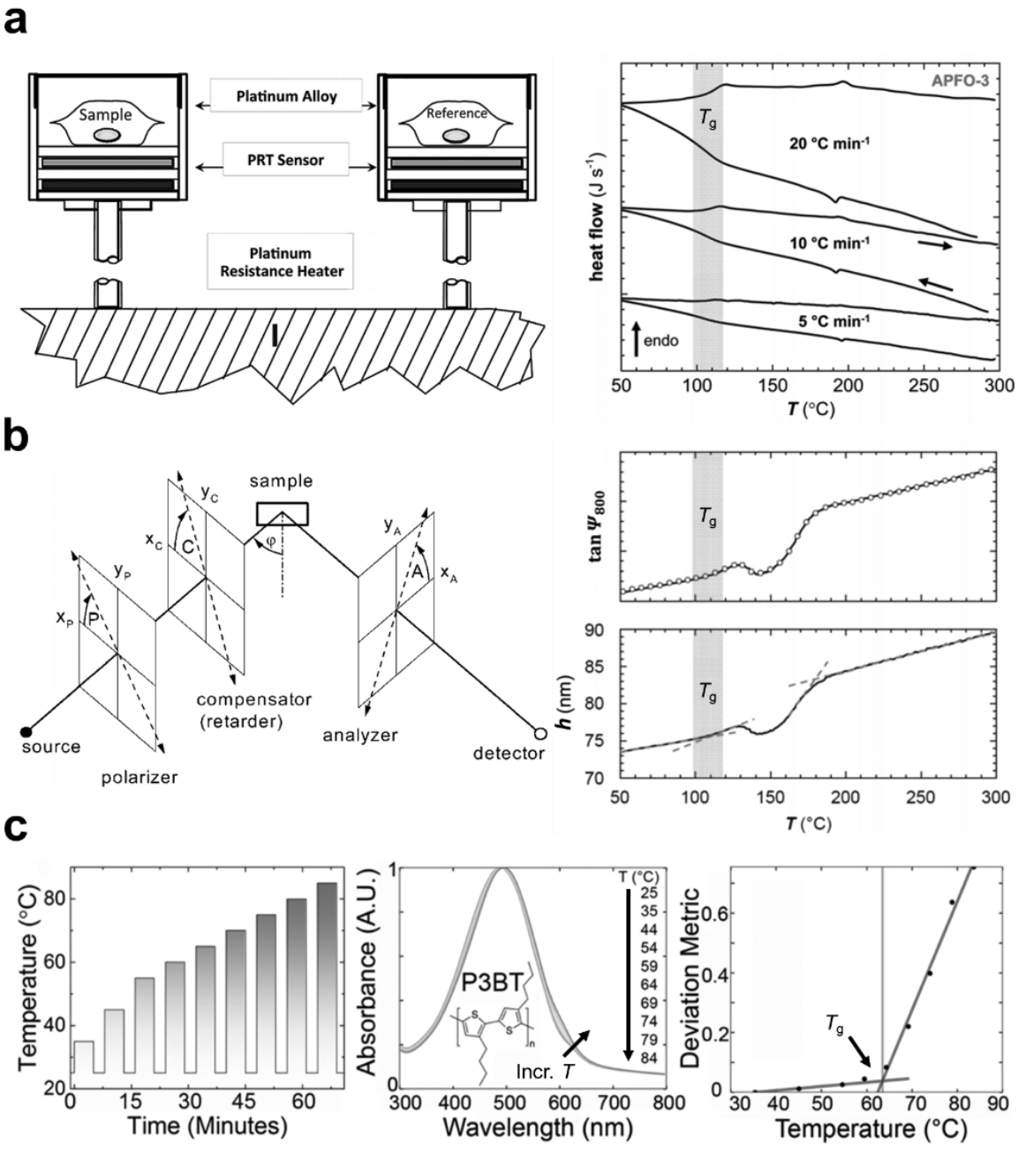
a
Sample
Reference
Platinum Alloy
PRT Sensor
Platinum
Resistance Heater
APFO-3
T_g
20 °C min⁻¹
10 °C min⁻¹
5 °C min⁻¹
endo
heat flow (J s⁻¹)
T (°C)
b
sample
source
polarizer
compensator
(retarder)
analyzer
detector
tan Ψ800
h (nm)
T (°C)
c
Temperature (°C)
Time (Minutes)
Absorbance (A.U.)
Wavelength (nm)
P3BT
Incr. T
T (°C)
Deviation Metric
Temperature (°C)

1.7 Theoretical Modeling

From a theoretical perspective, semiconducting polymers represent a mechanically unique class of polymers. The uniqueness arises in large part due to geometric constraints imposed by π-conjugation along the backbone. A theoretical foundation for describing semiconducting polymers is provided by many of the models reported in the extensive body of literature on the mechanical behavior of non-conjugated polymers. When considering mechanical properties, however, there are several attributes specific to semiconducting polymers that distinguish them from their non-conjugated counterparts. These attributes are a manifestation of nanoscale characteristics—such as the planarizing effects of π-conjugation along the backbone and the flexibility of side chains—and device-level considerations—such as film thickness and solid-state morphology. Existing theoretical treatments thus range from atomistic molecular dynamics of mechanisms of nanoscale deformation to continuum-scale modeling of the mechanical behavior of films of semicrystalline polymers.

1.7.1 Molecular Structure and Atomistic Simulations

The molecular structure of repeat units along a polymer chain is the first consideration for the overall mechanical behavior. The static geometry of these repeat units can be computed approximately using the well-developed numerical methods of quantum chemistry.[73–75] While density functional theory can yield reliable predictions of molecular geometry (**Figure 1.10a**), it falls short, in comparison to perturbation-based methods, when it comes to calculations of energy.[73,74] Moreover, the methods of computational quantum mechanics are too computationally expensive to describe the dynamics of even oligomeric chain segments, such that classical atomistic molecular dynamics must be employed.

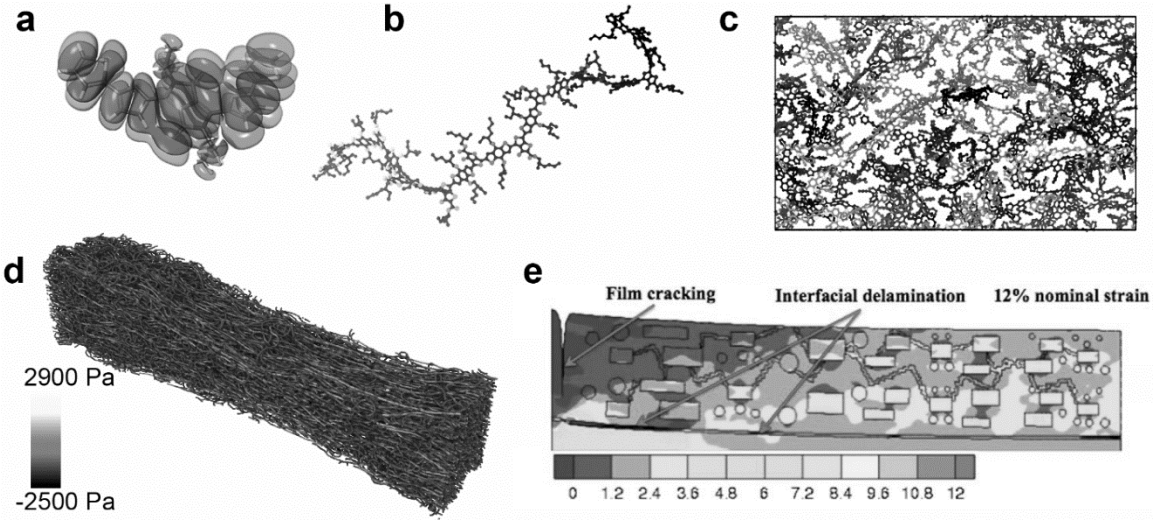

Figure 1.10. Theoretical and computational modeling of the mechanical properties of semiconducting polymers. (a) Illustration showing the highest-occupied molecular orbital (HOMO) of a diketopyrrolopyrrole (DPP) repeat unit obtained using density functional theory calculations. (b) Classical atomistic representation of a donor–acceptor polymer comprising branched alkyl side chains. (c) Atomistic simulations of a bulk donor–acceptor polymer under tensile strain; individual chains are colored distinctly. (d) A coarse-grained simulation of a P3HT film of high molecular weight subjected to tensile loading; polymer chains are colored based on their relative virial stress. (e) Multi-phase finite element simulation of a semicrystalline film of P3HT under tensile strain; the color scheme represents normalized normal stress. Reproduced with permission from ref 76. Copyright 2016, Wiley Periodicals, Inc.

Atomistic molecular dynamics simulations of semiconducting polymers generally use semi-empirical molecular force fields.[77,78] For conjugated polymers with complex backbone structures, many of the specific geometric, electrostatic, and energetic parameters must be obtained using quantum mechanical methods.[73,74] These parameters are typically associated with the planarizing intramolecular forces that exist between conjugated heterocyclic ring structures, such as dihedral rotations and bond stretches. The forces that control such molecular rotations are important in determining the time and temperature scales of stress relaxation through motion of polymer chains. These forces also influence the overall conformational structure of polymer chains, which subsequently

determines the degree of their entanglement. Atomistic models based on classical, semi-empirical force fields are only capable of describing ground-state dynamics, neglecting mechanical effects of higher order that may arise due to excited-state and charge-transfer processes. (Mechanical effects of higher order include changes in molecular geometry that minimize electrostatic potential energy in the presence of charged species: namely electrons and holes. Ground-state dynamics, however, usually overwhelm these effects.) Furthermore, these models do not allow for the possibility of scission of chemical bonds; such a description is difficult from a numerical perspective because breakage of covalent bonds is associated with a large release of energy. Nevertheless, atomistic models provide practical predictions of the conformational preferences (**Figure 1.10b**), nanoscale packing features, and tensile behavior of complex donor–acceptor polymers (**Figure 1.10c**).

1.7.2 Polymer-Chain Size and Phase Behavior

The next length scale of interest is the size of polymer chains, which, combined with the chemical structure of the monomer, determines the overall phase behavior during solution casting. Conjugated polymers embody a wide range of behaviors in the solution phase, among which is the formation of single-chain and multi-chain aggregates.[73,79–82] The tendency to form such aggregates is important with regard to the mechanical stability of thin films processed form solution, as it leads to the creation of voids and lower densities of entanglement in the solid state.[8] This outcome is especially true for materials that undergo a glass transition well above room temperature and lack molecular mechanisms to relax kinetically trapped conformations without treatment by thermal annealing or solvent vapor. The solid-state morphology and tensile behavior of conjugated homopolymers, such as P3HT,[42,83] and numerous low-bandgap, alternating copolymers[8] have been studied in

atomistic detail using modified force fields. An illustration of one such atomistic simulation is shown in **Figure 1.10c**.

Atomistic molecular dynamics simulations employ periodic boundary conditions and are thus used to model bulk samples. The stress–strain behavior of a bulk sample can be computed by imposing a constant strain rate in one dimension of the simulation box, and then by calculating the bulk stress in the axial dimension as the sum of all virial stresses acting on the particles. Atomistic simulations also provide predictions of packing at the molecular scale, tendency for entanglement, and mechanisms of deformation in semiconducting polymers of low molecular weight under tension. In addition, these simulations can be used to predict thermal properties, such as the glass transition temperature, by quenching a system from the melt phase and determining the temperature at which the coefficient of thermal expansion exhibits a change in slope. Atomistic simulations, however, do not consider any aspects of casting from solution and cannot be run long enough for crystallization to occur. In this regard, atomistic simulations can only be used to model the amorphous phase that is obtained by quenching from an equilibrated melt phase.

1.7.3 Coarse-Grained Simulations and Continuum-Based Methods

Although atomistic models can be used to describe the dynamics and mechanical behavior of systems of low molecular weight, the large length and time scales associated with polymers of high molecular weight make these simulations computationally prohibitive. For such large scales, coarse-grained models must be employed. In these models of comparatively low resolution, groups of atoms are mapped to “beads” that have prescribed interactions and are optimized to match the results of atomistic simulations in

either a melt or solution phase.[84–91] This coarse-graining procedure allows for the simulation of solution casting and may also be used to model a thin film in its entirety, such as the one shown in **Figure 1.10d**. These models have been employed to predict the mechanical behavior of P3ATs of high molecular weight and composite systems with fullerene molecules. Such simulations show reliable predictions of the tensile modulus, Poisson ratio, and glass transition temperature.[4,28] In addition, alignment of polymer chains due to plastic deformation and stress concentration within chains can be calculated (see **Figure 1.10d**). Finally, important theoretical properties, such as the density of entanglements, can be computed directly from coarse-grained simulations using algorithms of primitive-path analysis developed for non-conjugated polymers.[40,92–94] One particularly insightful observation that emerged from these simulations is that P3HT chains tend to fold on themselves when mixed with fullerenes.[10] This folding leads to a reduction in entanglement between chains and, consequently, a decrease in the toughness of the composite material.

For simulations of even larger scale that include bulk, semicrystalline domains, continuum-based methods must be employed. Finite element simulations consisting of three-phase heterogeneous models for P3HT have been developed to account for the crystallinity of ordered regions, elasto-viscoplasticity of amorphous regions, and even hypo-elasticity of tie chains between interconnected crystalline domains.[76,95] A typical simulation output that depicts the concentration of stress in a representative semicrystalline morphology is shown in **Figure 1.10e**. Although these simulations can provide detailed mechanisms of deformation that agree well with experiment, they require numerous mechanical parameters that are not known for most semiconducting polymers.

1.8 Composite Systems

The importance of composite systems is exemplified by the bulk heterojunction (BHJ)—an intimate blend of two or more semiconducting components—which functions as the active layer in organic solar cells. This structure introduces additional challenges to understanding the deformability of semiconducting polymers because the mechanical properties of a composite depend not only on those of its constituents but also on complex interactions between these components.

1.8.1 Effects of Molecular Mixing

In a BHJ, the electron donor is typically a semiconducting polymer and the electron acceptor may be a fullerene derivative.[96] In electron-donating polymers, side chains can have a high attachment density such as in P3HT, where each thiophene ring has a side chain attached. On the other hand, side chains could be sparse such as in poly(2,5-bis(3-tetradecyllthiophen-2-yl)thieno[3,2-*b*]thiophene) (PBTTT), where individual thiophene rings with side chains attached are separated by naked thienothiophene units. In polymers that exhibit lower attachment densities of side chains, greater free volume exists, which allows for the intercalation of fullerene crystals between the side chains. This intercalation results in a mixed, bimolecular blend where fullerene molecules can directly interact with the polymer backbone.[97]

When mixed with [6,6]-phenyl C_{61} butyric acid methyl ester ([60]PCBM), P3ATs generally do not allow for [60]PCBM intercalation, whereas PBTTTs and poly(terthiophenes) (e.g., PT2T) do (**Figure 1.11a**).[98] P3AT:fullerene blends, mixed in ratios of 1:1, form ternary morphologies that comprise fullerene-rich domains, polymer-rich aggregates, and a mixed, amorphous phase.[99] Moreover, PBTTT:fullerene blends form

a bimolecular phase that is well-ordered (i.e., bimolecular crystallites),[100] while the bimolecular phase of PT2T:fullerene blends is disordered. The latter may be inferred based on the disappearance of the vibronic peaks in the UV–vis absorption spectrum of PT2T upon adding [60]PCBM, as shown in **Figure 1.11b**.[101] (Vibronic peaks in a UV–vis absorption spectrum are indicative of polymer aggregation, such that their disappearance corresponds to a disruption in microstructural order.) An important consequence of molecular mixing is thus that the elastic moduli of polymer:fullerene blends are lower than simple averages of the moduli of the individual components. As shown in **Figure 1.11c**, a linear correlation may nevertheless be observed between the moduli of blends and those of the corresponding neat polymers.[101]

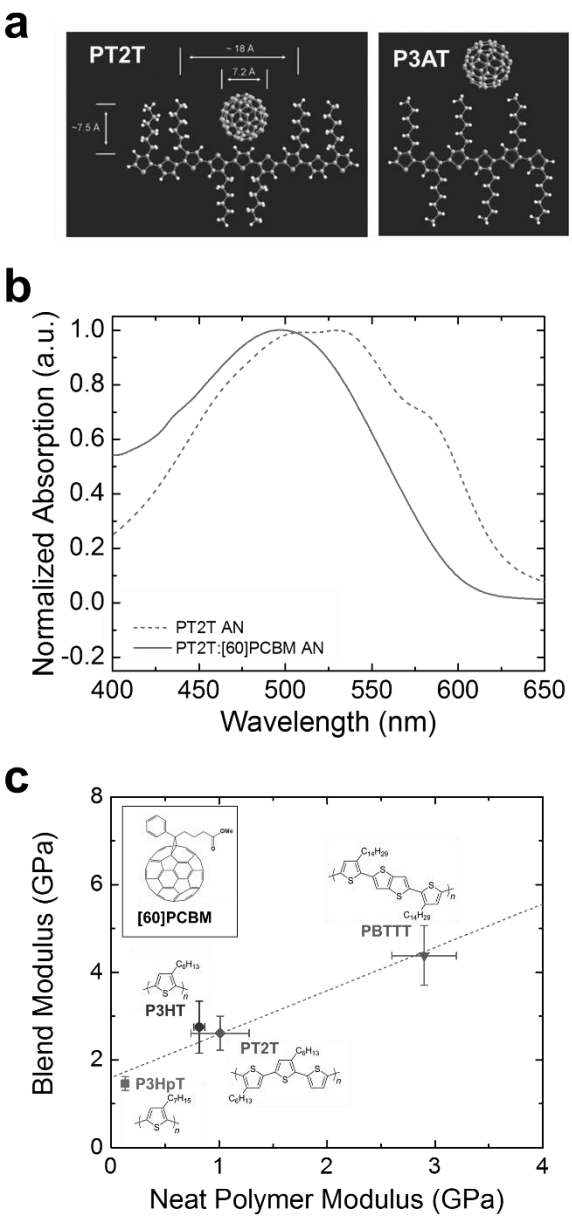

Figure 1.11. Effects of fullerene mixing on semiconducting polymers. (a) C_{60} can readily intercalate along the backbone of polymers that are structurally similar to PT2T, which has side chains that are sparsely attached, but it cannot intercalate along the backbone of polymers that are structurally similar to P3ATs, which have side chains that are densely attached. Reproduced with permission from ref 98. Copyright 2007, Wiley-VCH Verlag, GmbH & Co. KGaA. (b) UV–vis absorption spectra of neat PT2T and PT2T:[60]PCBM (both thermally annealed) showing the disruption of PT2T ordering—as suggested by the complete vanishing of the vibronic peaks—upon addition of [60]PCBM. (c) Linear correlation between the elastic moduli of polymer:fullerene blends and those of the corresponding neat polymers. Reproduced with permission from ref 101. Copyright 2015, Elsevier.

1.8.2 Polymer–Fullerene Composites

Methanofullerenes are fullerene derivatives commonly used as the electron-accepting component of a BHJ and, mechanically, are extremely brittle van der Waals solids. In general, fullerenes are produced as a mixture of various structures, though their separation is a resource-intensive and energetically expensive process.[102] Two common methanofullerenes are [60]PCBM, which comprises a spherical 60-carbon fullerene and a solubilizing side chain, and [6,6]-phenyl C_{71} butyric acid methyl ester ([70]PCBM), which comprises an ovoidal 70-carbon fullerene but has the same solubilizing side chain as in [60]PCBM (**Figure 1.12a**). The former packs efficiently and readily crystallizes to the point that it fractures at very low strain. On the other hand, [70]PCBM can withstand slightly more deformation because it packs less efficiently and is morphologically hindered due to its ovoidal shape and numerous isomers.[103] Methanofullerenes behave as anti-plasticizers when mixed with semiconducting polymers by increasing the glass transition temperature and elastic modulus and by reducing the strain at fracture and cohesive energy.[6,103,104] These effects on the thermomechanical properties of semiconducting polymers all result in more fragile polymer:fullerene systems overall.

The detrimental effects that [60]PCBM and [70]PCBM have on the mechanical performance of semiconducting polymers indicate that these fullerene derivatives, individually, are far from ideal electron acceptors for low-cost applications that require mechanical durability. Nonetheless, incompletely separated fullerenes combine the advantage of a lower embodied energy—i.e., the total input of energy for synthesis and processing of fullerenes—with a reduction in modulus and an increase in crack-onset strain.[103] Increases in compliance and extensibility, as shown in **Figure 1.12b** and **Figure**

1.12c, can be attributed to synergy between the inefficient packing of fullerene molecules in fullerene-rich domains and a reduction in polymer aggregation.[103] BHJ blends that comprise incompletely separated fullerenes, though still stiffer and more brittle than the polymeric component alone, exhibit greater deformability compared to BHJs consisting of completely separated fullerenes.[103] Thermal annealing of these blends, particularly those comprising polythiophene-based polymers, induces molecular aggregation and crystallization.[12] This improved molecular ordering, however, stiffens and embrittles the films, as demonstrated in **Figure 1.12b** and **Figure 1.12c**.[43,103]

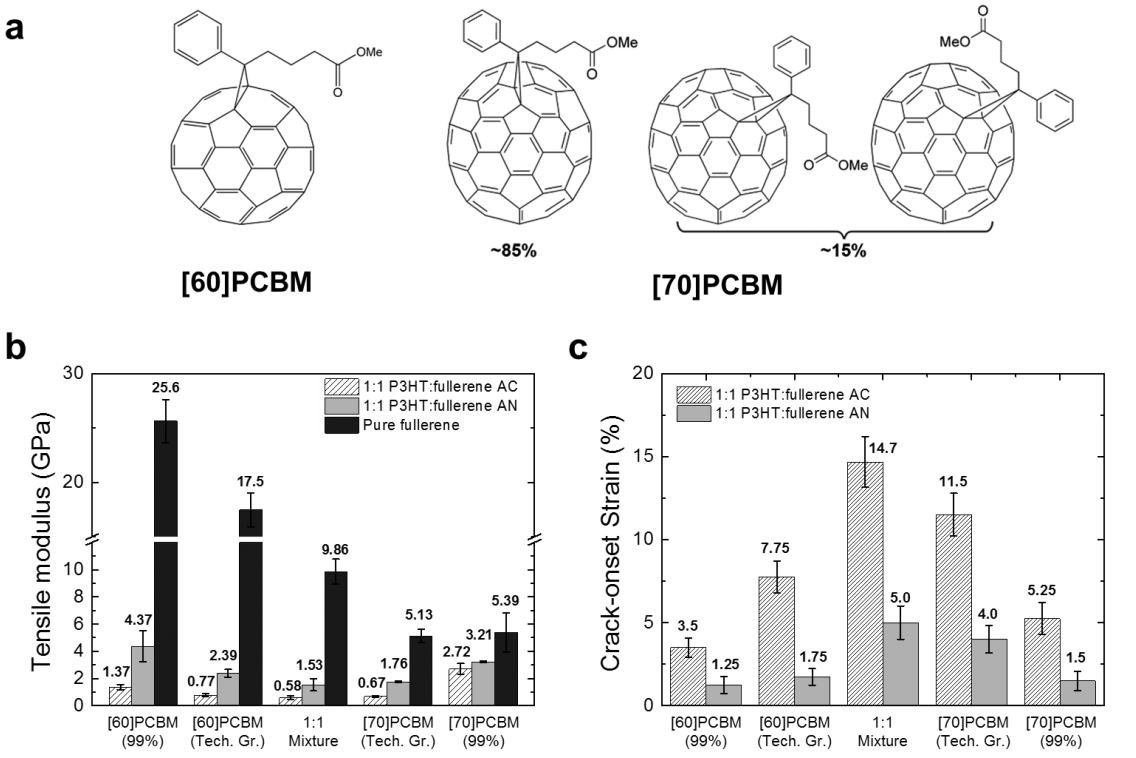

Figure 1.12. Effects of fullerene mixing on semiconducting polymers. (a) Molecular structures of [60]PCBM and [70]PCBM; the latter is predominantly a mixture of three different isomers. (b) Tensile moduli of polymer:fullerene composites as functions of the relative concentrations of [60]PCBM and [70]PCBM. Data for pure fullerene films and their respective composites, as-cast (AC) and after thermal annealing (AN), are included. Compared to composites with separated fullerenes, composites with mixed fullerenes exhibit lower elastic moduli and (c) higher crack-onset strains. Reproduced with permission from ref 103. Copyright 2015, American Chemical Society.

1.9 Conclusion and Outlook

Mechanical deformability is the characteristic that enables most touted advantages of organic electronic materials. Although the field of flexible and robust electronics is nascent with as of yet few commercialized products, significant efforts to determine how chemical structure and microstructural order influence the mechanical properties of semiconducting polymers have already been made. The mechanical properties of thin films of semiconducting polymers depend on molecular structure and also on molecular packing in the solid state. Indeed, a recurring finding, both experimentally and computationally, is that the thermomechanical properties of semiconducting polymers are controlled by conditions of solution and thermal processing, which directly influence crystallinity and nanoscale ordering. A complete understanding of the mechanical properties of these materials entails developing a framework for how specific molecular structures assemble in solution and ultimately in the solid state.

Determining the mechanical properties of thin films has proven difficult in numerous ways, primarily due to the impracticality of handling these materials in freestanding form. These challenges have led to the development of broadly applicable approaches to metrology, such as the film-on-elastomer and film-on-water methods, that can be readily applied to semiconducting polymers. Although these techniques allow for facile determination of the mechanical properties of thin films, the results of such mechanical analyses are dependent on the technique and testing conditions used. Another typical complication in characterizing the mechanical properties of thin films of semiconducting polymer lies in the diversity of the fracture behavior that these materials exhibit. In addition, the mechanics that govern ductile fracture—compared to brittle

fracture—are more sophisticated and less well understood due to the occurrence of plastic flow during events of ductile fracture.

A deeper understanding of the mechanical properties of semiconducting polymers will enable the production of organic electronics that are mechanically robust and resistant to fracture. For these devices to be a technological success, however, efforts to enhance their thermomechanical properties and reliability against mechanical deformation must not come second to optimizing electronic performance. Instead, the primary objective in developing robust and efficient devices should be to co-optimize the mechanical and optoelectronic properties of semiconducting polymers. For this purpose, computational methods and theoretical modeling are expected to play a crucial role in facilitating the co-optimization of mechanical and electronic properties by generating experimentally testable hypotheses. These efforts directed toward an improved understanding of the thermomechanical properties of semiconducting polymers may also reveal ways in which to create materials with properties inspired by biological tissue, including simultaneous toughness and compliance, degradability, and the capacity to self-repair.

1.10 Acknowledgements

This work was supported by a grant from the Air Force Office of Scientific Research Grant Number FA9550-16-1-0220. S.S. and D.R. were supported in part by the Graduate Research Fellowship Program of the National Science Foundation (DGE-1144086).

Chapter 1, in full, is currently in press for publication of the material by Mohammad A. Alkhadra, Andrew T. Kleinschmidt, Samuel E. Root, Daniel Rodriquez, Adam D. Printz, Suchol Savagatrup, and Darren J. Lipomi*. The thesis author was the primary investigator and author of this material.

1.11 References

(1) Xu, J. M. Plastic Electronics and Future Trends in Microelectronics. *Synth. Met.* **2000**, *115*, 1–3.

(2) *Flexible Electronics: Materials and Applications*, 1st ed.; Wong, W. S., Salleo, A., Eds.; Springer Science & Business Media, 2009.

(3) Facchetti, A. π-Conjugated Polymers for Organic Electronics and Photovoltaic Cell Applications. *Chem. Mater.* **2011**, *23*, 733–758.

(4) Root, S. E.; Savagatrup, S.; Printz, A. D.; Rodriquez, D.; Lipomi, D. J. Mechanical Properties of Organic Semiconductors for Stretchable, Highly Flexible, and Mechanically Robust Electronics. *Chem. Rev.* **2017**, *117*, 6467–6499.

(5) Mei, J.; Bao, Z. Side Chain Engineering in Solution-Processable Conjugated Polymers. *Chem. Mater.* **2014**, *26*, 604–615.

(6) Savagatrup, S.; Printz, A. D.; Wu, H.; Rajan, K. M.; Sawyer, E. J.; Zaretski, A. V.; Bettinger, C. J.; Lipomi, D. J. Viability of Stretchable Poly(3-Heptylthiophene) (P3HpT) for Organic Solar Cells and Field-Effect Transistors. *Synth. Met.* **2015**, *203*, 208–214.

(7) Müller, C. On the Glass Transition of Polymer Semiconductors and Its Impact on Polymer Solar Cell Stability. *Chem. Mater.* **2015**, *27*, 2740–2754.

(8) Root, S. E.; Jackson, N.; Savagatrup, S.; Arya, G.; Lipomi, D. J. Modelling the Morphology and Thermomechanical Behaviour of Low-Bandgap Conjugated Polymers and Bulk Heterojunction Films. *Energy Environ. Sci.* **2016**, *10*, 558–569.

(9) Root, S. E.; Alkhadra, M. A.; Rodriquez, D.; Printz, A. D.; Lipomi, D. J. Measuring the Glass Transition Temperature of Conjugated Polymer Films with Ultraviolet-Visible Spectroscopy. *Chem. Mater.* **2017**, *29*, 2646–2654.

(10) Root, S. E.; Savagatrup, S.; Pais, C. J.; Arya, G.; Lipomi, D. J. Predicting the Mechanical Properties of Organic Semiconductors Using Coarse-Grained Molecular Dynamics Simulations. *Macromolecules* **2016**, *49*, 2886–2894.

(11) Capaldi, F. M.; Boyce, M. C.; Rutledge, G. C. Molecular Response of a Glassy Polymer to Active Deformation. *Polymer* **2004**, *45*, 1391–1399.

(12) O'Connor, B.; Chan, E. P.; Chan, C.; Conrad, B. R.; Richter, L. J.; Kline, R. J.; Heeney, M.; McCulloch, I.; Soles, C. L.; DeLongchamp, D. M. Correlations between Mechanical and Electrical Properties of Polythiophenes. *ACS Nano* **2010**, *4*, 7538–7544.

(13) Ward, I. M.; Sweeney, J. *Mechanical Properties of Solid Polymers*, 3rd ed.; John

Wiley & Sons, 2012.

(14) Alkhadra, M. A.; Root, S. E.; Hilby, K. M.; Rodriquez, D.; Sugiyama, F.; Lipomi, D. J. Quantifying the Fracture Behavior of Brittle and Ductile Thin Films of Semiconducting Polymers. *Chem. Mater.* **2017**, *29*, 10139–10149.

(15) Balar, N.; O'Connor, B. T. Correlating Crack Onset Strain and Cohesive Fracture Energy in Polymer Semiconductor Films. *Macromolecules* **2017**, *50*, 8611–8618.

(16) Kim, J.-H.; Nizami, A.; Hwangbo, Y.; Jang, B.; Lee, H.-J.; Woo, C.-S.; Hyun, S.; Kim, T.-S. Tensile Testing of Ultra-Thin Films on Water Surface. *Nat. Commun.* **2013**, *4*, 2520.

(17) Printz, A. D.; Zaretski, A. V.; Savagatrup, S.; Chiang, A. S.-C.; Lipomi, D. J. Yield Point of Semiconducting Polymer Films on Stretchable Substrates Determined by Onset of Buckling. *ACS Appl. Mater. Interfaces* **2015**, *7*, 23257–23264.

(18) Kim, T.; Kim, J.-H.; Kang, T. E.; Lee, C.; Kang, H.; Shin, M.; Wang, C.; Ma, B.; Jeong, U.; Kim, T.-S.; Kim, B. J. Flexible, Highly Efficient All-Polymer Solar Cells. *Nat. Commun.* **2015**, *6*, 8547.

(19) Stafford, C. M.; Harrison, C.; Beers, K. L.; Karim, A.; Amis, E. J.; VanLandingham, M. R.; Kim, H. C.; Volksen, W.; Miller, R. D.; Simonyi, E. E. A Buckling-Based Metrology for Measuring the Elastic Moduli of Polymeric Thin Films. *Nat. Mater.* **2004**, *3*, 545–550.

(20) Rodriquez, D.; Savagatrup, S.; Valle, E.; Proctor, C. M.; McDowell, C.; Bazan, G. C.; Nguyen, T.-Q.; Lipomi, D. J. Mechanical Properties of Solution-Processed Small-Molecule Semiconductor Films. *ACS Appl. Mater. Interfaces* **2016**, *8*, 11649–11657.

(21) Volynskii, A. L.; Bazhenov, S.; Lebedeva, O. V.; Bakeev, N. F. Mechanical Buckling Instability of Thin Coatings Deposited on Soft Polymer Substrates. *J. Mater. Sci.* **2000**, *35*, 547–554.

(22) Roth, B.; Savagatrup, S.; De Los Santos, N. V.; Hagemann, O.; Carlé, J. E.; Helgesen, M.; Livi, F.; Bundgaard, E.; Søndergaard, R. R.; Krebs, F. C.; Lipomi, D. J. Mechanical Properties of a Library of Low-Band-Gap Polymers. *Chem. Mater.* **2016**, *28*, 2363–2373.

(23) Dundurs, J. Elastic Interaction of Dislocations with Inhomogeneities. In *Mathematical Theory of Dislocations*; Mura, T., Ed.; American Society of Mechanical Engineers: New York, 1969; pp 70–115.

(24) Beuth, J. L. Cracking of Thin Bonded Films in Residual Tension. *Int. J. Solids Struct.* **1992**, *29*, 1657–1675.

(25) Xia, Z. C.; Hutchinson, J. W. Crack Patterns in Thin Films. *J. Mech. Phys. Solids* **2000**, *48*, 1107–1131.

(26) Li, T.; Huang, Z.; Suo, Z.; Lacour, S. P.; Wagner, S. Stretchability of Thin Metal Films on Elastomer Substrates. *Appl. Phys. Lett.* **2004**, *85*, 3435–3437.

(27) Bruner, C.; Dauskardt, R. Role of Molecular Weight on the Mechanical Device Properties of Organic Polymer Solar Cells. *Macromolecules* **2014**, *47*, 1117–1121.

(28) Rodriquez, D.; Kim, J.-H.; Root, S. E.; Fei, Z.; Boufflet, P.; Heeney, M.; Kim, T.-S.; Lipomi, D. J. Comparison of Methods for Determining the Mechanical Properties of Semiconducting Polymer Films for Stretchable Electronics. *ACS Appl. Mater. Interfaces* **2017**, *9*, 8855–8862.

(29) Lu, N.; Wang, X.; Suo, Z.; Vlassak, J. Metal Films on Polymer Substrates Stretched Beyond 50%. *Appl. Phys. Lett.* **2007**, *91*, 221909.

(30) Sawyer, E. J.; Zaretski, A. V.; Printz, A. D.; de los Santos, N. V.; Bautista-Gutierrez, A.; Lipomi, D. J. Large Increase in Stretchability of Organic Electronic Materials by Encapsulation. *Extrem. Mech. Lett.* **2016**, *8*, 78–87.

(31) Keddie, J. L.; Jones, R. A. L.; Cory, R. A. Size-Dependent Depression of the Glass Transition Temperature in Polymer Films. *Europhys. Lett.* **1994**, *27*, 59–64.

(32) Wang, T.; Pearson, A. J.; Dunbar, A. D. F.; Staniec, P. A.; Watters, D. C.; Coles, D.; Yi, H.; Iraqi, A.; Lidzey, D. G.; Jones, R. A. L. Competition between Substrate-Mediated π-π Stacking and Surface-Mediated T_g Depression in Ultrathin Conjugated Polymer Films. *Eur. Phys. J. E. Soft Matter* **2012**, *35*, 9807.

(33) Si, L.; Massa, M. V.; Dalnoki-Veress, K.; Brown, H. R.; Jones, R. A. L. Chain Entanglement in Thin Freestanding Polymer Films. *Phys. Rev. Lett.* **2005**, *94*, 127801.

(34) Liu, D.; Orozco, R. O.; Wang, T. Deviations of the Glass Transition Temperature in Amorphous Conjugated Polymer Thin Films. *Phys. Rev. E* **2013**, *88*, 022601.

(35) Zhao, J.-H.; Kiene, M.; Hu, C.; Ho, P. S. Thermal Stress and Glass Transition of Ultrathin Polystyrene Films. *Appl. Phys. Lett.* **2000**, *77*, 2843.

(36) Lee, J. H.; Chung, J. Y.; Stafford, C. M. Effect of Confinement on Stiffness and Fracture of Thin Amorphous Polymer Films. *ACS Macro Lett.* **2012**, *1*, 122–126.

(37) Mulliken, A. D.; Boyce, M. C. Mechanics of the Rate-Dependent Elastic-Plastic Deformation of Glassy Polymers from Low to High Strain Rates. *Int. J. Solids Struct.* **2006**, *43*, 1331–1356.

(38) Richeton, J.; Ahzi, S.; Vecchio, K. S.; Jiang, F. C.; Adharapurapu, R. R. Influence

of Temperature and Strain Rate on the Mechanical Behavior of Three Amorphous Polymers: Characterization and Modeling of the Compressive Yield Stress. *Int. J. Solids Struct.* **2006**, *43*, 2318–2335.

(39) Koch, F. P. V.; Rivnay, J.; Foster, S.; Müller, C.; Downing, J. M.; Buchaca-Domingo, E.; Westacott, P.; Yu, L.; Yuan, M.; Baklar, M.; Fei, Z.; Luscombe, C.; Mclachlan, M. A.; Heeney, M.; Rumbles, G.; Silva, C.; Salleo, A.; Nelson, J.; Smith, P.; Stingelin, N. The Impact of Molecular Weight on Microstructure and Charge Transport in Semicrystalline Polymer Semiconductors–Poly(3-Hexylthiophene), a Model Study. *Prog. Polym. Sci.* **2013**, *38*, 1978–1989.

(40) Shanbhag, S.; Kröger, M. Primitive Path Networks Generated by Annealing and Geometrical Methods: Insights into Differences. *Macromolecules* **2007**, *40*, 2897–2903.

(41) Kröger, M. Shortest Multiple Disconnected Path for the Analysis of Entanglements in Two- and Three-Dimensional Polymeric Systems. *Comput. Phys. Commun.* **2005**, *168*, 209–232.

(42) Tummala, N. R.; Bruner, C.; Risko, C.; Brédas, J.-L.; Dauskardt, R. H. Molecular-Scale Understanding of Cohesion and Fracture in P3HT:Fullerene Blends. *ACS Appl. Mater. Interfaces* **2015**, *7*, 9957–9964.

(43) Savagatrup, S.; Printz, A. D.; Rodriquez, D.; Lipomi, D. J. Best of Both Worlds: Conjugated Polymers Exhibiting Good Photovoltaic Behavior and High Tensile Elasticity. *Macromolecules* **2014**, *47*, 1981–1992.

(44) Savagatrup, S.; Makaram, A. S.; Burke, D. J.; Lipomi, D. J. Mechanical Properties of Conjugated Polymers and Polymer-Fullerene Composites as a Function of Molecular Structure. *Adv. Funct. Mater.* **2014**, *24*, 1169–1181.

(45) Savagatrup, S.; Printz, A. D.; O'Connor, T. F.; Zaretski, A. V.; Rodriquez, D.; Sawyer, E. J.; Rajan, K. M.; Acosta, R. I.; Root, S. E.; Lipomi, D. J. Mechanical Degradation and Stability of Organic Solar Cells: Molecular and Microstructural Determinants. *Energy Environ. Sci.* **2015**, *8*, 55–80.

(46) Koch, F. P. V.; Heeney, M.; Smith, P. Thermal and Structural Characteristics of Oligo(3-Hexylthiophene)s $(3HT)_n$, $n = 4–36$. *J. Am. Chem. Soc.* **2013**, *135*, 13699–13709.

(47) Yiu, A. T.; Beaujuge, P. M.; Lee, O. P.; Woo, C. H.; Toney, M. F.; Fréchet, J. M. J. Side-Chain Tunability of Furan-Containing Low-Band-Gap Polymers Provides Control of Structural Order in Efficient Solar Cells. *J. Am. Chem. Soc.* **2012**, *134*, 2180–2185.

(48) Ho, V.; Boudouris, B. W.; Segalman, R. A. Tuning Polythiophene Crystallization

Through Systematic Side Chain Functionalization. *Macromolecules* **2010**, *43*, 7895–7899.

(49) Kim, J.-S.; Kim, J.-H.; Lee, W.; Yu, H.; Kim, H. J.; Song, I.; Shin, M.; Oh, J. H.; Jeong, U.; Kim, T.-S.; Kim, B. J. Tuning Mechanical and Optoelectrical Properties of Poly(3-Hexylthiophene) Through Systematic Regioregularity Control. *Macromolecules* **2015**, *48*, 4339–4346.

(50) Lipomi, D. J.; Chong, H.; Vosgueritchian, M.; Mei, J.; Bao, Z. Toward Mechanically Robust and Intrinsically Stretchable Organic Solar Cells: Evolution of Photovoltaic Properties with Tensile Strain. *Sol. Energy Mater. Sol. Cells* **2012**, *107*, 355–365.

(51) Zhao, Y.; Zhao, X.; Zang, Y.; Di, C. A.; Diao, Y.; Mei, J. Conjugation-Break Spacers in Semiconducting Polymers: Impact on Polymer Processability and Charge Transport Properties. *Macromolecules* **2015**, *48*, 2048–2053.

(52) Wu, H.-C.; Benight, S. J.; Chortos, A.; Lee, W.-Y.; Mei, J.; F To, J. W.; Lu, C.; He, M.; B-H Tok, J.; Chen, W.-C.; Bao, Z. A Rapid and Facile Soft Contact Lamination Method: Evaluation of Polymer Semiconductors for Stretchable Transistors. *Chem. Mater.* **2014**, *36*, 4544–4551.

(53) Savagatrup, S.; Zhao, X.; Chan, E.; Mei, J.; Lipomi, D. J. Effect of Broken Conjugation on the Stretchability of Semiconducting Polymers. *Macromol. Rapid Commun.* **2016**, *27*, 1623–1628.

(54) Liu, J.; Sun, Y.; Gao, X.; Xing, R.; Zheng, L.; Wu, S.; Geng, Y.; Han, Y. Oriented Poly(3-Hexylthiophene) Nanofibril with the π-π Stacking Growth Direction by Solvent Directional Evaporation. *Langmuir* **2011**, *27*, 4212–4219.

(55) Strobl, G. *The Physics of Polymers: Concepts for Understanding Their Structures and Behavior*, 1997, DOI: 10.1007/978-3-662-03488-0.

(56) Gutzow, I. S.; Schmelzer, J. W. P. *The Vitreous State: Thermodynamics, Structure, Rheology, and Crystallization*, 2nd ed.; Springer, 2013; Vol. 37.

(57) Reimschuessel, H. K. Glass-Transition Temperature of Comblike Polymers: Effects of Side-Chain Length and Backbone Chain Structure. *J. Polym. Sci., Part A: Polym. Chem.* **1979**, *17*, 2447–2457.

(58) Cowie, J. M. G.; Reid, V. M. C.; Mcewen, I. J. Effect of Side Chain Length on the Glass Transition of Copolymers from Styrene with n-Alkyl Citraconimides and with n-Alkyl Itaconimides. *Br. Polym. J.* **1990**, *23*, 353–357.

(59) Bruner, C.; Novoa, F.; Dupont, S.; Dauskardt, R. Decohesion Kinetics in Polymer Organic Solar Cells. *ACS Appl. Mater. Interfaces* **2014**, *6*, 21474–21483.

(60) *The Physics of Glassy Polymers*, 2nd ed.; Haward, R. N., Young, R. J., Eds.;

Springer Science & Business Media, 1997.

(61) Danley, R. L.; Reader, J. R.; Schaefer, J. W. Differential Scanning Calorimeter. U.S. Patent US5842788 A, 1998.

(62) Rieger, J. Glass Transition Temperature T_g of Polymers-Comparison of the Values from Differential Thermal Analysis (DTA, DSC) and Dynamic Mechanical Measurements (Torsion Pendulum). *Polym. Test.* **2001**, *20*, 199–204.

(63) Beaucage, G.; Composto, R.; Stein, R. S. Ellipsometric Study of the Glass Transition and Thermal Expansion Coefficients of Thin Polymer Films. *J. Polym. Sci., Part B: Polym. Phys.* **1993**, *31*, 319–326.

(64) Wunderlich, B. Study of the Change in Specific Heat of Monomeric and Polymeric Glasses during the Glass Transition. *J. Phys. Chem.* **1960**, *64*, 1052–1056.

(65) Campoy-Quiles, M.; Sims, M.; Etchegoin, P. G.; Bradley, D. D. C. Thickness-Dependent Thermal Transition Temperatures in Thin Conjugated Polymer Films. *Macromolecules* **2006**, *39*, 7673–7680.

(66) McCrackin, F. L.; Passaglia, E.; Stromberg, R. R.; Steinberg, H. L. Measurement of the Thickness and Refractive Index of Very Thin Films and the Optical Properties of Surfaces by Ellipsometry. *J. Res. Natl. Inst. Stand. Technol.* **1963**, *67A*, 363–377.

(67) Parks, G. S.; Huffman, H. M.; Cattoir, F. R. Studies on Glass. II. The Transition between the Glassy and Liquid States in the Case of Glucose. *J. Phys. Chem.* **1928**, *32*, 1366–1379.

(68) Holliday, S.; Donaghey, J. E.; McCulloch, I. Advances in Charge Carrier Mobilities of Semiconducting Polymers Used in Organic Transistors. *Chem. Mater.* **2013**, *26*, 647–663.

(69) Kim, D. H.; Lee, B. L.; Moon, H.; Kang, H. M.; Jeong, E. J.; Park, J. Il; Han, K. M.; Lee, S.; Yoo, B. W.; Koo, B. W.; Kim, J. Y.; Lee, W. H.; Cho, K.; Becerril, H. A.; Bao, Z. Liquid-Crystalline Semiconducting Copolymers with Intramolecular Donor-Acceptor Building Blocks for High-Stability Polymer Transistors. *J. Am. Chem. Soc.* **2009**, *131*, 6124–6132.

(70) *Principles of Thermal Analysis and Calorimetry*, 2nd ed.; Gaisford, S., Kett, V., Haines, P., Eds.; Royal Society of Chemistry, 2016.

(71) *Handbook of Ellipsometry*, 1st ed.; Tompkins, H. G., Irene, E. A., Eds.; Springer, 2005; Vol. 30.

(72) Müller, C.; Bergqvist, J.; Vandewal, K.; Tvingstedt, K.; Anselmo, A. S.; Magnusson, R.; Alonso, M. I.; Moons, E.; Arwin, H.; Campoy-Quiles, M.; Inganäs, O. Phase Behaviour of Liquid-Crystalline Polymer/Fullerene Organic Photovoltaic

Blends: Thermal Stability and Miscibility. *J. Mater. Chem.* **2011**, *21*, 10676.

(73) Jackson, N. E.; Kohlstedt, K. L.; Savoie, B. M.; Olvera de la Cruz, M.; Schatz, G. C.; Chen, L. X.; Ratner, M. A. Conformational Order in Aggregates of Conjugated Polymers. *J. Am. Chem. Soc.* **2015**, *137*, 6254–6262.

(74) Dubay, K. H.; Hall, M. L.; Hughes, T. F.; Wu, C.; Reichman, D. R.; Friesner, R. A. Accurate Force Field Development for Modeling Conjugated Polymers. *J. Chem. Theory Comput.* **2012**, *8*, 4556–4569.

(75) Marcon, V.; Raos, G. Free Energies of Molecular Crystal Surfaces by Computer Simulation: Application to Tetrathiophene. *J. Am. Chem. Soc.* **2006**, *128*, 1408–1409.

(76) Zhao, B.; Awartani, O.; O'Connor, B.; Zikry, M. A. Microstructural Behavior and Failure Mechanisms of Organic Semicrystalline Thin Film Blends. *J. Polym. Sci., Part B: Polym. Phys.* **2016**, *54*, 896–907.

(77) Jorgensen, W. L.; Maxwell, D. S.; Tirado-Rives, J. Development and Testing of the OPLS All-Atom Force Field on Conformational Energetics and Properties of Organic Liquids. *J. Am. Chem. Soc.* **1996**, *118*, 11225–11236.

(78) Do, K.; Huang, D. M.; Moule, A. J. A Comparitive MD Study of the Local Structure of Polymer Semiconductors P3HT and PBTTT. **2010**, *12*, 14735–14739.

(79) Schwarz, K. N.; Kee, T. W.; Huang, D. M. Coarse-Grained Simulations of the Solution-Phase Self-Assembly of Poly(3-Hexylthiophene) Nanostructures. *Nanoscale* **2013**, *5*, 2017–2027.

(80) Fauvell, T. J.; Zheng, T.; Jackson, N. E.; Ratner, M. A.; Yu, L.; Chen, L. X. The Photophysical and Morphological Implications of Single-Strand Conjugated Polymer Folding in Solution. *Chem. Mater.* **2016**, *28*, 2814–2822.

(81) Stewart, B.; Burrows, H. Molecular Dynamics Study of Self-Assembly of Aqueous Solutions of Poly[9,9-bis(4-Sulfonylbutoxyphenylphenyl) Fluorene-2,7-Diyl-2,2′-Bithiophene] (PBS-PF2T) in the Presence of Pentaethylene Glycol Monododecyl Ether ($C_{12}E_5$). *Materials* **2016**, *9*, 379.

(82) Newbloom, G. M.; Hoffmann, S. M.; West, A. F.; Gile, M. C.; Sista, P.; Cheung, H. K. C.; Luscombe, C. K.; Pfaendtner, J.; Pozzo, L. D. Solvatochromism and Conformational Changes in Fully Dissolved Poly(3-Alkylthiophene)s. *Langmuir* **2015**, *31*, 458–468.

(83) Tummala, N. R.; Risko, C.; Bruner, C.; Dauskardt, R. H.; Brédas, J.-L. Entanglements in P3HT and Their Influence on Thin-Film Mechanical Properties: Insights from Molecular Dynamics Simulations. *J. Polym. Sci., Part B: Polym. Phys.* **2015**, *53*, 934–942.

(84) Huang, D. M.; Faller, R.; Do, K.; Moul, A. J. Coarse-Grained Computer Simulations of Polymer/Fullerene Bulk Heterojunctions for Organic Photovoltaic Applications. *J. Chem. Theory Comput.* **2010**, *6*, 526–537.

(85) Tapping, P. C.; Clafton, S. N.; Schwarz, K. N.; Kee, T. W.; Huang, D. M. Molecular-Level Details of Morphology-Dependent Exciton Migration in Poly(3-Hexylthiophene) Nanostructures. *J. Phys. Chem. C* **2015**, *119*, 7047–7059.

(86) Agrawal, V.; Arya, G.; Oswald, J. Simultaneous Iterative Boltzmann Inversion for Coarse-Graining of Polyurea. *Macromolecules* **2014**, *47*, 3378–3389.

(87) Lee, C.-K.; Pao, C.-W.; Chu, C.-W. Multiscale Molecular Simulations of the Nanoscale Morphologies of P3HT:PCBM Blends for Bulk Heterojunction Organic Photovoltaic Cells. *Energy Environ. Sci.* **2011**, *4*, 4124–4132.

(88) Do, K.; Ravva, M. K.; Wang, T.; Brédas, J.-L. Computational Methodologies for Developing Structure–Morphology–Performance Relationships in Organic Solar Cells: A Protocol Review. *Chem. Mater.* **2016**, *29*, 346–354.

(89) Do, K.; Risko, C.; Anthony, J. E.; Amassian, A.; Brédas, J.-L. Dynamics, Miscibility, and Morphology in Polymer-Molecule Blends: The Impact of Chemical Functionality. *Chem. Mater.* **2015**, *27*, 7643–7651.

(90) Carrillo, J.-M. Y.; Seibers, Z.; Kumar, R.; Matheson, M. A.; Ankner, J. F.; Goswami, M.; Bhaskaran-Nair, K.; Shelton, W. A.; Sumpter, B. G.; Kilbey, S. M. Petascale Simulations of the Morphology and the Molecular Interface of Bulk Heterojunctions. *ACS Nano* **2016**, *10*, 7008–7022.

(91) Alessandri, R.; Uusitalo, J. J.; de Vries, A. H.; Havenith, R. W. A.; Marrink, S. J. Bulk Heterojunction Morphologies with Atomistic Resolution from Coarse-Grain Solvent Evaporation Simulations. *J. Am. Chem. Soc.* **2017**, *130*, 3697–3705.

(92) Karayiannis, N. C.; Kröger, M. Combined Molecular Algorithms for the Generation, Equilibration and Topological Analysis of Entangled Polymers: Methodology and Performance. *Int. J. Mol. Sci.* **2009**, *10*, 5054–5089.

(93) Hoy, R. S.; Foteinopoulou, K.; Kröger, M. Topological Analysis of Polymeric Melts: Chain-Length Effects and Fast-Converging Estimators for Entanglement Length. *Phys. Rev. E* **2009**, *80*, 031803.

(94) Everaers, R. Rheology and Microscopic Topology of Entangled Polymeric Liquids. *Science.* **2004**, *303*, 823–826.

(95) Zhao, B.; Zikry, M. A. The Effects of Structural Disorders and Microstructural Mechanisms on Semi-Crystalline P3HT Behavior. *Polymer.* **2015**, *57*, 1–11.

(96) Dennler, G.; Scharber, M. C.; Brabec, C. J. Polymer-Fullerene Bulk-Heterojunction

Solar Cells. *Adv. Mater.* **2009**, *21*, 1323–1338.

(97) Mayer, A. C.; Toney, M. F.; Scully, S. R.; Rivnay, J.; Brabec, C. J.; Scharber, M.; Koppe, M.; Heeney, M.; McCulloch, I.; McGehee, M. D. Bimolecular Crystals of Fullerenes in Conjugated Polymers and the Implications of Molecular Mixing for Solar Cells. *Adv. Funct. Mater.* **2009**, *19*, 1173–1179.

(98) Koppe, M.; Scharber, M.; Brabec, C.; Duffy, W.; Heeney, M.; McCulloch, I. Polyterthiophenes as Donors for Polymer Solar Cells. *Adv. Funct. Mater.* **2007**, *17*, 1371–1376.

(99) Campoy-Quiles, M.; Kanai, Y.; El-Basaty, A.; Sakai, H.; Murata, H. Ternary Mixing: A Simple Method to Tailor the Morphology of Organic Solar Cells. *Org. Electron.* **2009**, *10*, 1120–1132.

(100) Miller, N. C.; Cho, E.; Gysel, R.; Risko, C.; Coropceanu, V.; Miller, C. E.; Sweetnam, S.; Sellinger, A.; Heeney, M.; McCulloch, I.; Brédas, J. L.; Toney, M. F.; McGehee, M. D. Factors Governing Intercalation of Fullerenes and Other Small Molecules between the Side Chains of Semiconducting Polymers Used in Solar Cells. *Adv. Energy Mater.* **2012**, *2*, 1208–1217.

(101) Printz, A. D.; Savagatrup, S.; Rodriquez, D.; Lipomi, D. J. Role of Molecular Mixing on the Stiffness of Polymer:Fullerene Bulk Heterojunction Films. *Sol. Energy Mater. Sol. Cells* **2015**, *134*, 64–72.

(102) Anctil, A.; Babbitt, C. W.; Raffaelle, R. P.; Landi, B. J. Cumulative Energy Demand for Small Molecule and Polymer Photovoltaics. *Prog. Photovoltaics Res. Appl.* **2012**, *21*, 1541–1554.

(103) Savagatrup, S.; Rodriquez, D.; Printz, A. D.; Sieval, A. B.; Hummelen, J. C.; Lipomi, D. J. PCBM and Incompletely Separated Grades of Methanofullerenes Produce Bulk Heterojunctions with Increased Robustness for Ultra-Flexible and Stretchable Electronics. *Chem. Mater.* **2015**, *27*, 3902–3911.

(104) Dupont, S. R.; Oliver, M.; Krebs, F. C.; Dauskardt, R. H. Interlayer Adhesion in Roll-to-Roll Processed Flexible Inverted Polymer Solar Cells. *Sol. Energy Mater. Sol. Cells* **2012**, *97*, 171–175.

Chapter 2

Measuring the Glass Transition Temperature of Conjugated Polymer Films with Ultraviolet-Visible Spectroscopy

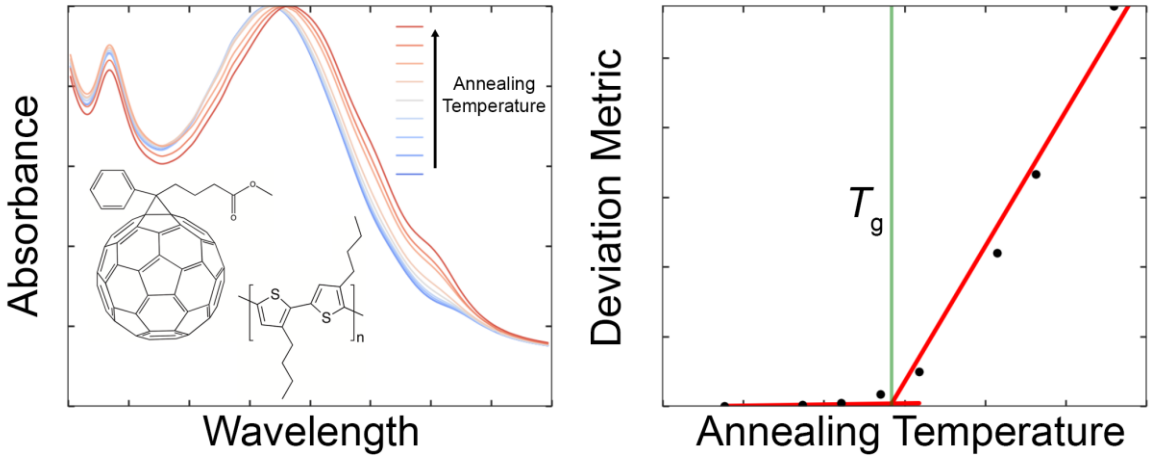

Image 2. Table of contents artwork for Chapter 2. Illustration of measurement technique.

Samuel E. Root,‡ Mohammad A. Alkhadra,‡ Daniel Rodriquez, Adam D. Printz, and Darren J. Lipomi*

(‡ Equal contribution)

Department of NanoEngineering, University of California, San Diego

9500 Gilman Drive, Mail Code 0448, La Jolla, CA 92093-0448

Abstract

The glass transition temperature (T_g) of a conjugated polymer can be used to predict its morphological stability and mechanical properties. Despite the importance of this parameter in applications from organic solar cells to wearable electronics, it is not easy to measure. The T_g is often too weak to detect using conventional differential scanning calorimetry (DSC). Alternative methods—e.g., variable temperature ellipsometry—require specialized equipment. This paper describes a technique for measuring the T_g of thin films of semicrystalline conjugated polymers using only a hot plate and an ultraviolet-visible (UV-vis) spectrometer. UV-vis spectroscopy is used to measure changes in the absorption spectrum due to molecular-scale rearrangement of polymers when heated past T_g, corresponding to the onset of the formation of photophysical aggregates. A deviation metric, defined as the sum of the squared deviation in absorbance between as-cast and annealed films, is used to quantify shifts in the absorption spectra. The glass transition is observed as a change in slope in a plot of the deviation metric versus temperature. To demonstrate the usefulness of this technique, a variety of semiconducting polymers are tested: P3BT, PBTTT-C14, F8BT, PDTSTPD, PTB7, PCDTBT, TQ1, and MEH-PPV. These polymers represent a range of solid-state morphologies, from highly ordered to predominantly amorphous. A successful measurement of T_g depends on the ability of the polymer to form photophysical aggregates. The results obtained using this method for P3BT, PBTTT-C14, F8BT, and PDTSTPD are in agreement with values of T_g that have been reported in the literature. Molecular dynamics simulations are used to show how the morphology evolves upon annealing: above the T_g, an initially kinetically trapped morphology undergoes structural

rearrangement to assume a more thermodynamically preferred structure. The temperature at which onset of this rearrangement occurs in the simulation is concomitant with the spectroscopically determined value of T_g.

2.1 Introduction

The glass transition temperature (T_g) is a critical property of polymers that can be used to predict the thermal[1] and mechanical stabilities[2] of organic semiconductor devices.[3] The glass transition describes the onset of relaxation processes in segments of the main chains of polymeric materials.[4–6] This parameter is of particular importance for the operational stability of organic electronic devices (which include π-conjugated polymers and small molecules) for at least two reasons.[1] First, devices operating above T_g may undergo deleterious morphological rearrangement. Changes in the morphology are deleterious particularly if a kinetically trapped structure formed upon solidification of a film is conducive to device performance, while a thermodynamically favorable structure that forms upon heating is not. For example, the domains in a highly phase-separated morphology of a bulk heterojunction (BHJ) organic solar cell that forms upon heating above T_g may be too large to allow efficient separation of charges.[1] Second, the T_g is intimately related to stress-relaxation processes of polymeric materials. For soft, compliant polymers intended for biological integration, it may be desirable to have a low T_g, and thus rubber-like mechanical behavior.[7,8] Although a variety of well-developed methods exist for measuring the T_g of bulk polymeric materials,[9] thin films present a significant challenge for these conventional methods. The challenge arises in part because of the small thermal signal produced by the minute mass of a thin film. Moreover, the

thermal properties of the bulk material do not necessarily represent those of a thin film.[10] This paper describes a facile technique to measure the T_gs of conjugated polymers that leverages their unique photophysical behavior. The technique works by finding the annealing temperature at which the thin-film absorption spectrum in the UV-vis range undergoes an abrupt change, indicating the onset of formation of photophysical aggregates.[11]

Thin films of conjugated polymers are generally prepared by casting from a solution using laboratory-scale techniques (e.g., spin coating) or industrial-scale techniques (e.g., slot-die coating, gravure, inkjet, or screen printing). Rapid solidification of the polymer that occurs upon evaporation of the solvent typically results in the formation of kinetically trapped structures that contain considerable free volume[12] and structural disorder.[13] Thermal annealing is a common post-processing step that allows kinetically trapped structures to undergo morphological rearrangement and aggregation.[14] These structural changes have important effects on device-scale optoelectronic[15] and mechanical properties.[2]

In a recent review on the glass transition of organic semiconductors,[1] four standard techniques to measure T_g were outlined: differential scanning calorimetry (DSC),[16] dynamic mechanical analysis (DMA),[17] broadband dielectric spectroscopy (BDS),[18] and variable-temperature ellipsometry (VTE).[19] These techniques are ubiquitous in the field of polymer science and have been widely applied to characterize the thermal properties of semiconducting polymers, for which the most common is DSC.[16] In many cases, DSC does not possess the sensitivity to detect the subtle glass transitions of polymeric semiconductors; it is commonplace for T_g to evade detection, even in cases

where DSC thermograms are reported.[15,20–26] Moreover, conventional DSC setups require bulk samples and thus cannot be used to characterize thin films (DMA and BDS are also typically restricted to bulk materials).[1] Advanced techniques such as differential AC-chip calorimetry have been developed to mitigate some of these limitations,[27] however, they are usually unavailable in laboratories that focus on organic electronics.

The thermal behavior of a polymeric thin film becomes thickness-dependent below a critical threshold (~100 nm).[28] This phenomenon has been attributed to interfacial effects at the free surface and with the supporting substrate.[19,28] The dominant effect is the increased mobility of polymer chains at the free surface, which serves to decrease the T_g.[19] VTE is unique among the available thermal characterization techniques in that it can probe thermal transitions of thin films, as opposed to bulk samples.[19] Unfortunately, ellipsometric systems, especially those with temperature-controlled stages, are expensive and not widely available. Therefore, use of this technique is mainly restricted to research groups that have specialized expertise.

Thin films of conjugated polymers absorb strongly in the UV-vis range, and various optical techniques have been developed to characterize their thermomechanical properties.[20,29,30] Lindqvist et al. have developed a simple technique to measure thermal transitions in fullerene-based BHJ films by taking advantage of the increased scattering of micrometer-sized fullerene crystals that form when the film is annealed above the T_g.[20] As such, this technique is not applicable to neat conjugated polymer films.

In this work, we measured the T_g by taking advantage of the shift in the UV-vis absorption spectrum that occurs after thermally annealing many neat conjugated polymer films.[11,31] This shift has been widely attributed to the formation of ordered aggregates and

is generally accompanied by an improvement in the charge transport properties of the thin film.[11] The amorphous phase of conjugated polymer thin films undergoes significant structural rearrangement only when the annealing temperature approaches T_g. We thus hypothesized that it would be possible to estimate the T_g of conjugated polymer thin films by quantifying the change in the absorption spectrum that resulted from thermal annealing. We expected that, once the annealing temperature surpassed the T_g, there would be an easily discernible change in the absorption spectrum. Hence, we defined a deviation metric (DM_T) as the sum of the squared deviation in the absorbance between as-cast and annealed films (at annealing temperature, T):

$$DM_T \equiv \sum_{\lambda_{min}}^{\lambda_{max}} [I_{RT}(\lambda) - I_T(\lambda)]^2 \quad (1)$$

where $I_{RT}(\lambda)$ and $I_T(\lambda)$ are the normalized absorption intensities of the as-cast (room temperature) and annealed films, respectively, λ is the wavelength, and λ_{min} and λ_{max} are the lower and upper bounds of the optical sweep, respectively. We expected that, at the T_g, there would be a sharp increase in the slope of DM_T when plotted against annealing temperature.

2.2 Experimental Design

2.2.1 Selection of Materials

To test the validity of our proposed methodology, we selected materials whose T_gs had been measured successfully using other techniques. Moreover, it was important to use materials of significant interest to the research community. Since the T_g of the popular regioregular poly(3-hexylthiophene) (P3HT) is near or somewhat below room temperature, we selected poly(3-butylthiophene) (P3BT) instead (structure shown in

Figure 2.1). An additional advantage of using P3BT was that we were able to apply the weakly interacting H-aggregate model developed by Spano and coworkers to provide a detailed analysis of vibronic progression as a function of annealing temperature.[32,33] This analysis allowed us to deconvolute spectral shifts and determine microstructural mechanisms responsible for the abrupt shift in the absorption spectrum near the T_g. Additionally, to demonstrate the applicability of our technique to composite systems of organic semiconductors, we tested a BHJ film comprising P3BT and [6,6]-phenyl C_{61} butyric acid methyl ester (PCBM).

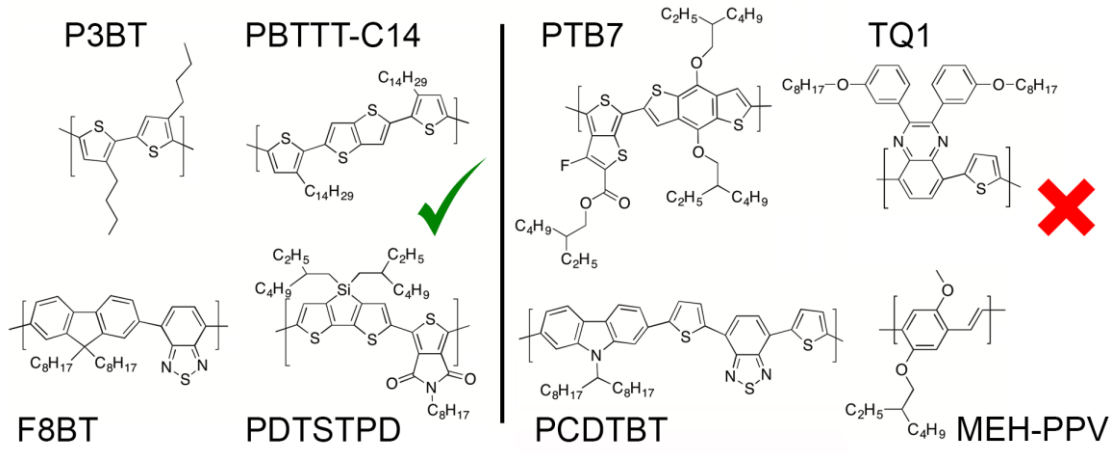

Figure 2.1. Chemical structures and common names of conjugated polymers involved in this study. Refer to **Experimental Methods** for systematic names. The technique works best for semicrystalline polymers.

To assess the transferability of our proposed methodology, we performed the experiment on several conjugated polymers with complex structures. The following materials were tested: F8BT, PBTTT-C14, PDTSTPD, PTB7, PCDTBT, TQ1, and MEH-PPV. These materials were chosen because they exhibit a wide range of ordering in the solid state, from highly ordered (e.g., the liquid-crystalline PBTTT-C14) to minimal long-range order (e.g., TQ1). In particular, PDTSTPD was chosen because its T_g has been

reported,[34,35] and we have previously performed molecular dynamics (MD) simulations to predict its thermal and mechanical properties.[36] To gain a detailed mechanistic understanding of our results, we performed additional MD simulations to demonstrate how the thermal annealing of a kinetically trapped structure results in morphological rearrangement. We expected that materials with stronger tendencies to crystallize would produce shifts in the absorption spectra that were more pronounced, corresponding to a more easily observable T_g. Accordingly, we did not expect this technique to work for predominantly amorphous materials (refer to **Section A.1** of the **Appendix A**). These amorphous materials are generally blended with fullerenes to form BHJs and do not perform especially well in transistor devices. Thus, the properties of the neat polymers are not as relevant as those of the BHJ, and the optical technique of Lindqvist et al. (which relies on the presence of the fullerene) can be applied instead.[20]

2.2.2 Design of Annealing Protocol

The experimental protocol was specifically designed so that it would only require basic equipment readily available to any research group interested in conjugated polymers: a spin coater, a hot plate, a glovebox, and a UV-vis spectrometer. All thermal annealing was carried out inside a glovebox (N_2 atmosphere) to eliminate possible effects of photochemical degradation at elevated temperatures that could occur under ambient conditions. For example, Cho et al. observed a significant degradation in the π–π^* absorption band of PCDTBT when annealed above the T_g in air.[37] Thermal annealing was carried out using a standard hot plate, and heat transfer calculations were performed to account for thermal insulation by the glass slide substrate, as described in detail in **Section A.2** of the **Appendix A**. The UV-vis characterization was performed *ex situ*

because a UV-vis spectrometer with a controlled atmosphere and temperature-controlled stage is not a common piece of equipment. This is not to say that *in situ* measurements are not viable, as Pingel et al. studied the thermal dependence of UV-vis absorption *in situ* for deuterated P3HT.[33] However, no evidence of the glass transition was observed in those experiments because the T_g of P3HT is below room temperature. For our experiments, each film was subjected to a thermal cycling protocol, like the one shown in **Figure 2.2a**. UV-vis spectra of the cooled films under ambient conditions were taken between annealing steps. To analyze the data and extract the T_g, we developed a code to automate and standardize the bilinear regression analysis based on a custom R^2 maximization algorithm (we released this algorithm in an open-sourced format; refer to **Section A.3** of the **Appendix A**).

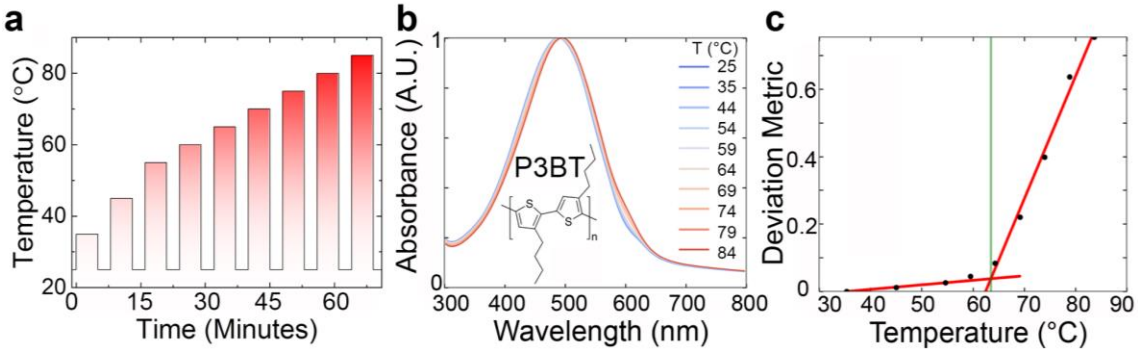

Figure 2.2. Overview of UV-vis absorption T_g measurement technique for P3BT. (a) Thermal history of polymer thin film. Absorption measurements were taken at ambient temperature for the as-cast film and between successive annealing steps. (b) Thin-film absorption spectra for the annealing temperatures indicated. (c) Evolution of the deviation metric as a function of annealing temperature, showing a distinct increase at the T_g of P3BT.

2.3. Results and Discussion

2.3.1 Proof-of-Concept: P3BT

The results of our proposed technique—as applied to P3BT—are shown in **Figure 2.2**. The thermal cycling protocol is given in **Figure 2.2a**. After each annealing step, a UV-vis spectrum was recorded (**Figure 2.2b**). We observed that the spectra exhibited a clear redshift as well as a distinct change in shape around 600 nm with increased annealing temperature. These shifts in the absorption spectra result from the formation of weakly interacting H-aggregates, as explained in the next section. Spectra were processed using the deviation metric, and this quantity was plotted against annealing temperature (**Figure 2.2c**); a clear transition was observed. Using our bilinear curve-fitting algorithm, the T_g was estimated to be 60 ± 3 °C. Encouragingly, this measurement was in excellent quantitative agreement with reported values in the literature, which range from 59 to 67 °C.[38,39]

2.3.2 Weakly Interacting H-Aggregate Analysis

To identify the microstructural changes responsible for the evolution of the absorption spectra upon annealing, we applied the weakly interacting H-aggregate model, developed by Spano and coworkers.[32,40] When two segments of planar thiophene backbones come into co-facial contact, an excitonic coupling produces a redshift in the absorption. This spectral signature is known as an H-aggregate,[41] and the absorption spectra of poly(3-alkylthiophenes) can be comprehensively analyzed using this model.[32] To perform this analysis, a Frank-Condon progression was fit to the UV-vis spectra (assuming a Gaussian line shape), and the absorption of the aggregated regions was deconvoluted from that of the amorphous phase. A representative fit obtained from this

process is shown in **Figure 2.3a**. After correcting for the unequal absorption coefficients of the two domains, the fraction of aggregated polymeric chromophores was determined.

As shown in **Figure 2.3b**, we found that the aggregate fraction increased with annealing temperature and exhibited a transition near the T_g. Interestingly, not only did we observe a change in the slope, but also an increase in the error (based on the standard deviation between independently tested films). It is possible that the increase in the statistical uncertainty is due to minor differences in the cooling rates of separately annealed films. The H-aggregate model can also be used to characterize the quality of structural ordering present in aggregate regions.

The free exciton bandwidth (W) is the dispersion of energy that arises due to interchain coupling in the aggregate domains. This parameter is inversely related to the conjugation length of the interacting chromophoric species.[32,42] As shown in **Figure 2.3c**, the inverse exciton bandwidth ($1/W$) exhibits exhibits a sharp transition when the film is annealed above the T_g. This observation is in agreement with previous results of Yazawa et al., who used temperature-dependent Fourier-transform infrared absorption measurements to correlate the glass transition in P3BT with the thermal activation of the dihedral twist between two thiophene rings.[39] We also found that the $1/W$ exhibited a sharper transition than did the aggregate fraction.

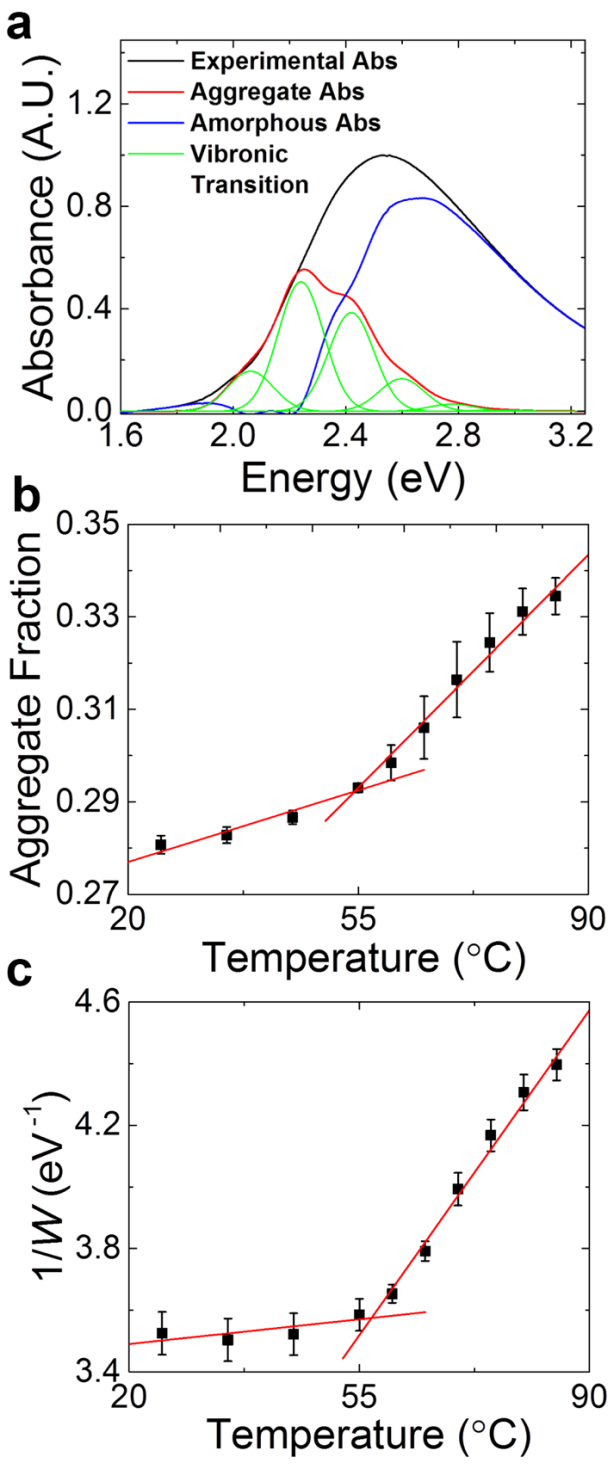

Figure 2.3. Weakly interacting H-aggregate analysis of P3BT. (a) Representative deconstructed absorption spectrum used to calculate (b) the aggregate fraction and (c) the inverse exciton bandwidth, 1/*W*.

2.3.3 Bulk Heterojunction Film

Conjugated polymers are typically blended with solubilized fullerene derivatives to form the active layer of BHJ organic photovoltaic devices. The thermal behavior of such composites is important for both optimization of device processing and operational stability.[1] Fullerenes are known to slow the dynamics of conjugated polymers.[43] Due to the strong dispersive forces and spherical geometries, fullerenes act as anti-plasticizers and increase the T_g of the composite.[2,44] To demonstrate the applicability of our approach for such composites, we have characterized a BHJ layer composed of P3BT and PCBM. The results of our technique are shown in **Figure 2.4**. As expected, we found that the addition of PCBM served to increase the T_g by about 15 °C. Moreover, we found that the addition of 1,8-diiodooctane, a common processing additive, resulted in a significant decrease in the T_g of the BHJ film (**Section A.4** of the **Appendix A**).

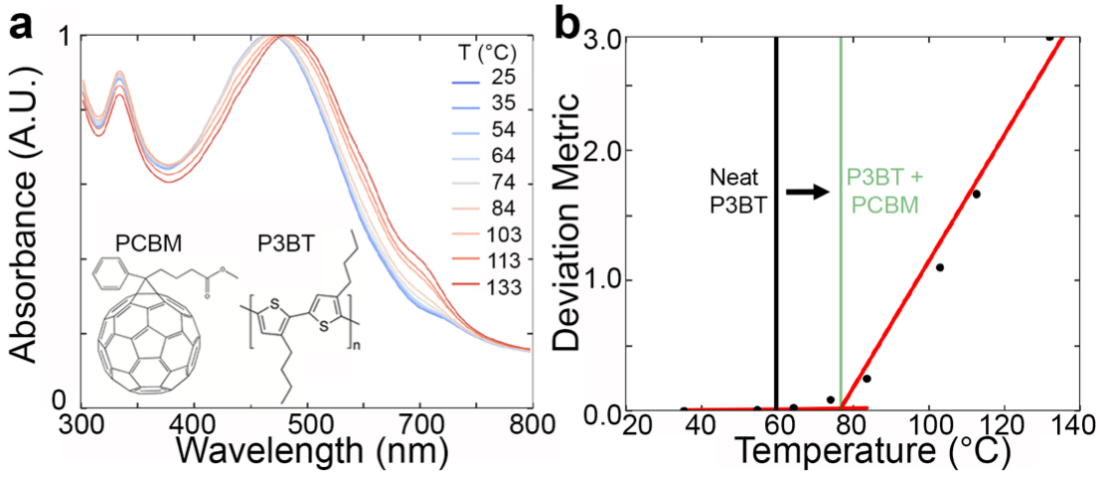

Figure 2.4. Thermal characterization of a BHJ film P3BT:PCBM (0.8:1 by mass). (a) UV-vis absorption spectra for different annealing temperatures. (b) Deviation metric showing a distinct transition at 75 °C. The addition of PCBM resulted in a ≈15 °C shift in the T_g.

2.3.4 PBTTT-C14

The PBTTT family of polymers are known to exhibit a highly-ordered, liquid-crystalline mesophase. As shown in **Figure 2.5a**, our technique revealed a distinct transition occurring at 102 ± 1 °C for PBTTT-C14. Previous DSC measurements have revealed two discrete exotherms upon cooling. These two transitions occur at ≈100 °C and ≈230 °C and have been rigorously assigned to the crystallization of the side chains and the backbone, respectively.[45–47] However, the DSC thermograms reported for PBTTT-C14 revealed no indication of a glass transition. We have rationalized this finding through the argument that the weak signal of the glass transition could be obscured by the endothermic melting of the side chains, as both occur in the same temperature range. This argument is further substantiated by the temperature-dependent UV-vis spectroscopic ellipsometry measurements of DeLongchamp et al., which revealed that the thermochromic behavior of PBTTT-C14 remains approximately constant until heated to ≈120 °C.[46] These results suggest that segmental relaxation of the conjugated backbone can be intrinsically coupled to the dynamics of the side chains, which could lead to convoluted signals in DSC thermograms.

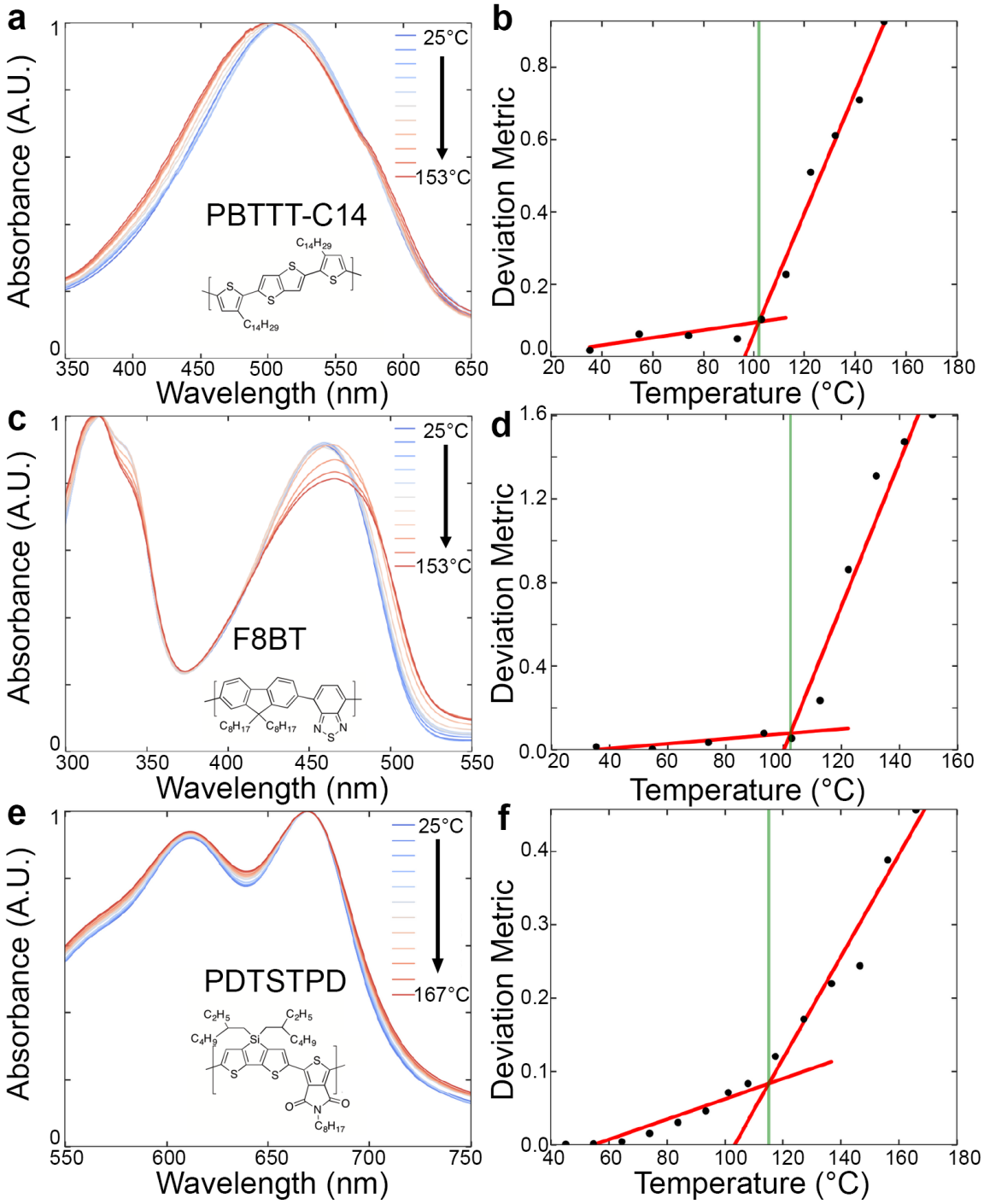

Figure 2.5. Application of technique to representative semiconducting polymers. UV-vis absorption spectra and corresponding deviation metric showing the measurement of the T_g for (a) PBTTT-C14, (b) F8BT, and (c) PDTSTPD.

2.3.5 F8BT

The polyfluorene copolymer, F8BT, has been of particular interest for photovoltaic applications due to its ability to act as the electron acceptor in BHJ devices.[48] As shown in **Figure 2.5b**, our technique revealed a pronounced transition at 104 ± 6 °C. F8BT has been previously characterized with both DSC and VTE. DSC measurements revealed an exothermic feature at 125 °C, which Sirringhaus and coworkers assigned to the glass transition; an additional, more pronounced exothermic transition at 240 °C has been assigned to the crystallization temperature.[49] The authors argued that cold crystallization might also be occurring at the T_g as the chains become mobile. Additionally, VTE experiments revealed a sharp transition in the ellipsometric angle at ≈100 °C.[50] The slight negative deviation in our measurement from the DSC measurements was likely due to thin-film effects, since our measurement agreed with the transition in the ellipsometric angle obtained with thin films using VTE.

2.3.6 PDTSTPD

The donor-acceptor polymer PDTSTPD is a commercially available conjugated polymer that exhibits a high photovoltaic conversion efficiency when blended with fullerenes and incorporated into a BHJ device.[34,35,51] The T_g has been reported to be 109 °C based on DSC measurements.[34] In close agreement with these results, we have measured the T_g to be 106 ± 12 °C (**Figure 2.5c**). We note that the transition was not quite as pronounced as it was for the other polymers tested, leading to substantially more uncertainty in the measured value. We ascribed this finding to two factors: a small overall change in the absorption spectrum with annealing, and the occurrence of morphological rearrangement during sub-T_g annealing of this material.[52] When the best fits are not

entirely obvious, the fitting algorithm described in **Section A.3** of the **Appendix A** is especially important for the accurate determination of the T_g.

Molecular dynamics simulations have previously predicted a value of 107 ± 10 °C for the T_g of PDTSTPD.[53] This prediction was achieved by subjecting an initially melted polymeric simulation to a thermal quenching protocol at constant pressure. The density was monitored as a function of temperature, and the glass transition was taken as the intersection of linear fits to the melted and glassy regions. The thermal history in our proposed measurement technique is fundamentally different: an initially kinetically trapped morphology is gradually heated until polymeric motion becomes activated and chain segments can relax to a state closer to thermodynamic equilibrium. To obtain an improved understanding of this process, we performed additional simulations that provide a closer representation of the experimental protocol.

First, we generated a simulated morphology to represent an as-cast film that was kinetically trapped at room temperature. The procedure for simulating solution casting was guided by solution-phase UV-vis absorption measurements and previous work.[54] As shown in **Figure 2.6a**, the UV-vis absorption spectra of a dilute solution (0.015 mg mL^{-1}, chloroform) and an as-cast thin film of PDTSTPD both contain aggregate absorption peaks. Fauvell et al. recently demonstrated that this low-energy visible absorption is due to self-aggregation-induced ordering (rather than in-chain charge transfer, as previously thought).[54] Thus, to generate the as-cast morphology, self-aggregated chains were randomly packed at low concentration and allowed to condense at room temperature and atmospheric pressure until the density stabilized (**Figure 2.6b**). A detailed description of this process and the results of such simulations can be found in an earlier publication.[36] It

has been previously demonstrated that simulation morphologies generated in this manner give a closer match to the experimentally determined tensile modulus of an as-cast film.

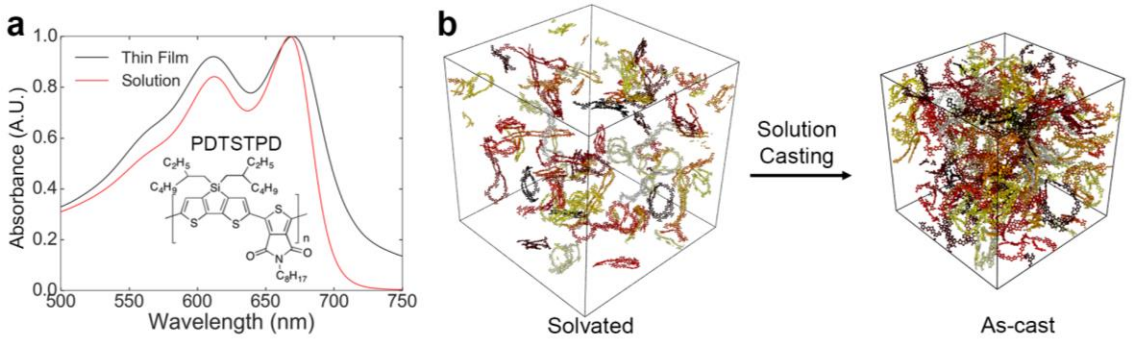

Figure 2.6. Simulated solution casting: experimental justification and MD snapshots. (a) Comparison between thin-film and solution-phase absorption spectra showing aggregate behavior in a dilute solution. (b) Snapshots showing the trajectory of the simulated solution casting; individual molecules are colored separately, and side chains are not shown.

The morphology generated by solution casting was far from thermodynamic equilibrium and contained significant void space and disorder, as shown in **Figure 2.7** (**1**). The system was subjected to a heating protocol in which temperature was gradually increased while density was monitored. We observed that the density decreased slightly until approximately 110 °C (**2**). We attributed this initial thermal expansion to increased vibrations of the amorphous glass about metastable equilibrium positions. Above 110 °C there was a clear transition; the density started to increase with temperature. This behavior was evidently the result of chain segments escaping from metastable packing conformations and approaching an equilibrium state with better intermolecular packing. The density continued to increase with temperature until about 250 °C (**3**) where it peaked, and the thermal expansion due to molecular vibrations dominated. Finally, at approximately 330 °C (**4**), an equilibrium melt was achieved, corresponding to the melting temperature measured using DSC for a structural analog of the simulated

polymer containing a branched side chain on the thienopyrrolodione (TPD) moiety.[51] When the melted system was subsequently quenched to room temperature (**5**), the density increased to a value substantially greater than that of the initial morphology.

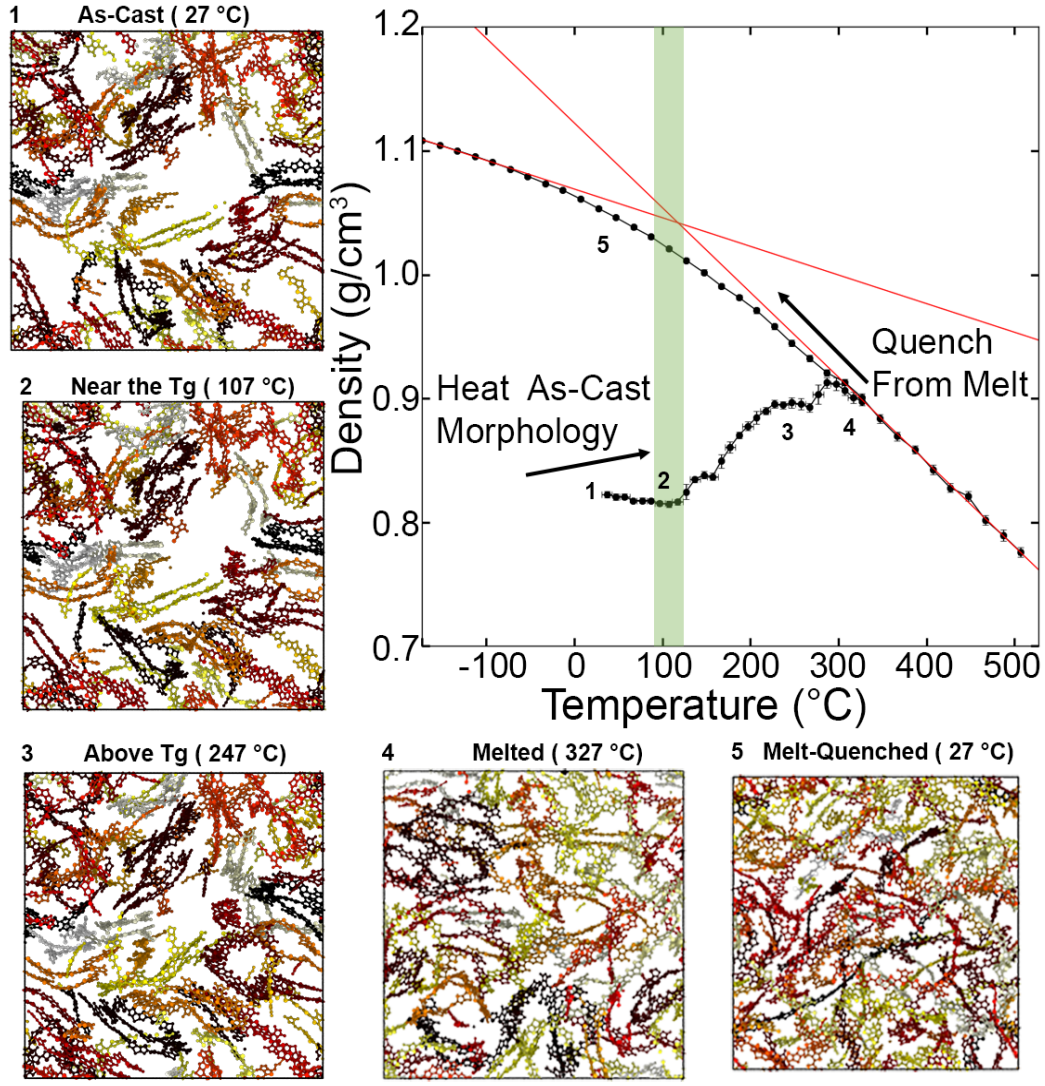

Figure 2.7. MD simulations showing the thermally activated molecular and microstructural rearrangement of an as-cast morphology of PDTSTPD subjected to thermal annealing. Plot of density against temperature showing that the onset of structural rearrangement occurred at approximately 107 °C. Images depicting 2 nm slices of simulation morphologies; individual molecules are colored separately, and side chains are not shown.

2.4 Conclusion

The glass transition temperature is of paramount importance in determining the mechanical properties and thermal reliability of organic electronic devices. However, this property is not easy to measure using conventional techniques and often goes unreported. Facile techniques with broad applicability and which use simple equipment are necessary. This paper described a new method to determine the glass transition temperature of thin films of semicrystalline conjugated polymers. The technique uses quantitative analysis of the UV-vis absorption spectra of polymer films subjected to thermal annealing, and requires only commonplace equipment. We tested the robustness of the technique through comparison with the literature for various well-characterized conjugated polymers and a BHJ composite (**Figure 2.8**). It is important to note that this technique works best for materials with a strong tendency to form ordered photophysical aggregates upon thermal annealing. For P3BT, an H-aggregate analysis of the absorption spectra revealed that the observed transition was dominated by an increase in the average conjugation length due to thermal relaxation of kinetically trapped dihedral states. MD simulations demonstrated in atomistic detail how a kinetically trapped morphology might rearrange due to the annealing of a solution-cast thin film. This technique should be of interest to organic materials chemists aiming to characterize the thermal properties of newly synthesized polymeric semiconductors and identify structure-property relationships required for molecular design.

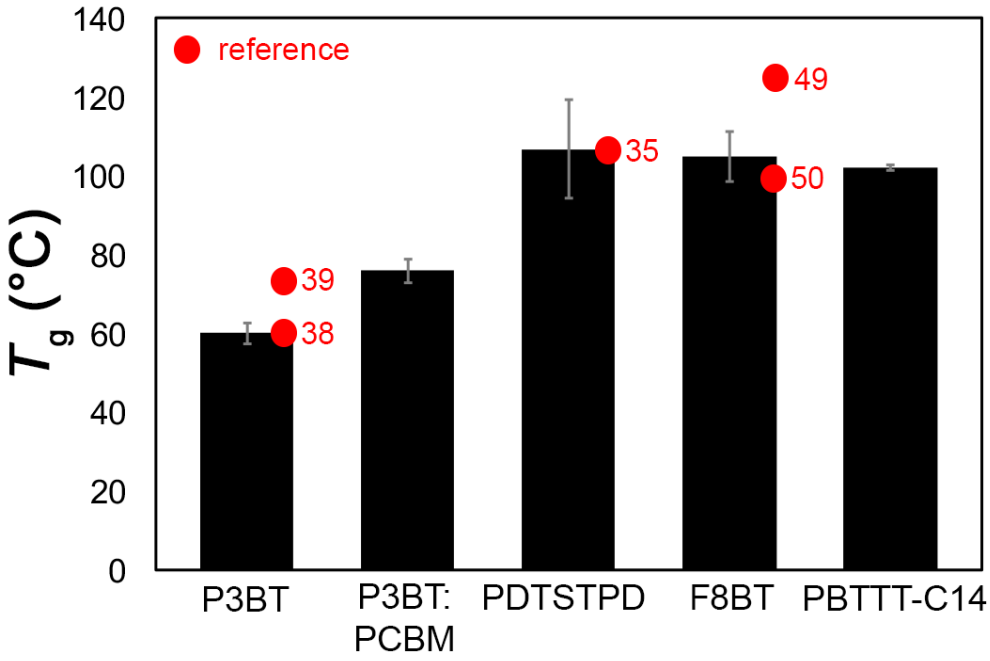

Figure 2.8. Summary of T_g measurements along with comparisons to the results of conventional techniques from the literature. Error bars are based on standard deviations between at least three separate films.

2.5 Experimental Methods

2.5.1 Materials

Poly(3-butylthiophene) (P3BT, M_n = 50−70 kDa, PDI = 2.1−3.0) was purchased from Rieke metals and was used as received. Poly[2,5-bis(3-tetradecylthiophen-2-yl)thieno[3,2-b]thiophene] (PBTTT-C14, M_n > 12 kDa, PDI = 1.8), poly(9,9-dioctylfluorene-*alt*-benzothiadiazole) (F8BT, M_n = 20−100 kDa), and poly[*N*-9′-heptadecanyl-2,7-carbazole-*alt*-5,5-(4′,7′-di-2-thienyl-2′,1′,3′-benzothiadiazole)] (PCDTBT, M_n = 20−100 kDa) were purchased from Lumtec and were used as received. Poly[(5,6-dihydro-5-octyl-4,6-dioxo-4*H*-thieno[3,4-*c*]pyrrole-1,3-diyl)[4,4-bis(2-ethylhexyl)-4*H*-silolo[3,2-*b*:4,5-*b*′;]dithiophene-2,6-diyl]] (PDTSTPD, M_n = 7−35 kDa, PDI = 1.4−2.9), poly({4,8-bis[(2-ethylhexyl)oxy]benzo[1,2-*b*:4,5-b′]dithiophene-2,6-

diyl}{3-fluoro-2-[(2-ethylhexyl)carbonyl]thieno[3,4-*b*]thiophenediyl}) (PTB7, M_n = 80−200 kDa, PDI < 3.0), poly[[2,3-bis(3-octyloxyphenyl)-5,8-quinoxalinediyl]-2,5-thiophenediyl] (TQ1, M_n = 12−45 kDa, PDI < 3.3), poly[2-methoxy-5-(2-ethylhexyloxy)-1,4-phenylenevinylene] (MEH-PPV, M_n = 40−70 kDa, PDI ≈ 6), [6,6]-phenyl C_{61} butyric acid methyl ester (PCBM), and 1,8-diiodooctane (DIO) were purchased from Sigma-Aldrich and were used as received. Chloroform, acetone, and isopropyl alcohol (IPA) were obtained from Sigma-Aldrich and were used as received. Alconox was obtained from Alconox, Inc. and was used as received.

2.5.2 Preparation of Substrates

Glass slides, cut into squares (1 in × 1 in) with a diamond-tipped scribe, were used as substrates for the polymer thin films. The slides were thoroughly cleaned in an ultrasonic bath in the following sequence of 10-min steps: powdered Alconox detergent dissolved in deionized (DI) water, DI water only, acetone, and then IPA. After that, the slides were dried with compressed (house) air and then treated with plasma (30 W) for five minutes at a base pressure of 200 mTorr of air to remove residual organic debris and improve surface wettability.

2.5.3 Preparation of Films

Solutions of P3BT, P3BT:PCBM (0.8:1 by mass), PBTTT-C14, PDTSTPD, and F8BT in chloroform (10 mg mL^{-1}) were prepared and allowed to stir overnight. Prior to use, all solutions were slightly heated (~15 s) with a heat gun to promote dissolution of the polymer. Next, the solutions were filtered with 0.20 μm PTFE filters, immediately after which they were spin-coated (Headway Research PWM32) onto the cleaned glass substrates at 2000 rpm (ramping at 1000 rpm s^{-1}) for 120 seconds. These conditions

produced films of thicknesses ranging from 80 to 100 nm as determined by profilometry (Dektak 150 Surface Profiler). All films were dried under dynamic vacuum in the antechamber of a nitrogen-atmosphere glovebox (MBRAUN) for exactly 60 min to remove any residual chloroform.

2.5.4 Spectroscopic Characterization and Analysis

Once the freshly prepared thin films had dried under dynamic vacuum for an hour, their as-cast (UV-vis) spectra were acquired using an Agilent 8453 UV-vis spectrometer; the range of wavelengths measured was from 300 to 750 nm with a sampling increment of 1 nm (a pristine glass slide was used as a baseline for the absorption). The glass-supported films were then immediately heated for 5 minutes on the surface of a hot plate in a nitrogen-atmosphere glovebox, after which they were suspended in air and allowed to cool to room temperature (T_R, ~25 °C) for 3 min prior to acquiring their 'annealed' spectra. Starting at T_R, each film was annealed in various increments of temperature (5 °C, 10 °C, or 20 °C) depending on how far its nominal T_g was from T_R. The measurements were concluded once the annealing temperature sufficiently surpassed the nominal T_g of the polymer under investigation. To correlate trends in aggregation and aggregate quality with annealing temperature, we have used the following model for H-aggregate absorption:

$$A \propto \sum_{m=0} \left(\frac{S^m}{m!}\right)\left(1 - \frac{We^{-S}}{2E_p}\sum_{n\neq \mathrm{m}} \frac{S^n}{n!\,(n-m)}\right)^2 \times \exp\left(\frac{\left(E - E_0 - mE_p - \frac{1}{2}WS^m e^{-S}\right)^2}{2\sigma^2}\right) \quad (2)$$

where A is the absorption by an aggregate as a function of the photon energy E, W is the free exciton bandwidth, E_0 is the energy of the $0 \rightarrow 0$ vibronic transition, S is the Huang-Rhys factor (set to 1 for P3ATs), and E_p is the intermolecular vibration energy, which (in the case where $S = 1$) is the difference in energy between the vibrational levels in the excited state (set to 0.179 eV as determined by Raman spectroscopy). The terms m and n are the ground- and excited-state vibrational levels and σ is the Gaussian linewidth.[32] The fitting parameters E_0, W, σ, and a scaling factor were found using MATLAB to perform a least squares fit to the experimental absorption spectrum in the region of 1.93 to 2.25 eV.

2.5.5 Molecular Dynamics Simulations

All simulations and visualizations were performed with LAMMPS[55] and OVITO,[56] respectively. A detailed description of the atomistic model parametrization from electronic structure calculations as well as the simulation process for generating the as-cast morphology can be found elsewhere.[36,57] Briefly, 60 independent and isolated 12-mers were subjected to a simulated annealing process using Langevin dynamics (800 K to 300 K over the course of 5 ns, NVT ensemble) in order to generate self-aggregated chain structures. These self-aggregated structures were randomly packed into a low-density simulation box (0.01 g cm^{-3}) and were subjected to NPT dynamics at 300 K and 1 atm using a Nosé-Hoover style thermostat (time constant = 100.0 fs) and barostat (time constant = 1000.0 fs) until the density converged (5 ns). Finally, the as-cast morphology was subjected to a thermal annealing protocol consisting of alternating runs between ramping the temperature (20 K ns^{-1}) and equilibrating (1 ns), while outputting the simulation trajectory and thermodynamic parameters.

2.6 Acknowledgements

This work was supported by the Air Force Office of Scientific Research (AFOSR) Grant Number FA9550-16-1-0220. Additional support was provided by the Hellman Fellowship awarded to D. J. L. and the Achievement Reward for College Scientists (ARCS) Fellowship awarded to S. E. R. Computational resources to support this work were provided by the Extreme Science and Engineering Discovery Environment (XSEDE) Program through the National Science Foundation grant number ACI-1053575.[58] Additionally, we would like to thank Professor Andrea Tao for use of the UV-vis spectrometer.

Chapter 2, in full, is a reprint of the material as it appears in *Chemistry of Materials*, 2017, 28, 2646–2654. The American Chemical Society, 2017. Samuel E. Root,‡ Mohammad A. Alkhadra,‡ Daniel Rodriquez, Adam D. Printz, and Darren J. Lipomi* (‡ Equal contribution). The thesis author was a primary investigator and author of this paper.

2.7 References

(1) Müller, C. On the Glass Transition of Polymer Semiconductors and Its Impact on Polymer Solar Cell Stability. *Chem. Mater.* **2015**, *27*, 2740–2754.

(2) Savagatrup, S.; Printz, A. D.; O'Connor, T. F.; Zaretski, A. V.; Rodriquez, D.; Sawyer, E. J.; Rajan, K. M.; Acosta, R. I.; Root, S. E.; Lipomi, D. J. Mechanical Degradation and Stability of Organic Solar Cells: Molecular and Microstructural Determinants. *Energy Environ. Sci.* **2015**, *8*, 55–80.

(3) Mateker, W. R.; Mcgehee, M. D. Progress in Understanding Degradation Mechanisms and Improving Stability in Organic Photovoltaics. *Adv. Mater.* **2017**, 14–16.

(4) Strobl, G. *Physics of Polymers: Concepts for Understanding Their Structures and Behavior*, 1997, DOI: 10.1007/978-3-662-03488-0.

(5) Bennemann, C.; Donati, C.; Baschnagel, J.; Glotzer, S. C. Growing Range of Correlated Motion in a Polymer Melt on Cooling towards the Glass Transition. *Nature* **1999**, *399*, 246–249.

(6) Williams, M. L.; Landel, R. F.; Ferry, J. D. The Temperature Dependence of Relaxation Mechanisms in Amorphous Polymers and Other Glass-Forming Liquids. *J. Am. Chem. Soc.* **1955**, *77*, 3701–3707.

(7) O'connor, T. F.; Rajan, K. M.; Printz, A. D.; Lipomi, D. J. Toward Organic Electronics with Properties Inspired by Biological Tissue. *J. Mater. Chem. B* **2015**, *3*, 4947–4952.

(8) Printz, A. D.; Lipomi, D. J. Competition between Deformability and Charge Transport in Semiconducting Polymers for Flexible and Stretchable Electronics. *Appl. Phys. Rev.* **2016**, *3*, 21302.

(9) Turi, E. *Thermal Characterization of Polymeric Materials*; Elsevier: 2012.

(10) Müller, C.; Andersson, L. M.; Garriga, M.; Campoy-quiles, M. Determination of Thermal Transition Depth Profiles in Polymer Semiconductor Films with Ellipsometry. *Macromolecules* **2013**, *46*, 7325–7331.

(11) Schwartz, B. J. Conjugated Polymers as Molecular Materials: How Chain Conformation and Film Morphology Influence Energy Transfer and Interchain Interactions. *Annu. Rev. Phys. Chem.* **2003**, *54*, 141–172.

(12) Nikolka, M.; Nasrallah, I.; Rose, B.; Ravva, M. K.; Broch, K.; Harkin, D.; Charmet, J.; Hurhangee, M.; Brown, A.; Illig, S.; Too, P.; Jongman, J.; McCulloch, I.; Brédas, J.-L.; Sirringhaus, H.; Sadhanala, A. High Operational and

Environmental Stability of High-Mobility Conjugated Polymer Field-Effect Transistors through the Use of Molecular Additives. *Nat. Mater.* **2016**, *16*, 356–362.

(13) Noriega, R.; Rivnay, J.; Vandewal, K.; Koch, F. P. V; Stingelin, N.; Smith, P.; Toney, M. F.; Salleo, A. A General Relationship between Disorder, Aggregation and Charge Transport in Conjugated Polymers. *Nat. Mater.* **2013**, *12*, 1038–1044.

(14) Holliday, S.; Donaghey, J. E.; McCulloch, I. Advances in Charge Carrier Mobilities of Semiconducting Polymers Used in Organic Transistors. *Chem. Mater.* **2014**, *26*, 647–663.

(15) Schroeder, B. C.; Chiu, Y.-C.; Gu, X.; Zhou, Y.; Xu, J.; Lopez, J.; Lu, C.; Toney, M. F.; Bao, Z. Non-Conjugated Flexible Linkers in Semiconducting Polymers: A Pathway to Improved Processability without Compromising Device Performance. *Adv. Electron. Mater.* **2016**, *2*, 1600104.

(16) Danley, R. L.; Reader, J. R.; Schaefer, J. W. Differential Scanning Calorimeter. U.S. Patent US5842788 A, 1998.

(17) Rotter, G.; Ishida, H. Dynamic Mechanical Analysis of the Glass Transition: Curve Resolving Applied to Polymers. *Macromolecules* **1992**, *25*, 2170–2176.

(18) Kremer, F.; Andreas, S. *Broadband Dielectric Spectroscopy*; Springer: 2003.

(19) Beaucage, G.; Composto, R.; Stein, R. S. Ellipsometric Study of the Glass Transition and Thermal Expansion Coefficients of Thin Polymer Films. *J. Polym. Sci. Part B Polym. Phys.* **1993**, *31*, 319–326.

(20) Lindqvist, C.; Wang, E.; Andersson, M. R.; Müller, C. Facile Monitoring of Fullerene Crystallization in Polymer Solar Cell Blends by UV-Vis Spectroscopy. *Macromol. Chem. Phys.* **2014**, *215*, 530–535.

(21) Tessarolo, M.; Guerrero, A.; Gedefaw, D.; Bolognesi, M.; Prosa, M.; Xu, X.; Mansour, M.; Wang, E.; Seri, M.; Andersson, M. R.; Muccini, M.; Garcia-Belmonte, G. Predicting Thermal Stability of Organic Solar Cells through an Easy and Fast Capacitance Measurement. *Sol. Energy Mater. Sol. Cells* **2015**, *141*, 240–247.

(22) Sung, M. J.; Luzio, A.; Park, W.-T.; Kim, R.; Gann, E.; Maddalena, F.; Pace, G.; Xu, Y.; Natali, D.; de Falco, C.; Dang, L.; McNeill, C. R.; Caironi, M.; Noh, Y.-Y.; Kim, Y.-H. High-Mobility Naphthalene Diimide and Selenophene-Vinylene-Selenophene-Based Conjugated Polymer: N-Channel Organic Field-Effect Transistors and Structure-Property Relationship. *Adv. Funct. Mater.* **2016**, *26*, 4984−4997.

(23) Lan, L.; Chen, Z.; Ying, L.; Huang, F.; Cao, Y. Acenaphtho[1,2-B]quinoxaline

Diimides Derivative as a Potential Small Molecule Non-Fullerene Acceptor for Organic Solar Cells. *Org. Electron.* **2016**, *30*, 176–181.

(24) Patel, S. N.; Su, G. M.; Luo, C.; Wang, M.; Perez, L. A.; Fischer, D. A.; Prendergast, D.; Bazan, G. C.; Heeger, A. J.; Chabinyc, M. L.; Kramer, E. J. NEXAFS Spectroscopy Reveals the Molecular Orientation in Blade-Coated Pyridal[2,1,3]thiadiazole-Containing Conjugated Polymer Thin Films. *Macromolecules* **2015**, *48*, 6606–6616.

(25) Hufnagel, M.; Thelakkat, M. Simultaneous Morphological Stability and High Charge Carrier Mobilities in Donor–Acceptor Block Copolymer/PCBM Blends. *J. Polym. Sci., Part B: Polym. Phys.* **2016**, *54*, 1125–1136.

(26) Cho, E. C.; Chang-Jian, C. W.; Hsiao, Y. S.; Lee, K. C.; Huang, J. H. Influence of the Bridging Atom on the Electrochromic Performance of a Cyclopentadithiophene Polymer. *Sol. Energy Mater. Sol. Cells* **2016**, *150*, 43–50.

(27) Huth, H.; Minakov, A. A.; Serghei, A.; Kremer, F.; Schick, C. Differential AC-Chip Calorimeter for Glass Transition Measurements in Ultra Thin Polymeric Films. *Eur. Phys. J.: Spec. Top.* **2007**, *141*, 153–160.

(28) Keddie, J. L.; Jones, R. A. L.; Cory, R. A. Size-Dependent Depression of the Glass Transition Temperature in Polymer Films. *Epl* **1994**, *27*, 59–64.

(29) Printz, A. D.; Zaretski, A. V.; Savagatrup, S.; Chiang, A. S.-C.; Lipomi, D. J. Yield Point of Semiconducting Polymer Films on Stretchable Substrates Determined by Onset of Buckling. *ACS Appl. Mater. Interfaces* **2015**, *7*, 23257–23264.

(30) Printz, A. D.; Chiang, A. S. C.; Savagatrup, S.; Lipomi, D. J. Fatigue in Organic Semiconductors: Spectroscopic Evolution of Microstructure due to Cyclic Loading in poly(3-Heptylthiophene). *Synth. Met.* **2016**, *217*, 144–151.

(31) Kim, D. H.; Lee, B. L.; Moon, H.; Kang, H. M.; Jeong, E. J.; Park, J. Il; Han, K. M.; Lee, S.; Yoo, B. W.; Koo, B. W.; Kim, J. Y.; Lee, W. H.; Cho, K.; Becerril, H. A.; Bao, Z. Liquid-Crystalline Semiconducting Copolymers with Intramolecular Donor-Acceptor Building Blocks for High-Stability Polymer Transistors. *J. Am. Chem. Soc.* **2009**, *131*, 6124–6132.

(32) Clark, J.; Chang, J. F.; Spano, F. C.; Friend, R. H.; Silva, C. Determining Exciton Bandwidth and Film Microstructure in Polythiophene Films Using Linear Absorption Spectroscopy. *Appl. Phys. Lett.* **2009**, *94*, 163306.

(33) Pingel, P.; Zen, A.; Abellón, R. D.; Grozema, F. C.; Siebbeles, L. D. A.; Neher, D. Temperature-Resolved Local and Macroscopic Charge Carrier Transport in Thin P3HT Layers. *Adv. Funct. Mater.* **2010**, *20*, 2286–2295.

(34) Chu, T. Y.; Lu, J.; Beaupré, S.; Zhang, Y.; Pouliot, J. R.; Zhou, J.; Najari, A.; Leclerc, M.; Tao, Y. Effects of the Molecular Weight and the Side-Chain Length on the Photovoltaic Performance of Dithienosilole/thienopyrrolodione Copolymers. *Adv. Funct. Mater.* **2012**, *22*, 2345–2351.

(35) Chu, T.-Y.; Lu, J.; Beaupre, S.; Zhang, Y.; Pouliot, J.-R.; Wakim, S.; Zhou, J.; Leclerc, M.; Li, Z.; Ding, J.; Tao, Y. Bulk Heterojunction Solar Cells Using Thieno[3,4-C]pyrrole-4,6-Dione and Dithieno[3,2-b:2′,3′-d]silole Copolymer with a Power Conversion Efficiency of 7.3%. *J. Am. Chem. Soc.* **2011**, *133*, 4250–4253.

(36) Root, S. E.; Jackson, N.; Savagatrup, S.; Arya, G.; Lipomi, D. J. Modelling the Morphology and Thermomechanical Behaviour of Low-Bandgap Conjugated Polymers and Bulk Heterojunction Films. *Energy Environ. Sci.* **2017**, *10*, 558–569.

(37) Cho, S.; Seo, J. H.; Park, S. H.; Beaupré, S.; Leclerc, M.; Heeger, A. J. A Thermally Stable Semiconducting Polymer. *Adv. Mater.* **2010**, *22*, 1253–1257.

(38) Chen, S.; Ni, J. Structure/properties of Conjugated Conductive Polymers. 1. Neutral Poly(3-Alkythiophene) S. *Macromolecules* **1992**, *25*, 6081–6089.

(39) Yazawa, K.; Inoue, Y.; Yamamoto, T.; Asakawa, N. Twist Glass Transition in Regioregulated poly(3-Alkylthiophene). *Phys. Rev. B: Condens. Matter Mater. Phys.* **2006**, *74*, 094204.

(40) Spano, F. C. Modeling Disorder in Polymer Aggregates: The Optical Spectroscopy of Regioregular poly(3-Hexylthiophene) Thin Films. *J. Chem. Phys.* **2005**, *122*, 234701.

(41) Spano, F. C. The Spectral Signatures of Frenkel Polarons in H- And J-Aggregates. *Acc. Chem. Res.* **2010**, *43*, 429–439.

(42) Awartani, O.; Lemanski, B. I.; Ro, H. W.; Richter, L. J.; De Longchamp, D. M.; O'Connor, B. T. Correlating Stiffness, Ductility, and Morphology of polymer:Fullerene Films for Solar Cell Applications. *Adv. Energy Mater.* **2013**, *3*, 399–406.

(43) Guilbert, A. A. Y.; Zbiri, M.; Jenart, M. V. C.; Nielsen, C. B.; Nelson, J. New Insights into the Molecular Dynamics of P3HT:PCBM Bulk Heterojunction: A Time-of-Flight Quasi-Elastic Neutron Scattering Study. *J. Phys. Chem. Lett.* **2016**, *7*, 2252–2257.

(44) Root, S. E.; Savagatrup, S.; Pais, C. J.; Arya, G.; Lipomi, D. J. Predicting the Mechanical Properties of Organic Semiconductors Using Coarse-Grained Molecular Dynamics Simulations. *Macromolecules* **2016**, *49*, 2886–2894.

(45) McCulloch, I.; Heeney, M.; Bailey, C.; Genevicius, K.; Macdonald, I.; Shkunov, M.; Sparrowe, D.; Tierney, S.; Wagner, R.; Zhang, W.; Chabinyc, M. L.; Kline, R.

J.; McGehee, M. D.; Toney, M. F. Liquid-Crystalline Semiconducting Polymers with High Charge-Carrier Mobility. *Nat. Mater.* **2006**, *5*, 328–333.

(46) Delongchamp, D. M.; Kline, R. J.; Jung, Y.; Lin, E. K.; Fischer, D. A.; Gundlach, D. J.; Cotts, S. K.; Moad, A. J.; Richter, L. J.; Toney, M. F.; Heeney, M.; McCulloch, I. Molecular Basis of Mesophase Ordering in a Thiophene-Based Copolymer. *Macromolecules* **2008**, *41*, 5709–5715.

(47) Miller, N. C.; Gysel, R.; Miller, C. E.; Verploegen, E.; Beiley, Z.; Heeney, M.; McCulloch, I.; Bao, Z.; Toney, M. F.; McGehee, M. D. The Phase Behavior of a Polymer-Fullerene Bulk Heterojunction System That Contains Bimolecular Crystals. *J. Polym. Sci., Part B: Polym. Phys.* **2011**, *49*, 499–503.

(48) Kim, Y.; Cook, S.; Choulis, S. a.; Nelson, J.; Durrant, J. R.; Bradley, D. D. C. Organic Photovoltaic Devices Based on Blends of Regioregular Poly(3-Hexylthiophene) and Poly(9,9-Dioctylfluorene-Co-Benzothiadiazole). *Chem. Mater.* **2004**, *16*, 4812–4818.

(49) Banach, M. J.; Friend, R. H.; Sirringhaus, H. Influence of the Molecular Weight on the Thermotropic Alignment of Thin Liquid Crystalline Polyfluorene Copolymer Films. *Macromolecules* **2003**, *36*, 2838–2844.

(50) Campoy-Quiles, M.; Sims, M.; Etchegoin, P. G.; Bradley, D. D. C. Thickness-Dependent Thermal Transition Temperatures in Thin Conjugated Polymer Films. *Macromolecules* **2006**, *39*, 7673–7680.

(51) Yuan, M. C.; Chou, Y. J.; Chen, C. M.; Hsu, C. L.; Wei, K. H. A Crystalline Low-Bandgap Polymer Comprising Dithienosilole and thieno[3,4-C]pyrrole-4,6-Dione Units for Bulk Heterojunction Solar Cells. *Polymer* **2011**, *52*, 2792–2798.

(52) Bergqvist, J.; Lindqvist, C.; Bäcke, O.; Ma, Z.; Tang, Z.; Tress, W.; Gustafsson, S.; Wang, E.; Olsson, E.; Andersson, M. R.; Inganäs, O.; Müller, C. Sub-Glass Transition Annealing Enhances Polymer Solar Cell Performance. *J. Mater. Chem. A* **2014**, *2*, 6146–6152.

(53) Root, S. E.; Jackson, N.; Savagatrup, S.; Arya, G.; Lipomi, D. J. Modelling the Morphology and Thermomechanical Behaviour of Low-Bandgap Conjugated Polymers and Bulk Heterojunction Films. *Energy Environ. Sci.* **2017**, *10*, 558–569.

(54) Fauvell, T. J.; Zheng, T.; Jackson, N. E.; Ratner, M. A.; Yu, L.; Chen, L. X. The Photophysical and Morphological Implications of Single-Strand Conjugated Polymer Folding in Solution. *Chem. Mater.* **2016**, *28*, 2814−2822.

(55) Plimpton, S. Fast Parallel Algorithms for Short-Range Molecular Dynamics. *J. Comput. Phys.* **1995**, *117*, 1–19.

(56) Stukowski, A. Visualization and Analysis of Atomistic Simulation Data with

OVITO–the Open Visualization Tool. *Modell. Simul. Mater. Sci. Eng.* **2010**, *18*, 015012.

(57) Jackson, N. E.; Kohlstedt, K. L.; Savoie, B. M.; Olvera de la Cruz, M.; Schatz, G. C.; Chen, L. X.; Ratner, M. A. Conformational Order in Aggregates of Conjugated Polymers. *J. Am. Chem. Soc.* **2015**, *137*, 6254–6262.

(58) Towns, J.; Cockerill, T.; Foster, I.; Gaither, K.; Dahan, M.; Grimshaw, A.; Hazlewood, V.; Lathrop, S.; Lifka, D.; Peterson, G. D.; Roskies, R.; Scott, J. R.; Wilkins-Diehr, N. XSEDE: Accelerating Scientific Discovery. *Comput. Sci. Eng.* **2014**, *16*, 62−74.

Chapter 3

Fracture Mechanics of Brittle and Ductile Thin Films of Semiconducting Polymers

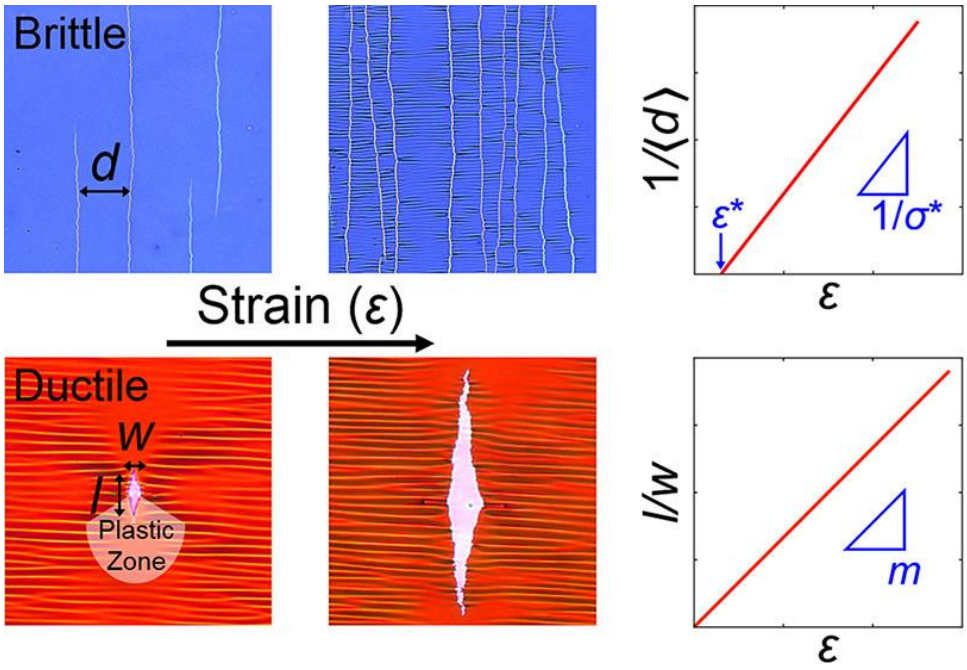

Image 3. Table of contents artwork for Chapter 3. Illustration of fracture mechanisms.

Mohammad A. Alkhadra,‡ Samuel E. Root,‡ Kristan M. Hilby, Daniel Rodriquez, Fumitaka Sugiyama, and Darren J. Lipomi*

(‡ Equal contribution)

Department of NanoEngineering, University of California, San Diego, 9500 Gilman Drive Mail Code 0448, La Jolla, CA 92093-0448.

Abstract

One of the primary complications in characterizing the mechanical properties of thin films of semiconducting polymers is their diverse range of fracture behavior. Experimentally, fracture can be characterized by observing the propagation of cracks and voids in an elongated film. For brittle polymers, we find that films bifurcate in such a way that the crack density increases linearly with applied strain ($R^2 \geq 0.91$) at small strains. Linear regression is used to estimate the fracture strength and strain at fracture of each material using an existing methodology. For the case of ductile polymers, however, we find that diamond-shaped microvoids, which originate at pinholes and defects within the film, propagate with an aspect ratio that increases linearly with applied strain ($R^2 \geq 0.98$). We define the rate of change of the aspect ratio of a microvoid with respect to applied strain as the "microvoid-propagation number." This dimensionless film parameter, previously unreported, is a useful measure of ductility in thin films supported by an elastomer. To explore the significance of this parameter, we correlate the microvoid-propagation number with nominal ductility using several ductile polymer films of approximately equal thickness. Since the fracture of a film supported by a substrate depends on the elastic mismatch, we study the effect of this mismatch on the propagation of microvoids and observe that the microvoid-propagation number increases with increasing elastic mismatch. Moreover, we demonstrate the dependence of microvoid propagation on the thickness of the film and find that thicker films exhibit greater resistance to the propagation of fracture. We hypothesize that this behavior may be attributed to a larger volume of the plastic zone and a higher density of entanglements. To understand how the mechanical properties of a film influence the fracture behavior on a substrate, we perform tensile tests

of notched and unnotched films floated on the surface of water. We find a linear correlation ($R^2 = 0.99$) between the logarithm of the microvoid-propagation number and the fracture stress.

3.1 Introduction

The development of semiconducting polymers that are resistant to fracture requires a comprehensive understanding of their mechanical properties. These materials essentially always take the form of thin films supported by a rigid, flexible, or stretchable substrate. The challenges associated with force-based measurements of the mechanical response of such supported films, however, have led to the development of a suite of optical metrology techniques.[1–4] This paper describes how a range of fracture behavior in films of semiconducting polymers supported by an elastomer can be characterized using optical microscopy (**Figure 3.1**). We applied a metrology technique, described by Stafford and coworkers,[2] to thin films of polymers that undergo brittle fracture. In addition, we developed a novel technique to characterize the fracture behavior of thin films of ductile polymers We quantified the propagation of diamond-shaped microvoids in ductile films using the rate of change in the aspect ratio of these microvoids with applied strain. We then used this methodology to show that the propagation of ductile microvoids is inhibited in thicker films. To supplement these analyses, we performed tensile tests of pseudo freestanding films—supported only by water—in both notched and unnotched configurations. We then determined quantitative and qualitative relationships between the fracture behavior of a film supported by an elastomer and the mechanical response of the film on water. Our approach should be useful for predicting and comparing the mechanical

robustness of thin films of ductile polymers for applications in flexible and stretchable electronics.

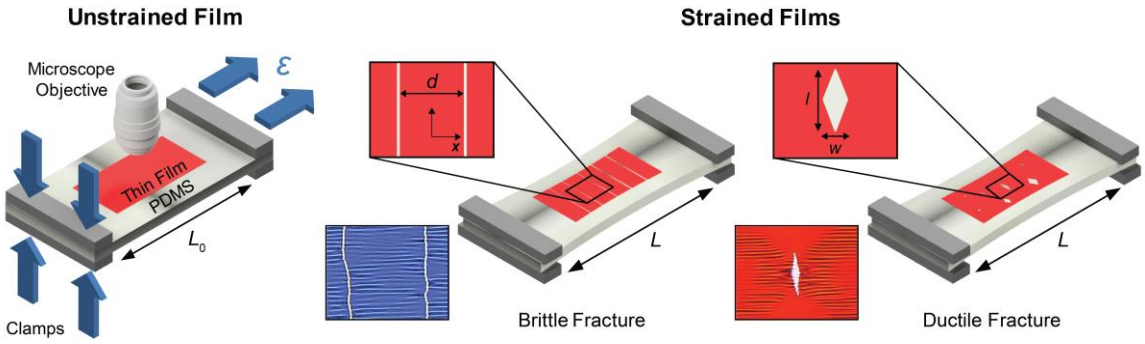

Figure 3.1. Overview of the experimental methodology and corresponding fracture modes in thin films of semiconducting polymers. A spin-coated film supported by a poly(dimethylsiloxane) (PDMS) substrate is incrementally strained under an optical microscope. Schematic illustrations (top) and representative optical micrographs (bottom) demonstrating fracture by either a brittle or a ductile mechanism. Blue arrows indicate the direction of an applied force, for either clamping or applying tensile strain.

3.2 Theoretical and Experimental Considerations

The mismatch in elastic modulus (E) between a rigid film and a compliant substrate affects the initiation and propagation of cohesive fracture that channels through the film.[5] For linear elastic films, Beuth showed that the strain-energy release rate (G, in units of J m^{-2}), defined as the energy dissipated per unit area of fracture surface created, is a function of the elastic mismatch between the film and the substrate.[6] This dependence proceeds from the concentration of stress at the interface of a strained bilayer structure caused by elastic mismatch. Elastic mismatch may be quantified using Dundurs' parameters α and β:[6,7]

$$\alpha = \frac{\overline{E}_f - \overline{E}_s}{\overline{E}_f + \overline{E}_s}, \ \beta = \frac{1}{2}\frac{\mu_f(1-2\nu_s) - \mu_s(1-2\nu_f)}{\mu_f(1-\nu_s) + \mu_s(1-\nu_f)} \quad (1)$$

where $\overline{\boldsymbol{E}} = \boldsymbol{E}/(\mathbf{1} - \boldsymbol{\nu}^{\mathbf{2}})$, $\boldsymbol{\nu}$ is the Poisson ratio, $\boldsymbol{\mu} = \boldsymbol{E}/(\mathbf{2}(\mathbf{1} + \boldsymbol{\nu}))$, and subscripts "f" and "s" denote the film and substrate, respectively. The dependence of G on β is weak when $\alpha > 0$, in which case β may be neglected.[8] For a stiff film and a relatively compliant substrate,

$\boldsymbol{E_f} \gg \boldsymbol{E_s}$ implies that $\alpha \approx 1$. The likelihood for fracture to initiate and propagate increases as Dundurs' parameter α tends to 1 because of the rapid increase in G with increasing elastic mismatch. The Griffith fracture criterion states that fracture occurs when G exceeds the critical value G_c, known as the cohesive fracture energy.[9]

For linear elastic materials, events of fracture may be characterized using the cohesive fracture energy and the stress intensity factor (K), a theoretical construct that relates the applied stress to the intensity of stress near the tip of a crack.[10] For materials that exhibit extensive plastic deformation, however, these parameters of linear elastic fracture mechanics are not sufficient to describe ductile fracture.[11,12] This insufficiency arises because the total energy due to ductile fracture is dissipated not only in the immediate vicinity of the fracture tip, but also in an outer region of extensive plastic deformation. To determine parameters for the fracture toughness of ductile materials, the method of the Essential Work of Fracture (EWF) was developed by Cotterell and Reddel.[11] The theory underlying this technique, however, assumes that the sample is not supported by a substrate that can bear the applied load. In the presence of an elastic substrate, adhesion and elastic mismatch strongly influence fracture, while intrinsic mechanical properties such as toughness are less important.[13] In general, the relationship between the intrinsic mechanical properties and the fracture behavior of ductile films supported by a substrate has not been thoroughly investigated.

Based on the theory of linear elastic fracture mechanics in thin films,[6,8] a stiffer substrate would delay the onset of fracture and inhibit its propagation, and a more compliant substrate would hasten the onset of fracture and promote its propagation.[5,14] Although the elastic moduli of the polymers we examined spanned multiple orders of

magnitude, we standardized the experimental procedure for tensile testing by holding the elastic modulus of the substrate approximately constant at 0.5 ± 0.2 MPa, which is much lower than the moduli of the films. In addition, we studied the role of varying the elastic modulus of the substrate on microvoid propagation in ductile films by varying the ratio of elastomer base to crosslinking agent. We note that this approach also affects the adhesion between the film and the substrate. To simplify our analysis, however, we assume that the film is well-bonded to the substrate in all cases.

Fracture may also be influenced by environmental conditions such as moisture, heat, and ultraviolet (UV) radiation.[15] In our experiments, however, effects of heat and UV radiation were trivial due to the controlled environment of the laboratory. We also reduced the influence of moisture content on our samples (e.g., moisture-assisted debonding[15] at the interface between the film and the substrate) by maintaining the relative humidity in our laboratory at approximately 65%.

3.3 Brittle Fracture

Chung and Lee et al. established a methodology that combines wrinkling and cracking of brittle films, such that the elastic modulus, fracture strength, and strain at fracture[16] can be determined simultaneously.[2] This methodology is carried out by transferring a rigid, brittle film onto a stretchable substrate and incrementally applying uniaxial tensile strain (ε) while measuring the average spacing between cracks (**Figure 3.2a**). The validity of this methodology, however, is contingent on the formation of approximately equally spaced, parallel cracks that propagate orthogonal to the direction of applied strain. Such a fragmentation pattern is characteristic of inherently brittle materials whose elastic behavior terminates with rupture—rather than plastic yield—at low strains.[17]

In investigating the fracture mechanics of thin films of semiconducting polymers, we observed experimentally that this process of brittle fracture occurs commonly.

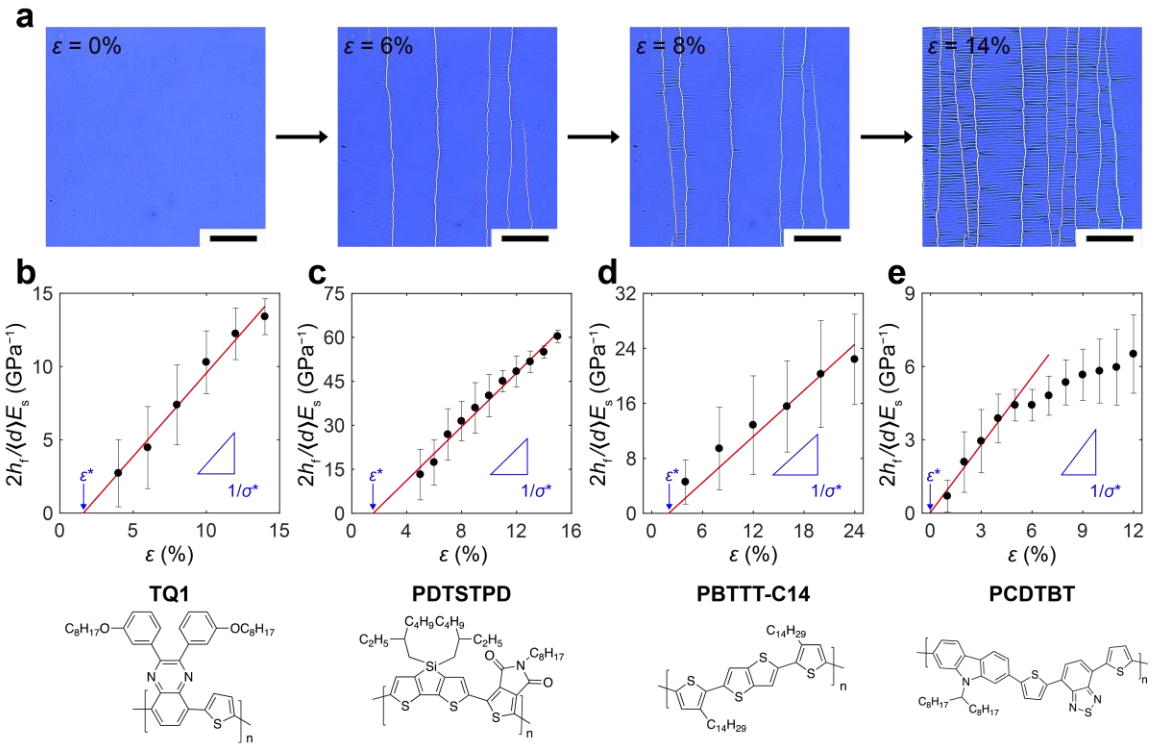

Figure 3.2. The combined wrinkling–cracking methodology applied to thin films of semiconducting polymers that exhibit brittle fracture. (a) Optical micrographs demonstrating the progressive elongation and systematic fragmentation of a thin film of TQ1 on PDMS; scale bars = 100 μm. Graphs of the scaled crack density $\left(\frac{2h_f}{\langle d\rangle E_s}\right)$ as a function of applied strain (ε) for (b) TQ1 ($h_f = 206 \pm 6$ nm), (c) PDTSTPD ($h_f = 159 \pm 8$ nm), (d) PBTTT-C14 ($h_f = 78 \pm 5$ nm), and (e) PCDTBT ($h_f = 137 \pm 8$ nm). Mean values and error bars (standard deviations) are based on data acquired from at least three separate measurements. Solid red lines correspond to linear regressions. Refer to **Experimental Methods** for systematic names.

The combined wrinkling–cracking methodology is restricted to the case in which the average width of fragments ($\langle \boldsymbol{d} \rangle$) is inversely proportional to the applied strain. It is also assumed that cracks in the film are unaccompanied by yielding or fracture of the substrate, any slip at the film–substrate interface is negligible, and tensile stress (σ) is

maximal at the midpoint between adjacent cracks. Under these assumptions, $\langle \boldsymbol{d} \rangle$ is given by[18–20]

$$\langle d \rangle = \frac{2h_f \sigma^*}{E_s(\varepsilon - \varepsilon^*)};\ \varepsilon > \varepsilon^*,\ \langle d \rangle < d_c = \frac{4h_f E_f}{E_s} \tag{2}$$

where h_f, σ^*, and ε^* are the thickness, fracture strength, and strain at fracture of the film, E_f and E_s are the elastic moduli of the film and substrate, respectively, and d_c is the critical width of fragments for which eq 2 is valid.[2] Rearrangement of eq 2 yields a functional form of the scaled crack density $\left(\frac{\boldsymbol{2h_f}}{\langle \boldsymbol{d} \rangle \boldsymbol{E_s}}\right)$ versus applied strain, which allows direct calculation of the fracture strength from the slope of the linear region of the graph. Extrapolation of this linear regression to the *x*-axis $\left(\frac{\boldsymbol{1}}{\langle \boldsymbol{d} \rangle} = \boldsymbol{0}\right)$ provides a reliable estimate of the strain at fracture. The fracture strength and strain at fracture are closely related to the damage and failure mechanisms of polymer films and, by extension, organic electronic devices.[13]

On applying uniaxial tensile strain, a buckling instability is produced by a transverse compressive strain due to the Poisson effect.[1] A periodic wrinkling pattern with a well-defined wavelength (λ) appears parallel to the direction of applied strain.[2] At low strains, and for a sufficiently thick substrate, the buckling wavelength can yield quantitative estimates of the elastic modulus of the film according to

$$\frac{E_f}{1 - \nu_f^2} = \frac{3E_s}{1 - \nu_s^2}\left(\frac{\lambda}{2\pi h_f}\right)^3 \tag{3}$$

where ν_f and ν_s are the Poisson ratios of the film and substrate, respectively.[1] The elastic modulus of the film is relevant for deformable applications and wearable devices, and it can be tailored to minimize interfacial stress and interlayer delamination that would otherwise result in catastrophic failure of these devices.[13]

We employed the combined wrinkling–cracking methodology to analyze the fracture of films of brittle semiconducting polymers. The mechanical response and fracture of a thin film of TQ1 subjected to uniaxial strain is illustrated in **Figure 3.2a**; as shown in Figure 2b, fragmentation occurred linearly with strain. A similar response was observed for thin films of PDTSTPD, PBTTT-C14, and PCDTBT, as shown in **Figure 3.2c-e**, respectively. The large uncertainties associated with the scaled crack densities in **Figure 3.2b** and **Figure 3.2d** manifest as large errors on estimates of the strain at fracture (refer to **Table 3.1**). This uncertainty could be due to the highly statistical nature of crack formation,[21] which depends on film defects and surface roughness. In contrast, the uncertainties associated with the slopes of the regressions are comparatively smaller, as indicated by the small errors on estimates of the fracture strength.

In **Figure 3.2e**, the rate of change of the scaled crack density with respect to applied strain begins to decrease for $\varepsilon \geq 6\%$. Stafford and coworkers attribute such behavior[22] to an insufficiency in the amount of stress induced on the film by the substrate for existing fragments to continue to bifurcate.[2] In any case, the relationship between scaled crack density and strain is linear ($R^2 \geq 0.91$) at low strains, and linear regression was used to determine the fracture strength and strain at fracture. Estimating Poisson ratios of $\nu_f = 0.35$ and $\nu_s = 0.5$,[23] eq 3 was used to calculate the elastic modulus of the film for each material based on the corresponding wavelength of wrinkles produced at low strains. The results of this analysis are summarized in **Table 3.1**.

Table 3.1. Tabulated values of the mechanical properties measured using the combined wrinkling–cracking methodology. Molecular weights were determined by gel-permeation chromatography (GPC), and glass transition temperatures (T_g) were measured for thin films ($h_f \geq 80$ nm).

Material	M_n (kDa) [$Đ$]	h_f (nm)	E_f (MPa)	ε^* (%)	σ^* (MPa)	T_g (°C)
TQ1	4 [1.4]	206 ± 6	120 ± 80	2 ± 2	9 ± 2	≈ 100, ref 53
PDTSTPD	15 [2.5]	159 ± 8	60 ± 10	2 ± 1	2.2 ± 0.2	110 ± 10, ref 54
PBTTT-C14‡	6 [2.2]	78 ± 5	180 ± 30	2 ± 2	9 ± 1	102 ± 1, ref 54
PCDTBT	1 [4.3]	137 ± 9	1100 ± 200	0 ± 1	11 ± 3	$130. \pm 3$, ref 29

‡Spun from a heated solution at $T \approx 80$ °C

Based on the strains at fracture reported in **Table 3.1**, the materials examined clearly underwent brittle fracture at low strains. The most plausible explanation for this mechanical response is the relatively low molecular weights of the materials coincident with their relatively high glass transition temperatures (T_g). Semiconducting polymers with molecular weights near or below the entanglement molecular weight comprise unconnected, chain-extended crystals that cannot endure large stresses and, as a result, manifest extreme brittleness.[5,24] In this instance, chain pullout is the favored mechanism of fracture.[25,26] Analogously, semiconducting polymers with T_gs well above room temperature often—though not always—fail in a brittle manner because segmental relaxation cannot occur on short, experimental time scales.[27] Considering the data in Table 1, the materials we examined using the combined wrinkling–cracking methodology fractured near $\varepsilon = 2\%$. Moreover, the product of the elastic modulus of the film and the strain at fracture is approximately equal to the fracture strength for each of the respective polymers. These materials therefore absorbed the applied mechanical energy entirely

elastically and, in turn, ruptured without exhibiting any plastic yield or deformation, which is characteristic of brittle fracture.[17]

Films of semiconducting polymers exhibit strong, substrate-dependent variations in the T_g with thickness, though these variations occur predominantly when a film is thinned below approximately 80 nm.[28–30] In addition, Chung et al. observed no notable thickness dependence of the mechanical properties of thin films of tantalum and atactic polystyrene over the range of thicknesses investigated in their study (50 nm $\leq h_f \leq$ 1000 nm).[2] We thus expect there to be no significant thickness dependence of the mechanical properties of the materials listed in Table 1. Although the combined wrinkling–cracking methodology works well for brittle materials, this type of analysis cannot be applied to ductile materials, which are necessary for applications that demand mechanical compliance and extreme deformability.

3.4 Ductile Fracture

Ductility, in the classical sense, is defined as the capacity of a material to sustain large and permanent deformation under tensile loading.[16] In the field of organic electronics, measuring the crack-onset strain (COS) of thin films of semiconducting polymers on elastomeric substrates has been adopted as the standard method of evaluating ductility.[31] This measure alone, however, does not provide a rigorous standard. One reason is that estimation of the crack-onset strain is limited by the finite resolution of an optical microscope. Another reason is that fracture at defects is by nature highly statistical, and, since experimenters are susceptible to confirmation bias,[32,33] visual inspection can be imprecise. The crack-onset strain also provides no information with regard to the propagation of microvoids after their initiation. In fact, consideration of fracture in ductile

polymers has been limited to the initiation phase, while the propagation of microvoids has been neglected. A more definitive metric is therefore needed to evaluate the ductility of polymer films supported by an elastic substrate.

For ductile materials, fracture in a film initiates at defects—sites to which mechanical stress is highly localized—and grows progressively with increasing strain.[34] These microvoids, compared to the cracks observed in films of brittle materials, exhibit less of a tendency to propagate with increasing strain, which corresponds to the greater cohesion of ductile materials.[21,35] For the case of PTB7 of high molecular weight, a diamond-shaped microvoid, illustrated in **Figure 3.3a**, originated in the film at low strain ($\varepsilon \approx 10\%$) with a small aspect ratio (l/w). Although there existed regions in the film where multiple sites of fracture developed within close proximity to each other, only isolated microvoids were considered for the analysis. As the film was further elongated, we observed that the microvoid propagated progressively with an aspect ratio that increased linearly, as shown in **Figure 3.3b**. The rate of change of the aspect ratio of the microvoid with respect to applied strain is given by the slope (m) of a linear regression. This parameter, which we term the microvoid-propagation number, describes the ability of a specimen supported by an elastomer to resist fracture propagation and is an effective measure of ductility.

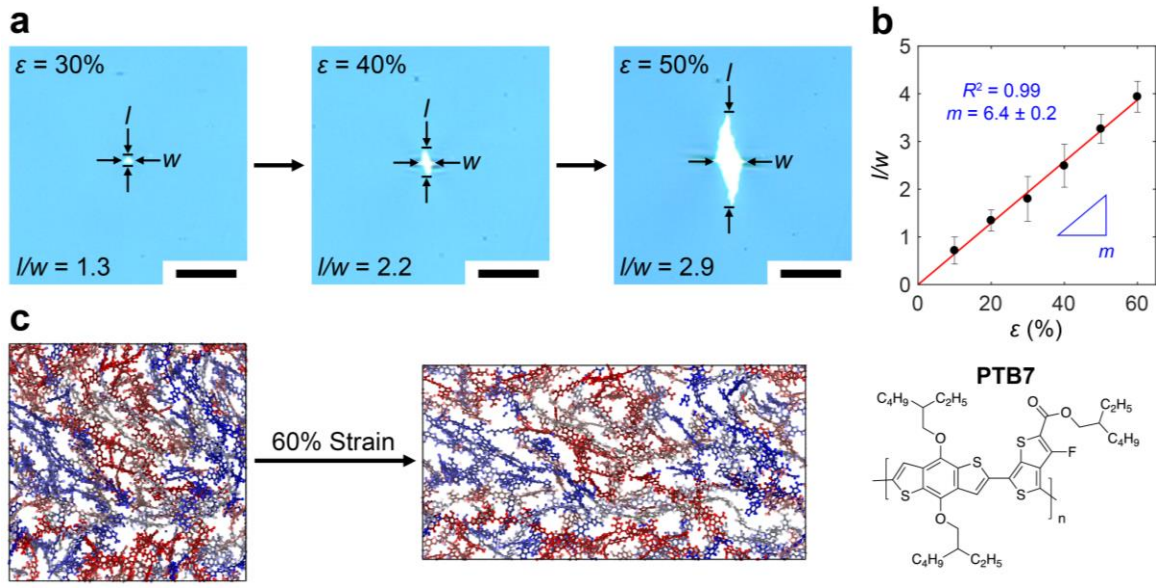

Figure 3.3. Propagation of ductile microvoids in a thin film of PTB7 (h_f = 110. ± 8 nm and E_f = 90 ± 30 MPa) under tensile strain. (a) Optical micrographs depicting the progressive elongation and consequent growth of a microvoid in a thin film of PTB7 on PDMS; scale bars = 25 μm. (b) Plot of the aspect ratio (l/w) of the microvoid as a function of applied strain (ε). To normalize the relationship for microvoids that appear at different strains, the graph is shifted vertically so that the intercepts pass through the origin. Mean values and error bars (standard deviations) are based on data acquired from three separate measurements. Solid red line corresponds to a linear regression with slope m. (c) A 4 nm slice of a molecular dynamics simulation box showing the molecular yielding of PTB7 with applied strain. Hydrogen atoms are removed for clarity, and separate polymer chains are colored distinctly.

For events of ductile fracture, elastic strain energy can be dissipated in two ways: through the formation of both cohesive and adhesive fracture surfaces, and through the plastic deformation of polymer chains. To portray the molecular mechanism of the process of plastic dissipation, we performed molecular dynamics simulations in which PTB7 was subjected to tensile strain using protocols described elsewhere.[36,37] As demonstrated in **Figure 3.3c**, we observed significant morphological rearrangement and alignment of polymer chains. These irreversible deformations ultimately lower the strain-energy release rate that drives the propagation of microvoids. Given that many ductile polymers exhibit

such dissipation processes, the formation and propagation of diamond-shaped microvoids is a commonly observed mechanism of fracture in these materials.[35,38] We note that plastic deformation may also take the form of crazing that could occur at the tip of the microvoid. This effect, which commonly occurs in glassy polymers strained below the T_g,[39] would inhibit the propagation of microvoids. Crazing, however, is typically associated with a whitening of the crazed region due to the scattering of light, which was not evident in any of our microscope images.

3.4.1 Nominal Ductility

To correlate the propagation of microvoids with nominal ductility, we measured the microvoid-propagation number and crack-onset strain for a number of semiconducting polymers (**Figure 3.4**). We defined the crack-onset strain as the strain at which the length (l) of any existing microvoid in the film exceeded approximately 20 μm. We believe that this is a more rigorous definition of the crack-onset strain that could compensate for limitations in the resolution of optical microscopy and aid in mitigating biases of the experimenter. To further standardize the experimental procedure, films were tested at an average thickness of 130 $\pm$ 10 nm. Figures 4a shows a strong correlation between the microvoid-propagation number and crack-onset strain that can be generalized for thin films of ductile polymers, the chemical structures of which are provided in Figure 4b. Balar and O'Connor determined that crack-onset strain can be correlated with cohesive fracture energy for both brittle and ductile films of semiconducting polymers.[38] Although measuring the cohesive fracture energy is beyond the scope of this work, we expect the microvoid-propagation number to decrease with increasing cohesive energy.

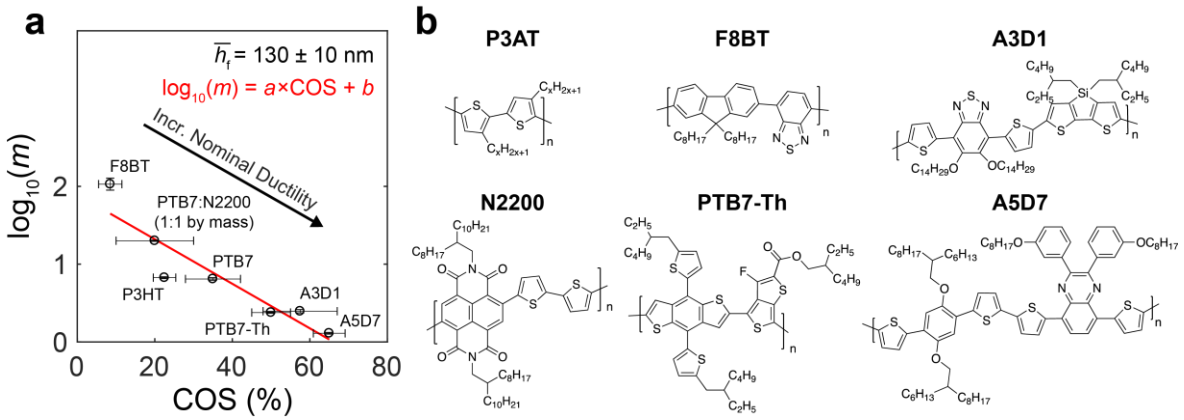

Figure 3.4. Characterization of ductile fracture for various semiconducting polymers. (a) Correlation of the microvoid-propagation number with nominal ductility for thin films tested at an average thickness of 130 $\pm$ 10 nm. The crack-onset strain (COS) is defined as the applied strain at which the length (l) of any existing microvoid in the film (excluding those that are present prior to the application of strain) exceeds approximately 20 μm. Vertical error bars are based on 95% confidence bounds of linear regressions, and horizontal error bars (standard deviations) are based on data acquired from at least three separate measurements. Solid red line corresponds to a linear regression with slope $a = -3 \pm 1$ and y-intercept $b = 1.9 \pm 0.6$ (errors are based on 95% confidence bounds). (b) Chemical structures of the materials used to characterize ductile fracture; refer to **Experimental Methods** for systematic names.

3.4.2 Role of Substrate

Rodriquez and Kim et al. demonstrated that the crack density of thin films of P3HT (40 kDa) supported by PDMS increased with increasing elastic mismatch at a given strain.[5] To examine the effect of elastic mismatch on the propagation of fracture in ductile polymers, we determined the microvoid-propagation number for films of P3BT supported by PDMS of varying elastic modulus, as shown in **Figure 3.5**. The results of this experiment indicate that the microvoid-propagation number increases with increasing elastic mismatch and is a stronger function of this mismatch than is the crack-onset strain. This behavior is consistent with the fact that the strain-energy release rate increases rapidly with increasing elastic mismatch. Although adhesive fracture could serve as an additional dissipation mechanism that would inhibit the propagation of microvoids, data obtained

from contact angle measurements (refer to **Experimental Methods**) suggest that the adhesion of P3BT to PDMS of varying elastic modulus (over the range studied) is similar.

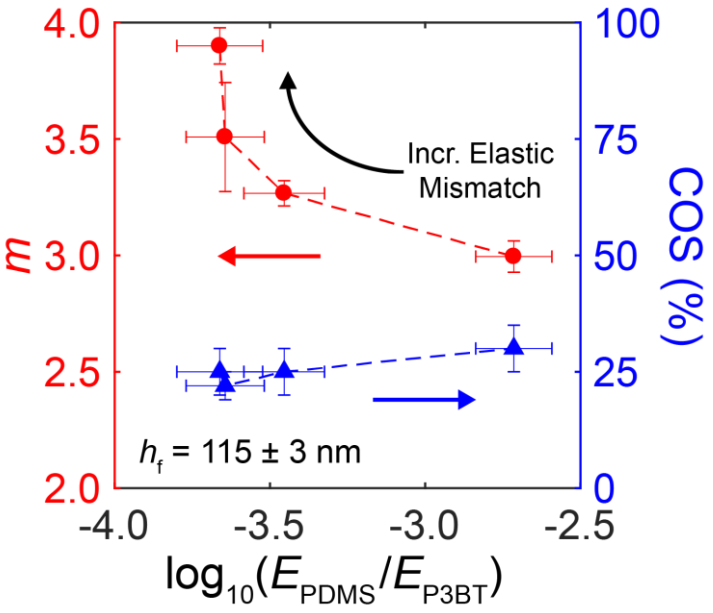

Figure 3.5. Role of the elastic modulus of the PDMS substrate (E_{PDMS}) on the fracture behavior of films of P3BT ($E_f = E_{P3BT} = 0.25 \pm 0.07$ GPa). The microvoid-propagation number (m) increases with increasing elastic mismatch and is a stronger function of this mismatch than is the crack-onset strain (COS). Dashed lines are guides to the eye.

In addition to the formation of surfaces of cohesive fracture, adhesive fracture is an important dissipation mechanism that occurs in thin films of polymers supported by a compliant substrate.[13] **Figure 3.6a** illustrates the surface topography of a fractured film of F8BT on PDMS obtained by atomic force microscopy. For ductile polymers, delamination and wrinkling of the film near the center of a microvoid result from the distribution of stress along the length of the microvoid, with the maximum stress being induced at the advancing tip.[17,40] Delamination of a film from the substrate is an important process that dissipates elastic strain energy by diverting it from the propagating tip of a microvoid. This process of interfacial debonding also results in localized necking[41] that could lead to the formation of ductile microvoids.[38] We expect that the adhesion of different semiconducting

polymers to PDMS is similar, such that delamination at the center of a microvoid is comparable in all cases.

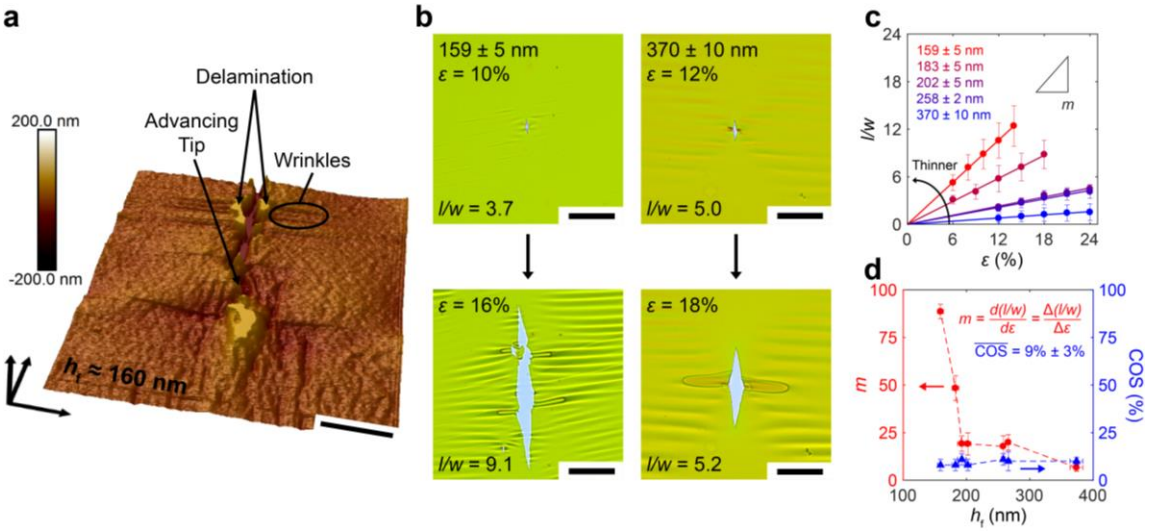

Figure 3.6. Topography of a cracked surface and dependence of ductile fracture on thickness in films of F8BT ($E_f = 1.0 \pm 0.3$ GPa). (a) Atomic force micrograph (tapping mode) of the height image of a crack in a strained film of F8BT supported by PDMS; scale bar = 3 μm. (b) Optical micrographs depicting the effect of an additional 6% strain (ε) on the aspect ratio (l/w) of microvoids in films of F8BT of different thicknesses; scale bars = 50 μm. (c) Graphs of the aspect ratio as a function of applied strain for films of different thicknesses. To normalize the relationship for microvoids that appear at different strains for a given thickness, the graph is shifted vertically so that the intercepts pass through the origin. Mean values and error bars (standard deviations) are based on data acquired from at least three separate measurements. Solid lines correspond to linear regressions. (d) Graphs of the microvoid-propagation number (m) and the crack-onset strain (COS) as functions of thickness (h_f). Vertical error bars on m are based on 95% confidence bounds of regressions in (c); vertical error bars on COS (standard deviations) are based on data acquired from at least three separate measurements; mean thicknesses and horizontal error bars (standard deviations) are based on data acquired from at least five separate measurements. Dashed lines are guides to the eye.

3.4.3 Role of Film Thickness

In the neighborhood of the tip of a microvoid, there exists a region—the plastic dissipation zone—where energy is dissipated due to plastic deformation.[17] Mai and Cotterell reported that the shape of this plastic zone in bulk samples of ductile engineering and commodity plastics depends on the geometry of the specimen.[12] We therefore

investigated the dependence of the propagation of ductile microvoids on the thickness of the film.

The optical micrographs in **Figure 3.6b** show the effect of an additional 6% strain on the aspect ratio of microvoids in films of F8BT of different thicknesses. Microvoids in a thicker film, in contrast to a thinner one, propagate with an aspect ratio that is comparatively less sensitive to applied strain, as demonstrated in **Figure 3.6c**. The graph of the microvoid-propagation number as a function of the thickness of the film is plotted in **Figure 3.6d**, from which the strong dependence on thickness of the rate of propagation of microvoids in ductile films becomes evident. Since the initiation of microvoids is statistical, and not all microvoids originate at a specific applied strain, we underscore the significance of the rate of propagation of microvoids—as opposed to the magnitude of the aspect ratio—in its dependence on thickness. In contrast to the microvoid-propagation number, the crack-onset strain exhibited little to no dependence on thickness (**Figure 3.6d**); films of F8BT of varying thickness (159 ± 5 nm $\leq h_f \leq 370 \pm 10$ nm) had a crack-onset strain of 9% ± 3% on average. This result strongly indicates that the microvoid-propagation number and the crack-onset strain, although correlated, capture distinct aspects of ductile fracture in thin films of semiconducting polymers. The crack-onset strain is a manifestation of the degree of non-uniformity in a film,[38] and it depends on the relative dimensions of local inhomogeneities and the thickness of the film.[13]

The dependence of the microvoid-propagation number on the thickness of the film may be ascribed to the greater sensitivity of the cohesive fracture energy to thickness in samples of high molecular weight.[42] Compared to polymers of low molecular weight, there is a greater tendency for polymers of high molecular weight to exhibit interchain

entanglement, which leads to larger plastic zones around the tips of microvoids.[43,44] Bruner and Dauskardt contended that larger plastic zones inhibit the propagation of fracture by relaxing the stress applied to a film, whereas smaller plastic zones allow extensive propagation of fracture by contributing little to the relaxation of stress.[42] Moreover, Mai and Cotterell argue that the width of the fracture process zone—a necked region of damage that lies directly in the path of an advancing microvoid (**Figure 3.7a**)—increases with increasing thickness in thin plates of metals.[12,45] We therefore propose that the plastic zone in a thinner film is geometrically confined by the boundaries of the specimen to a smaller volume, which results in a higher propensity for microvoids to propagate. It is also possible that effects of thin-film confinement—particularly a reduction in the density of entanglements—would lower the cohesion of the film and lead to more rapid propagation of microvoids. From the perspective of theoretical solid mechanics, the problem of relating the propagation of ductile microvoids to the intrinsic mechanical properties of a thin film is currently unsolved. Nonetheless, it would be interesting and useful to learn if a continuum-based approach could be used to predict this dependence on thickness.

3.4.4 Plastic Dissipation Zone

Over the course of this study, we repeatedly observed the formation of wrinkles with a characteristic X-shape that appeared around diamond-shaped microvoids, as shown in **Figure 3.7b** (right) for instance. We hypothesize that this pattern is determined by the dimensions of the plastic dissipation zone. **Figures 3.7a** schematically illustrates a strained film of semiconducting polymer on PDMS under conditions of plane stress (load forces act only parallel to the plane of the thin film). To test our hypothesis and characterize plastic deformation around the tip of a microvoid, we performed a simple experiment in which we

partially released the strain applied to an elongated film and inspected the wrinkles that formed in plastically deformed regions.[3] Optical micrographs of a fractured film of P3BT are presented in **Figure 3.7b**, the first of which shows these characteristic wrinkles. Elongation of the sample resulted in the propagation of the microvoid, and subsequent release of this additional strain led to severe wrinkling in the zone ahead of the advancing tip. The regions horizontally adjacent to the microvoid, however, displayed no such wrinkling, which suggests the existence of zones of partial elastic recovery.

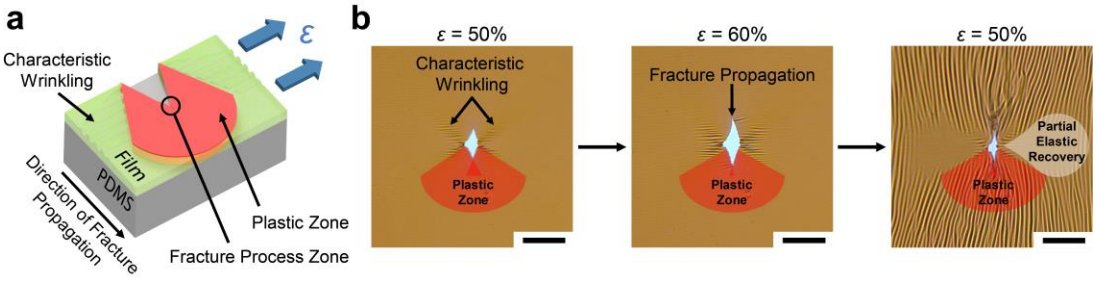

Figure 3.7. Approximate geometry of the plastic zone in thin films of ductile semiconducting polymers that form diamond-shaped microvoids upon fracture. (a) Schematic illustrating a strained film on PDMS and the proposed shape of the plastic zone under conditions of plane stress. Blue arrows indicate the direction of applied tensile strain (ε). (b) Optical micrographs depicting the effect of an additional 10% strain, followed by the release of this applied strain, on the topography of a film of P3BT ($h_f = 115 \pm 3$ nm); scale bars = 50 μm. The zone ahead of the advancing tip of the microvoid exhibited severe wrinkling upon release of the additional strain; regions horizontally adjacent to the microvoid displayed no such wrinkling.

3.4.5 Tensile Testing of Pseudo Freestanding Films

It is well-known that deformation and fracture in thin films supported by polymeric substrates are influenced by the adhesion and elastic mismatch between the film and the substrate.[46] To isolate these effects from the intrinsic mechanical properties of the film, we implemented a tensile test, originally developed by Kim and coworkers, in which pseudo freestanding films are supported by water (**Figure 3.8a**).[47] The "film-on-water" technique resembles a conventional pull test in that it is used to obtain a trace of force versus

displacement in a single step. As shown in **Figure 3.8b**, we measured force–displacement curves of unnotched films of four semiconducting polymers and transformed them into stress−strain curves using the dimensions of the corresponding sample. Based on these data and the results in **Figure 3.4**, we infer that films with a smaller microvoid-propagation number exhibit greater ductility, with or without the support of a substrate. Plotting the logarithm of the microvoid-propagation number versus fracture strength also reveals a correlation between these two parameters, as portrayed in the inset of **Figure 3.8b**. The microvoid-propagation number is thus informative of the stress that a thin film under tension can sustain at fracture.

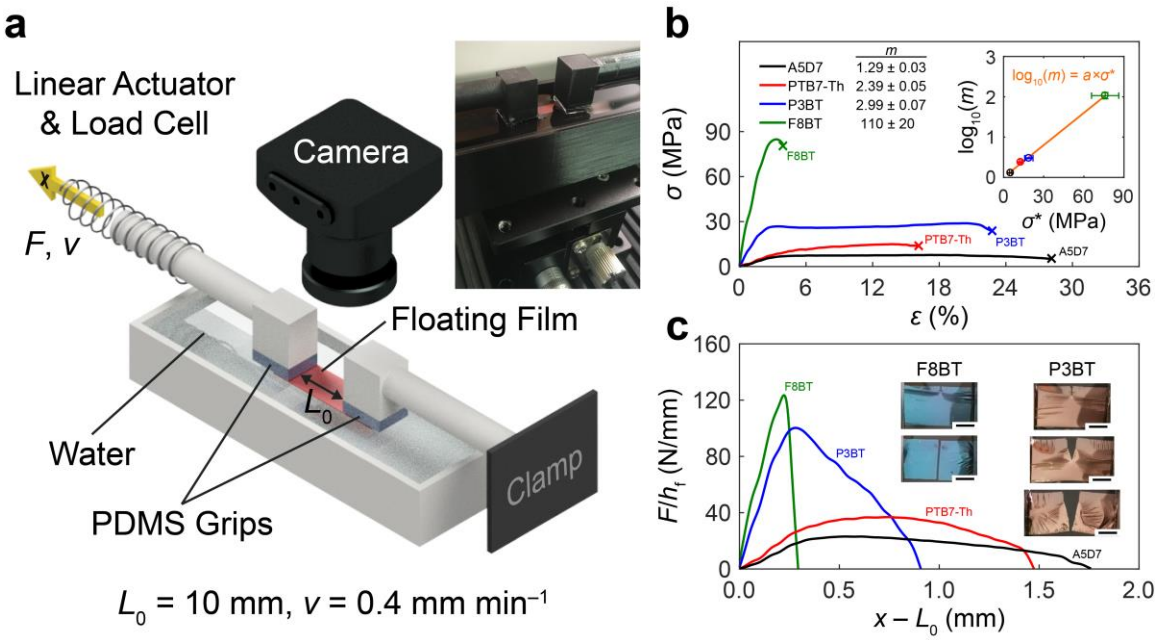

Figure 3.8. Tensile testing of pseudo freestanding films of semiconducting polymers. (a) Schematic diagram of the experimental setup, which consists of a linear actuator, a load cell, and a camera. (b) Representative stress–strain curves of unnotched films obtained using the film-on-water technique. Inset is a plot of the logarithm of the microvoid-propagation number ($\log_{10}(m)$) versus fracture strength (σ^*); values of m are for films tested at an average thickness of 130 ± 10 nm. Horizontal error bars (standard deviations) are based on data acquired from three separate measurements. Solid orange line corresponds to a linear regression with slope a = 0.027 ± 0.001 MPa^{-1} (error is based on 95% confidence bounds). (c) Representative traces of force per unit thickness (F/h_f) versus displacement ($x - L_0$) for notched films of the materials used in (b). Notches at the edges of samples were 0.3 ± 0.1 times the width of the respective film, which was equal to 4.5 ± 0.5 mm on average. Inset photographs demonstrate notched samples before and after the application of uniaxial strain; scale bars = 2.5 mm.

For bulk samples of ductile polymers, the fracture toughness is generally characterized by subjecting a notched specimen to tensile loading while measuring the force.[10,12] To relate the microvoid-propagation number to this classical metric of elastoplastic fracture mechanics, we adapted the film-on-water technique by introducing a notch at the edge of the floating film. This experiment produced curves of force per unit thickness versus displacement, as plotted in **Figure 3.8c**. Comparison of these data with the microvoid-propagation number revealed excellent qualitative agreement in the

observed behavior. Of the four materials tested, the polymer with the largest microvoid-propagation number, F8BT, exhibited the least ductility: the film bifurcated once the applied load reached a critical value. Conversely, the material with the smallest microvoid-propagation number, A5D7, exhibited significant post-yielding behavior due to blunting at the crack tip. In comparing P3BT and PTB7-Th, the relationship between the propagation of fracture for the cases of films supported by PDMS and by water is more subtle. This subtlety is likely due to the large difference in elastic modulus between these two materials, which introduces effects of elastic mismatch when these films are supported by a substrate. To summarize, tensile testing of films on water revealed that the microvoid-propagation number is related to traditional metrics of the fracture toughness of a freestanding film. Developing an exact, quantitative relationship between the intrinsic mechanical properties—determined for a film on water—and the fracture behavior of the film supported by a substrate, however, demands a thorough theoretical treatment supplemented by further experimental testing and is thus the subject of ongoing research.

3.5 Conclusion

Understanding the fracture phenomena that govern the mechanical properties of thin films of semiconducting polymers is critical for the design and processing of flexible and stretchable organic electronics. Mechanical failure in polymer films, however, is naturally convoluted and often the consequence of concurrent events of fracture that occur at the molecular scale. Using the combined wrinkling–cracking methodology, we quantified the stiffness, strength, and ductility of thin films that exhibited brittle fracture at their respective molecular weights. For films that exhibited ductile fracture, on the other hand, we monitored the growth of isolated microvoids and observed how the aspect ratio

varied with applied strain. This measure of the tendency for fracture to propagate was quantified by the microvoid-propagation number, *m*, which provides insight into the degree of plasticity that a ductile film exhibits. We correlated this previously unreported film parameter with the crack-onset strain for various polymers tested at a common thickness. In addition, we demonstrated that the microvoid-propagation number is a strong function of the thickness of the film, a dependence that may be attributed to the geometry of the plastic zone and effects of thin-film confinement. To better understand how plasticity influences the mechanics of ductile fracture, the molecular-scale phenomena that control the growth of microvoids warrant further investigation. Nevertheless, the microvoid-propagation number should be a useful metric because it serves as a simple yet effective way to evaluate the ductility of thin films supported by an elastomer. The characterization of the resistance of a material to fracture is the backbone of fracture mechanics, and it is crucial in assessing the damage tolerance of semiconducting polymers for mechanically robust electronics.

3.6 Experimental Methods

3.6.1 Materials

Poly(9,9-dioctylfluorene-*alt*-benzothiadiazole) (F8BT, M_w = 20–100 kDa) and poly[*N*-9′-heptadecanyl-2,7-carbazole-*alt*-5,5-(4′,7′-di-2-thienyl-2′,1′,3′-benzothiadiazole)] (PCDTBT, M_w = 20–100 kDa) were purchased from Lumtec and used as received. Poly[2,5-bis(3-tetradecylthiophen-2-yl)-thieno[3,2-*b*]thiophene] (PBTTT-C14, $M_n > 12$ kDa, $Đ = 1.8$) was purchased from Solarmer Energy, Inc. and used as received. Poly[(5,6-dihydro-5-octyl-4,6-dioxo-4*H*-thieno[3,4-*c*]pyrrole-1,3-diyl)[4,4-bis(2-ethylhexyl)-4*H*-silolo-[3,2-*b*:4,5-*b*′;]dithiophene-2,6-diyl]] (PDTSTPD, M_n = 7−35

kDa, $Đ$ = 1.4−2.9), poly[[2,3-bis(3-octyloxyphenyl)-5,8-quinoxalinediyl]-2,5-thiophenediyl] (TQ1, M_n = 12−45 kDa, $Đ$ < 3.3), and poly({4,8-bis[(2-ethylhexyl)oxy]benzo-[1,2-*b*:4,5-b′]dithiophene-2,6-diyl}{3-fluoro-2-[(2-ethylhexyl)-carbonyl]thieno[3,4-*b*]thiophenediyl}) (PTB7, M_w = 80−200 kDa, $Đ \leq 3.0$) were purchased from Sigma-Aldrich Co. and used as received. Poly(3-butylthiophene) (P3BT, M_n = 50−70 kDa, $Đ$ = 2.1−3.0) was purchased from Rieke Metals, Inc. and used as received. Poly{[*N*,*N*′-bis(2-octyldodecyl)naphthalene-1,4,5,8-bis(dicarboximide)-2,6-diyl]-*alt*-5,5′-(2,2′-bithiophene)} (PNDI(2OD)2T, Polyera ActivInk™ N2200, M_n = 48 kDa, $Đ$ = 3.7) was purchased from Polyera Corp. and used as received. Poly[4,8-bis(5-(2-ethylhexyl)thiophen-2-yl)benzo[1,2-*b*;4,5-b′]dithiophene-2,6-diyl-*alt*-(4-(2-ethylhexyl)-3-fluorothieno[3,4-*b*]thiophene-)-2-carboxylate-2-6-diyl)] (PTB7-Th, $M_w > 40$ kDa, $Đ$ = 1.8–2.0) was purchased from Ossila Ltd. and used as received. Poly(3-hexylthiophene) (P3HT, M_n = 80 kDa, $Đ$ = 1.6) was produced and characterized by the Heeney laboratory using synthetic procedures described elsewhere.[5] A3D1 (M_n = 50 kDa, $Đ$ = 10.8) and A5D7 (M_n = 34 kDa, $Đ$ = 3.4) were selected from a library of low-bandgap polymers used in studies by Bundgaard et al.[48] and subsequently by Roth and Savagatrup et al.[35] PEDOT:PSS (Clevios™ PH 1000) was purchased from Heraeus and used as received. (Tridecafluoro-1,1,2,2-tetrahydrooctyl)-1-trichlorosilane (FOTS) was purchased from Gelest, Inc. and used as received. Chloroform, acetone, and isopropyl alcohol were purchased from Sigma-Aldrich Co. and used as received. Alconox was purchased from Alconox, Inc. and used as received.

3.6.2 Gel Permeation Chromatography

Since the suppliers reported wide ranges of molecular weight for some polymers used in this study, we independently measured the molecular weight and polydispersity of these materials using gel permeation chromatography (GPC). GPC was performed in chlorobenzene at 55 °C using an Agilent 1260 separation module equipped with a 1260 refractive index detector and a 1260 photodiode array detector. Molecular weights of polymers were calculated relative to linear polystyrene standards. Our measured values of M_n for the brittle polymers are presented in Table 1. For F8BT, we measured $M_n = 10$ kDa and $Đ = 3.2$. For PTB7, the chains eluted too rapidly, such that the peak retention time was outside the range of calibration standards, and thus no reliable data could be obtained.

3.6.3 Preparation of Substrates

Glass slides were prepared as the substrate for polymer films. The glass slides were cut into squares of 2.5 cm × 2.5 cm using a diamond-tipped scribe and then cleaned in sonication baths of powdered Alconox dissolved in deionized water, pure deionized water, acetone, and isopropyl alcohol for cycles of 10 min each. After sonication, the slides were dried using a stream of compressed air. To activate the surface of glass, improve wettability, and remove any residual organic debris, the slides were treated with air plasma (30 W) for 5 min at a base pressure of 200–250 mTorr. Since TQ1 and PCDTBT adhered too strongly to glass treated in this manner, glass slides treated with antiadhesive FOTS were used as substrates. Specifically, slides were treated with plasma, placed in a desiccator with a vial containing a few drops of FOTS, and then left under vacuum for at least 3 h.

3.6.4 Preparation of Films

Solutions of pure polymers and a blend of PTB7 and N2200 (1:1 by mass) were prepared at given concentrations in chloroform and allowed to stir overnight. After mixing,

the solutions were filtered with 1 μm glass fiber media syringe filters before spin coating. All films were then spun, either directly on glass or on a PEDOT:PSS/glass substrate, in two steps. (PTB7-Th was spun from a heated solution at $T \approx 80$ °C.) First, F8BT (20 mg mL^{-1} in chloroform) was spun at 750 rpm (375 rpm s^{-1} ramp), 1000 rpm (500 rpm s^{-1} ramp), 1300 rpm (650 rpm s^{-1} ramp), 1500 rpm (750 rpm s^{-1} ramp), 2000 rpm (1000 rpm s^{-1} ramp), and 3500 rpm (1750 rpm s^{-1} ramp), separately, for 2 min, and F8BT (10 mg mL^{-1} in chloroform) was spun at 1000 rpm (500 rpm s^{-1} ramp) for 2 min. TQ1 and PCDTBT (10 mg mL^{-1} in chloroform) were spun onto glass treated with FOTS at 500 rpm (250 rpm s^{-1} ramp) for 2 min. All other solutions had a concentration of 10 mg mL^{-1} in chloroform and were first spun at 1000 rpm (500 rpm s^{-1} ramp) for 2 min. Second, all films were spun at 2000 rpm (1000 rpm s^{-1} ramp) for 30 s. Thicknesses of films were obtained using a Veeco Dektak stylus profilometer; at least five measurements were taken for each film.

3.6.5 Preparation of PDMS Elastomers

For tensile (compression) testing, poly(dimethylsiloxane) (PDMS) was chosen as the substrate for mechanical measurements. To prepare, 20 g (50 g) of Sylgard 184 Silicone elastomer base was mixed with 2 g (5 g) of Sylgard 184 Silicone crosslinking agent and stirred until cloudy. The mixture was then spread into a petri dish with a diameter of 15 cm and a height of 1.5 cm. PDMS was degassed by placing the petri dish in a desiccator under vacuum until the bubbles ceased to be visible. The dish was then placed in an oven preheated to 70 °C for 50 min to allow the PDMS to cure. Next, the PDMS, with an approximate thickness of 1 mm (3 mm), was cut into rectangular slabs of 1 cm × 9 cm. The elastic modulus of these elastomers was determined to be 0.5 ± 0.2 MPa, on average, using an Instron pull tester. To test the role of elastic mismatch on the fracture behavior of

ductile films, additional PDMS elastomers were prepared: 20 g of Sylgard 184 Silicone elastomer base was mixed with 1, 1.5, or 2 g of Sylgard 184 Silicone crosslinking agent. This batch of PDMS was then allowed to cure in an oven at 70 °C for 40 min, which resulted in elastic moduli of 54 ± 8, 56 ± 5, and 90 ± 10 kPa, respectively. Otherwise, the preparation procedure was the same as described above.

3.6.6 Combined Wrinkling-Cracking Methodology

Slides with polymer films were scored into four, equally sized rectangular sections. Films of PDTSTPD and PBTTT-C14 were transferred to unstrained strips of PDMS by firmly pressing a scored portion of the film onto PDMS and submerging the film–PDMS bilayer in deionized water. While still in water, the slide with the remaining sections of the film was removed, after which the PDMS was dried with compressed air. Films of TQ1 and PCDTBT were not transferred while submerged in water because they had been spun onto glass slides treated with FOTS. Instead, these films were scored into thin segments, placed onto strips of PDMS, and quickly removed with an applied force directly perpendicular to the film–PDMS interface. The film–PDMS bilayers were then uniaxially stretched at one end using a linear translation stage ($L_0 = 1.27$ cm), and the mechanical response of each film was imaged using a Leica DM2700 optical microscope.

3.6.7 Microvoid Aspect Ratio

Scored films of ductile polymers were transferred to unstrained strips of PDMS by firmly pressing a scored portion of the film onto PDMS and submerging the bilayer in deionized water. While still in water, the slide with the remaining sections of the film was removed, after which the PDMS was dried with compressed air. The film–PDMS bilayer was then uniaxially stretched at one end using a linear translation stage ($L_0 = 1.27$ cm),

and the mechanical response of the film was probed by observing the growth of isolated microvoids under the microscope.

3.6.8 Buckling-Based Metrology for Measuring Elastic Moduli

Elastic moduli of the brittle films examined using the combined wrinkling–cracking methodology, namely TQ1, PDTSTPD, PBTTT-C14, and PCDTBT, were estimated by applying the buckling-based metrology of Stafford et al. (eq 3) to these films based on the wrinkling behavior under tension.[1,2] On the other hand, measuring the elastic moduli of ductile films, namely F8BT, PTB7, and P3BT, required compression-induced mechanical buckling to produce visible wrinkling patterns. As such, neat slabs of PDMS were strained to approximately 5% on a linear translation stage and fixed to rectangular glass slides. For each material, films prepared at three different thicknesses (using spin speeds of 500, 1000, and 1500 rpm with ramp rates of 250, 500, and 750 rpm s^{-1}, respectively) were scored and transferred to the pre-strained PDMS. The release of this pre-strain produced a buckling instability and, in turn, wrinkles in the films. For each film, the wrinkles were imaged under a microscope at several (> 7), arbitrary locations. To count the number of wrinkles in an image, we used a function in MATLAB based on the Savitzky-Golay smoothing filter and peak finder, which distinguishes between crests and troughs. To compute the buckling wavelength (λ), the width of an image was divided by the average number of wrinkles. Moreover, the thickness of the film (h_f) was measured (on glass) using a stylus profilometer, and the elastic modulus of PDMS (E_s) was determined using a commercial pull tester. Finally, the elastic modulus of the film (E_f) was calculated using eq 3.

3.6.9 Molecular Dynamics Simulations

All simulations and visualizations were performed using LAMMPS[49] and OVITO[50] respectively. A detailed description of the atomistic model parameterization from calculations of electronic structure, as well as the computational process for generating the simulation morphology, can be found elsewhere.[36,51] Briefly, 60 independent 12-mers were packed into a simulation box and subjected to NPT dynamics at 800 K using time increments of 2 fs for 5 ns to generate a well-equilibrated melt phase. This melt-phase structure was then subjected to an annealing protocol in which the temperature was ramped from 800 K to 300 K in intervals of 20 K and at time increments of 1 ns for runs of both ramping and equilibration. Simulations of mechanical deformation were run by imposing a constant strain rate (1×10^{-6} Å ps^{-1}) in the *x*-dimension and applying stress-free boundary conditions in both transverse dimensions.

3.6.10 Contact Angle Measurements

To qualitatively assess the adhesion between films of P3BT and strips of PDMS, we measured the advancing and receding contact angles of droplets of deionized water (~6 μL) on pristine surfaces of PDMS. Imaging and data analysis were performed with an automated goniometer (Ramé-Hart, Model No. 290-U1) using the method of add/remove volume. Advancing (receding) contact angles of droplets of deionized water on pristine surfaces of PDMS ranged from 119.0° ± 0.6° (109° ± 3°) to 125.9° ± 0.7° (117° ± 4°), which correspond to the PDMS substrates with the highest and lowest elastic moduli, respectively.

3.6.11 Atomic Force Microscopy

A solution of F8BT in chloroform, with a concentration of 15 mg mL^{-1}, was spun onto glass treated with FOTS in two steps (1000 rpm for the first) as described above. A

PDMS substrate was prepared as explained above, though its surface was subsequently activated by cleaning with ultraviolet–ozone (UV–O_3) for 2 h, followed by treatment with FOTS in the same manner that the glass slides were. The film of F8BT on glass was scored into thin segments and transferred to the PDMS treated with FOTS. To generate microvoids in the film, the film–PDMS bilayer was uniaxially stretched at one end using a linear translation stage. Once enough microvoids were produced, the substrate was fixed at the corresponding applied strain. A second, pristine PDMS slab (neither cleaned with UV–O_3 nor treated with FOTS) was prepared by curing at 70 °C for 50 min on the smooth surface of a silicon wafer. After that, the slab was cut into squares of 1 cm × 1 cm (approximately 1 mm thick) and used to strip the fractured film off the strained, surface treated PDMS for imaging. Atomic force micrographs of the height image were then obtained using a Veeco scanning probe microscope (SPM) in tapping mode, and the data were analyzed with NanoScope Analysis v1.40 software (Bruker Corp.).

3.6.12 Film-on-Water Tensile Testing

Kim and coworkers developed a tensile test in which pseudo freestanding films are supported by water.[47] The "film-on-water" technique resembles a conventional pull test in that it is used to obtain a trace of force versus displacement in a single step. This technique leverages the high surface tension and low viscosity of water to support thin films and allow unimpeded sliding of these films on the surface. To float a specimen on water, a sacrificial layer of PEDOT:PSS—onto which semiconducting polymers were spin coated—was used. (PEDOT:PSS was spun onto a glass slide at 1000 rpm (500 rpm s^{-1} ramp) for 3 min, followed by a second step at 2000 rpm (1000 rpm s^{-1} ramp) for 30 s.) The layer of PEDOT:PSS readily dissolved in water upon contact, which allowed the polymer

film to delaminate from the substrate. Once the film was afloat, van der Waals adhesion was made between the film and a load cell using grips coated with small slabs of PDMS. To obtain plots of force versus displacement, films were uniaxially strained at a rate of approximately $6.67 \times 10^{-4}\ s^{-1}$ ($L_0 = 10$ mm) until the test was terminated. Additional tests of fracture were performed by introducing notches at the edges of films, which were then subjected to uniaxial strain. Procedures for preparation and transfer of samples were otherwise identical for films that were and were not notched

3.7 Acknowledgments

This work was supported by the Air Force Office of Scientific Research (AFOSR) Grant Number FA9550-16-1-0220. Further support was provided by a gift from the B Quest Giving Fund made through Benefunder to D.J.L. and the Achievement Reward for College Scientists (ARCS) Fellowship awarded to S.E.R. Computational resources to support this work were provided by the Extreme Science and Engineering Discovery Environment (XSEDE) Program through the National Science Foundation Grant Number ACI-1053575.[52] The authors would like to acknowledge the laboratories of Profs. Martin Heeney (P3HT) and Frederik Krebs (A3D1 and A5D7) for providing materials for this study. In addition, the authors would like to thank Prof. Vlado A. Lubarda, Dr. Laure V. Kayser, Dr. Suchol Savagatrup, Dr. Charles B. Dhong, and Cody W. Carpenter for insightful discussion.

Chapter 3, in full, is a reprint of the material as it appears in *Chemistry of Materials*, 2017, 29, 10139–10149. The American Chemical Society, 2017. Mohammad A. Alkhadra,‡ Samuel E. Root,‡ Kristan M. Hilby, Daniel Rodriquez, Fumitaka Sugiyama,

and Darren J. Lipomi* (‡ Equal contribution). The thesis author was a primary investigator and author of this paper.

3.8 References

(1) Stafford, C. M.; Harrison, C.; Beers, K. L.; Karim, A.; Amis, E. J.; VanLandingham, M. R.; Kim, H. C.; Volksen, W.; Miller, R. D.; Simonyi, E. E. A Buckling-Based Metrology for Measuring the Elastic Moduli of Polymeric Thin Films. *Nat. Mater.* **2004**, *3*, 545–550.

(2) Chung, J. Y.; Lee, J.; Beers, K. L.; Stafford, C. M. Stiffness, Strength, and Ductility of Nanoscale Thin Films and Membranes: A Combined Wrinkling-Cracking Methodology. *Nano Lett.* **2011**, *184*, 3361–3365.

(3) Printz, A. D.; Zaretski, A. V; Savagatrup, S.; Chiang, A. S.-C.; Lipomi, D. J. Yield Point of Semiconducting Polymer Films on Stretchable Substrates Determined by Onset of Buckling. *ACS Appl. Mater. Interfaces* **2015**, *7*, 23257–23264.

(4) Savagatrup, S.; Makaram, A. S.; Burke, D. J.; Lipomi, D. J. Mechanical Properties of Conjugated Polymers and Polymer-Fullerene Composites as a Function of Molecular Structure. *Adv. Funct. Mater.* **2014**, *24*, 1169–1181.

(5) Rodriquez, D.; Kim, J.-H.; Root, S. E.; Fei, Z.; Boufflet, P.; Heeney, M.; Kim, T.-S.; Lipomi, D. J. Comparison of Methods for Determining the Mechanical Properties of Semiconducting Polymer Films for Stretchable Electronics. *ACS Appl. Mater. Interfaces* **2017**, *9*, 8855–8862.

(6) Beuth, J. L. Cracking of Thin Bonded Films in Residual Tension. *Int. J. Solids Struct.* **1992**, *29*, 1657–1675.

(7) Dundurs, J. Elastic Interaction of Dislocations with Inhomogeneities. In *Mathematical Theory of Dislocations*; Mura, T., Ed.; American Society of Mechanical Engineers: New York, 1969; pp 70–115.

(8) Xia, Z. C.; Hutchinson, J. W. Crack Patterns in Thin Films. *J. Mech. Phys. Solids* **2000**, *48*, 1107–1131.

(9) Griffith, A. A. The Phenomena of Rupture and Flow in Solids. *Philos. Trans. R. Soc., A* **1921**, *221*, 163–198.

(10) Martinez, A. B.; Gamez-Perez, J.; Sanchez-Soto, M.; Velasco, J. I.; Santana, O. O.; Ll Maspoch, M. The Essential Work of Fracture (EWF) Method - Analyzing the Post-Yielding Fracture Mechanics of Polymers. *Eng. Failure Anal.* **2009**, *16*, 2604–2617.

(11) Cotterell, B.; Reddel, J. K. The Essential Work of Plane Stress Ductile Fracture. *Int. J. Fract.* **1977**, *13*, 267–277.

(12) Mai, Y.-W.; Cotterell, B. On the Essential Work of Ductile Fracture in Polymers. *Int. J. Fract.* **1986**, *32*, 105–125.

(13) Root, S. E.; Savagatrup, S.; Printz, A. D.; Rodriquez, D.; Lipomi, D. J. Mechanical Properties of Organic Semiconductors for Stretchable, Highly Flexible, and Mechanically Robust Electronics. *Chem. Rev.* **2017**, *117*, 6467–6499.

(14) Li, T.; Huang, Z.; Suo, Z.; Lacour, S. P.; Wagner, S. Stretchability of Thin Metal Films on Elastomer Substrates. *Appl. Phys. Lett.* **2004**, *85*, 3435–3437.

(15) Rolston, N.; Printz, A. D.; Dupont, S. R.; Voroshazi, E.; Dauskardt, R. H. Effect of Heat, UV Radiation, and Moisture on the Decohesion Kinetics of Inverted Organic Solar Cells. *Sol. Energy Mater. Sol. Cells* **2017**, *170*, 239–245.

(16) *Mechanical Engineers' Handbook*, 3rd ed.; Kutz, M., Ed.; John Wiley & Sons, 2015; Vol. *1* (Materials and Engineering Mechanics).

(17) Ward, I. M.; Sweeney, J. *Mechanical Properties of Solid Polymers*, 3rd ed.; John Wiley & Sons, 2012.

(18) Volynskii, A. L.; Bazhenov, S.; Lebedeva, O. V.; Ozerin, A. N.; Bakeev, N. F. Multiple Cracking of Rigid Platinum Film Covering Polymer Substrate. *J. Appl. Polym. Sci.* **1999**, *72*, 1267–1275.

(19) Bazhenov, S. L.; Volynskii, A. L.; Alexandrov, V. M.; Bakeev, N. F. Two Mechanisms of the Fragmentation of Thin Coatings on Rubber Substrates. *J. Polym. Sci., Part B: Polym. Phys.* **2002**, *40*, 10–18.

(20) Volynskii, A. L.; Panchuk, D. A.; Moiseeva, S. V; Kechek'yan, A. S.; Dement'ev, A. I.; Yarysheva, L. M.; Bakeev, N. F. New Approach to Evaluation of the Stress Strain Properties of Nanolayers of Solid Materials. *Russ. Chem. Bull.* **2009**, *58*, 865–882.

(21) Awartani, O.; Lemanski, B. I.; Ro, H. W.; Richter, L. J.; De Longchamp, D. M.; O'Connor, B. T. Correlating Stiffness, Ductility, and Morphology of Polymer:Fullerene Films for Solar Cell Applications. *Adv. Energy Mater.* **2013**, *3*, 399–406.

(22) Heinrich, M.; Gruber, P.; Orso, S.; Handge, U. A.; Spolenak, R. Dimensional Control of Brittle Nanoplatelets. A Statistical Analysis of a Thin Film Cracking Approach. *Nano Lett.* **2006**, *6*, 2026–2030.

(23) Tahk, D.; Lee, H. H.; Khang, D.-Y. Elastic Moduli of Organic Electronic Materials by the Buckling Method. *Macromolecules* **2009**, *42*, 7079–7083.

(24) Koch, F. P. V.; Rivnay, J.; Foster, S.; Müller, C.; Downing, J. M.; Buchaca-Domingo, E.; Westacott, P.; Yu, L.; Yuan, M.; Baklar, M.; Fei, Z.; Luscombe, C.; Mclachlan, M. A.; Heeney, M.; Rumbles, G.; Silva, C.; Salleo, A.; Nelson, J.; Smith, P.; Stingelin, N. The Impact of Molecular Weight on Microstructure and Charge Transport in Semicrystalline Polymer Semiconductors–Poly(3-hexylthiophene), a Model Study. *Prog. Polym. Sci.* **2013**, *38*, 1978–1989.

(25) Washiyama, J.; Kramer, E. J.; Hui, C.-Y. Fracture Mechanisms of Polymer Interfaces Reinforced with Block Copolymers: Transition from Chain Pullout to Crazing. *Macromolecules* **1993**, *26*, 2928–2934.

(26) Washiyama, J.; Kramer, E. J.; Creton, C. F.; Hui, C.-Y. Chain Pullout Fracture of Polymer Interfaces. *Macromolecules* **1994**, *27*, 2019–2024.

(27) Müller, C. On the Glass Transition of Polymer Semiconductors and Its Impact on Polymer Solar Cell Stability. *Chem. Mater.* **2015**, *27*, 2740–2754.

(28) Campoy-Quiles, M.; Sims, M.; Etchegoin, P. G.; Bradley, D. D. C. Thickness-Dependent Thermal Transition Temperatures in Thin Conjugated Polymer Films. *Macromolecules* **2006**, *39*, 7673–7680.

(29) Wang, T.; Pearson, A. J.; Dunbar, A. D. F.; Staniec, P. A.; Watters, D. C.; Coles, D.; Yi, H.; Iraqi, A.; Lidzey, D. G.; Jones, R. A. L. Competition between Substrate-Mediated π-π Stacking and Surface-Mediated T_g Depression in Ultrathin Conjugated Polymer Films. *Eur. Phys. J. E: Soft Matter Biol. Phys.* **2012**, *35*, 129.

(30) Liu, D.; Orozco, R. O.; Wang, T. Deviations of the Glass Transition Temperature in Amorphous Conjugated Polymer Thin Films. *Phys. Rev. E* **2013**, *88*, 022601.

(31) Kim, J.-H.; Lee, I.; Kim, T.-S.; Rolston, N.; Watson, B. L.; Dauskardt, R. H. Understanding Mechanical Behavior and Reliability of Organic Electronic Materials. *MRS Bull.* **2017**, *42*, 115–123.

(32) Wason, P. C. On the Failure to Eliminate Hypotheses in a Conceptual Task. *Q. J. Exp. Psychol.* **1960**, *12*, 129–140.

(33) Goldstein, E. B. *Cognitive Psychology: Connecting Mind, Research and Everyday Experience*, 3rd ed.; Cengage Learning, 2010.

(34) Seitz, J. T. The Estimation of Mechanical Properties of Polymers from Molecular Structure. *J. Appl. Polym. Sci.* **1993**, *49*, 1331–1351.

(35) Roth, B.; Savagatrup, S.; de los Santos, N. V.; Hagemann, O.; Carlé, J. E.; Helgesen, M.; Livi, F.; Bundgaard, E.; Søndergaard, R. R.; Krebs, F. C.; Lipomi, D. J. Mechanical Properties of a Library of Low-Band-Gap Polymers. *Chem. Mater.* **2016**, *28*, 2363–2373.

(36) Root, S. E.; Jackson, N.; Savagatrup, S.; Arya, G.; Lipomi, D. J. Modelling the Morphology and Thermomechanical Behaviour of Low-Bandgap Conjugated Polymers and Bulk Heterojunction Films. *Energy Environ. Sci.* **2017**, *10*, 558–569.

(37) Root, S. E.; Savagatrup, S.; Pais, C. J.; Arya, G.; Lipomi, D. J. Predicting the Mechanical Properties of Organic Semiconductors Using Coarse-Grained Molecular Dynamics Simulations. *Macromolecules* **2016**, *49*, 2886–2894.

(38) Balar, N.; O'Connor, B. T. Correlating Crack Onset Strain and Cohesive Fracture Energy in Polymer Semiconductor Films. *Macromolecules* **2017**, *50*, 8611–8618.

(39) McLeish, T. C. B.; Plummer, C. J. G.; Donald, A. M. Crazing by Disentanglement: Non-Diffusive Reptation. *Polymer* **1989**, *30*, 1651–1655.

(40) Serier, B.; Bachir Bouiadjra, B.; Belhouari, M. Finite Element Analysis of Bi-Material Interface Notch Crack Behaviour. *Comput. Mater. Sci.* **2003**, *27*, 517–522.

(41) Li, T.; Suo, Z. Ductility of Thin Metal Films on Polymer Substrates Modulated by Interfacial Adhesion. *Int. J. Solids Struct.* **2007**, *44*, 1696–1705.

(42) Bruner, C.; Dauskardt, R. H. Role of Molecular Weight on the Mechanical Device Properties of Organic Polymer Solar Cells. *Macromolecules* **2014**, *47*, 1117–1121.

(43) Kusy, R. P.; Katz, M. J. Effect of Molecular Weight on the Fracture Morphology of Poly(ethytmethacrylate) in Cleavage. *J. Mater. Sci.* **1976**, *11*, 1381–1384.

(44) Lee, S.; Moon, G. D.; Jeong, U. Continuous Production of Uniform Poly(3-hexylthiophene) (P3HT) Nanofibers by Electrospinning and Their Electrical Properties. *J. Mater. Chem.* **2009**, *19*, 743–748.

(45) Pardoen, T.; Marchal, Y.; Delannay, F. Thickness Dependence of Cracking Resistance in Thin Aluminium Plates. *J. Mech. Phys. Solids* **1999**, *47*, 2093–2123.

(46) Lu, N.; Wang, X.; Suo, Z.; Vlassak, J. Metal Films on Polymer Substrates Stretched beyond 50%. *Appl. Phys. Lett.* **2007**, *91*, 221909.

(47) Kim, J.-H.; Nizami, A.; Hwangbo, Y.; Jang, B.; Lee, H.-J.; Woo, C.-S.; Hyun, S.; Kim, T.-S. Tensile Testing of Ultra-Thin Films on Water Surface. *Nat. Commun.* **2013**, *4*, 1–6.

(48) Bundgaard, E.; Livi, F.; Hagemann, O.; Carlé, J. E.; Helgesen, M.; Heckler, I. M.; Zawacka, N. K.; Angmo, D.; Larsen-Olsen, T. T.; Dos Reis Benatto, G. A.; Roth, B.; Madsen, M. V.; Andersson, M. R.; Jørgensen, M.; Søndergaard, R. R.; Krebs, F. C. Matrix Organization and Merit Factor Evaluation as a Method to Address the Challenge of Finding a Polymer Material for Roll Coated Polymer Solar Cells. *Adv. Energy Mater.* **2015**, *5*, 1402186.

(49) Plimpton, S. Fast Parallel Algorithms for Short-Range Molecular Dynamics. *J. Comput. Phys.* **1995**, *117*, 1–19.

(50) Stukowski, A. Visualization and Analysis of Atomistic Simulation Data with OVITO–the Open Visualization Tool. *Modell. Simul. Mater. Sci. Eng.* **2010**, *18*, 015012.

(51) Jackson, N. E.; Kohlstedt, K. L.; Savoie, B. M.; Olvera de la Cruz, M.; Schatz, G. C.; Chen, L. X.; Ratner, M. A. Conformational Order in Aggregates of Conjugated Polymers. *J. Am. Chem. Soc.* **2015**, *137*, 6254–6262.

(52) John, T.; Cockerill, T.; Foster, I.; Gaither, K. XSEDE: Accelerating Scientific Discovery. *Comput. Sci. Eng.* **2014**, *16*, 62–74.

(53) Kroon, R.; Gehlhaar, R.; Steckler, T. T.; Henriksson, P.; Müller, C.; Bergqvist, J.; Hadipour, A.; Heremans, P.; Andersson, M. R. New Quinoxaline and Pyridopyrazine-Based Polymers for Solution-Processable Photovoltaics. *Sol. Energy Mater. Sol. Cells* **2012**, *105*, 280–286.

(54) Root, S. E.; Alkhadra, M. A.; Rodriquez, D.; Printz, A. D.; Lipomi, D. J. Measuring the Glass Transition Temperature of Conjugated Polymer Films with Ultraviolet-Visible Spectroscopy. *Chem. Mater.* **2017**, *29*, 2646–2654.

Appendix A

Supporting information for Chapter 2

Measuring the Glass Transition Temperature of Conjugated Polymer Films with UV-vis Spectroscopy

Samuel E. Root,‡ Mohammad A. Alkhadra,‡ Daniel Rodriquez, Adam D. Printz, and Darren J. Lipomi*

‡ (S.E.R. and M.A.A.) These authors contributed equally.

Department of NanoEngineering, University of California, San Diego

9500 Gilman Drive, Mail Code 0448, La Jolla, CA 92093-0448

A.1. Amorphous Conjugated Polymers

This technique did not work well for predominantly amorphous materials. **Figure A.1** shows the results obtained for PTB7, PCDTBT, TQ1, and MEH-PPV. These materials are all known to lack significant long-range order.[1–4] While PCDTBT has been demonstrated to self-assemble into to a unique bilayer structure upon thermal annealing,[5] this structure has a notably large π-stacking distance (4.4 Å) and only short-range order is observed in the π-stacking direction. Therefore, the aggregation state of the polymer is not significantly affected by thermal annealing (**Figure A.1b**). For TQ1, we found that the UV-vis spectrum substantially changed upon annealing (**Figure A.1c)**, however, we found that there was no discernible T_g when the deviation metric was plotted against the annealing temperature.

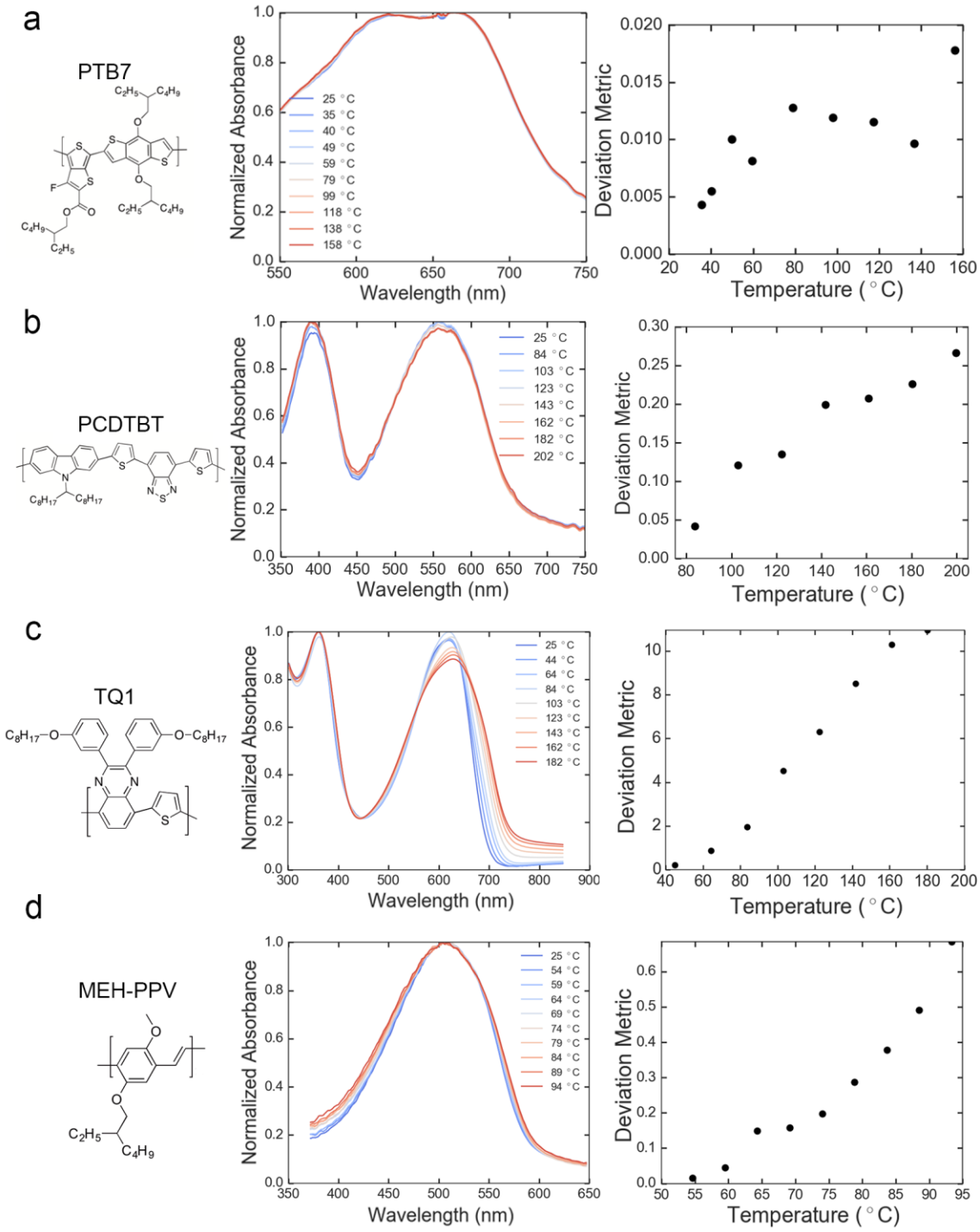

Figure A.1. Results of UV-vis absorption T_g measurement technique for the predominantly amorphous donor-acceptor (DA) copolymers (a) PTB7, (b) PCDTBT, (c) TQ1, and (d) MEH-PPV.

A.2 Heat Transfer Calculations

Since the conjugated polymers involved in this study were spin coated onto glass slides, the annealing temperatures of the thin film being tested differed slightly from those of the hot plate surface (**Figure A.2**). Therefore, heat transfer correction factor was computed. To find the temperature profile of the glass slide on the hot plate, we made use of the general differential equation (eq. 1) for energy transfer, below, derived from Welty's text[6]:

$$\nabla \cdot k\nabla T + \dot{q} + \Phi = \rho c_v \frac{DT}{Dt} = \rho c_v \left(\frac{\partial T}{\partial t} + \mathbf{v} \cdot \nabla T\right) \quad (1)$$

where T is the temperature of the slide, k is the thermal conductivity of glass, $\dot{q}$ is the volumetric rate of thermal energy generation, Φ is the viscous dissipation, ρ is the density of glass, c_v is the specific heat (under constant volume), and t is time. In order to simplify the above equation, which is essentially a re-statement of the first law of thermodynamics, we made the following assumptions in our analysis:

1) No generation effects $\Rightarrow \dot{q} = 0$.
2) Negligible viscous dissipation $\Rightarrow \Phi = 0$.
3) Negligible fluid motion $\Rightarrow \mathbf{v} = \mathbf{0} \Rightarrow \mathbf{v} \cdot \nabla T = 0$.
4) Passing of enough time to reach steady-state heat transfer $\Rightarrow \frac{\partial T}{\partial t} = 0$.

   Assumptions 3 and 4 give $\frac{DT}{Dt} = \frac{\partial T}{\partial t} + \mathbf{v} \cdot \nabla T = 0$. We are left with $\nabla \cdot k\nabla T = 0$.
5) Constant thermal conductivity (k) of glass $\Rightarrow \nabla \cdot k\nabla T = k\nabla^2 T = 0$, so $\nabla^2 T = 0$.
6) One-dimensional heat transfer in the z-direction $\Rightarrow T = T(z)$. Hence,

$$\nabla^2 T = \frac{\partial^2 T}{\partial z^2} = \frac{d^2 T}{dz^2} = 0 \tag{2}$$

It must be noted that the thermal conductivity of glass does indeed change with temperature, though this change has been neglected for simplicity, and an averaged value was used instead. Assuming Pyrex® glass properties, Welty reports that *k* ranges from 1.09 $\frac{\text{W}}{\text{m·K}}$ at 293 K to 1.45 $\frac{\text{W}}{\text{m·K}}$ at 573 K.[6] Assuming soda lime glass properties, Janssen reports that *k* ranges from 0.9 $\frac{\text{W}}{\text{m·K}}$ to 1.3 $\frac{\text{W}}{\text{m·K}}$ over a similar temperature range.[7] So, $k = 1.15\ \frac{\text{W}}{\text{m·K}}$ was taken as an approximate value over the entire temperature range used in this study. We require two boundary conditions on $T(z)$:

1) Taking $z = 0$ to be the bottom of the glass slide,

$$T(z = 0) = T_{\text{HP}} \tag{3}$$

where T_{HP} is the hot plate temperature.

2) Taking $z = l$ to be the thickness of the glass slide, the heat flux at the glass-air interface is given by

$$q_z = \frac{\dot{Q}}{A} = -k \frac{dT}{dz}\bigg|_{z=l} = h\Delta T \tag{4}$$

where ΔT is the temperature difference between the top surface of the glass slide and the ambient (glovebox) atmosphere, and *h* is the convective heat transfer coefficient computed using convective heat transfer correlations.

Regarding the second boundary condition (eq. 4), we note that a polymer thin film is sufficiently thin to safely assume that its temperature (T_s) is equal to that of the top

surface of the glass slide. Hence, $T(z = l) = T_s$. The temperature profile of the glass slide in the upwards direction from the hot plate, z, can be expressed as follows:

$$T(z) = \alpha z + \beta \tag{5}$$

where α and β are constants of integration; recall, we chose the z-axis pointing upwards with $z = 0$ at the surface of the hot plate (**Figure A.2a**).

In light of the linear temperature profile (eq. 5), the first boundary condition (eq. 3) gives

$$T(z = 0) = \beta = T_{HP} \tag{6}$$

and the second (eq. 4) gives

$$-k \left.\frac{dT}{dz}\right|_{z=l} = -k\alpha = h(T_s - T_\infty) \approx h(T_{HP} - T_\infty) \tag{7}$$

where T_∞ is the bulk fluid temperature, measured to be 25 °C. We approximated T_s with T_{HP} to avoid having to iterate (recall, T_s is unknown). It follows that

$$\alpha = \alpha(T_{HP}) = \frac{h}{-k}(T_{HP} - T_\infty) \tag{8}$$

To compute α, we must first compute *h* using natural (free) convection correlations for a horizontal plate geometry with the hot surface facing up. Fluid properties are temperature dependent, and so the properties involved in the correlations were evaluated at the 'average' temperature $T_f = \frac{1}{2}(T_s + T_\infty) \approx \frac{1}{2}(T_{HP} + T_\infty)$. Although annealing occurred in a nitrogen atmosphere (i.e., in the glovebox), the properties of the ambient fluid were approximated with those of air (≈ 78%$_{vol}$ N_2), which are more readily available in the literature.[6] The following correlation for laminar heat transfer from a horizontal plate, developed by Raithby and Hollands,[8] was used to determine the average Nusselt number $\overline{\mathrm{Nu}}_{L^*}$:

$$\overline{\mathrm{Nu}}_{L^*} = \frac{0.560\ \mathrm{Ra}_{L^*}^{1/4}}{[1 + (0.492/\mathrm{Pr})^{9/16}]^{4/9}}, \qquad 1 < \mathrm{Ra}_{L^*} < 10^7 \tag{9}$$

where a characteristic length scale $L^* = Area/Perimeter$ is used in the Rayleigh (Ra) and Nusselt numbers, the Prandtl number $\mathrm{Pr} = \frac{\nu}{\alpha} = \frac{\mu/\rho}{k/c_p\rho} = \frac{c_p\mu}{k}$, μ is the dynamic viscosity, ν is the kinematic viscosity, c_p is the specific heat (under constant pressure), $\mathrm{Ra}_{L^*} = \mathrm{Pr} \times \mathrm{Gr}_{L^*}$ and the Grashof number $\mathrm{Gr}_{L^*} = \frac{g\beta(T_{\mathrm{HP}} - T_\infty){L^*}^3}{\nu^2}$ (we assumed $T_\mathrm{s} \approx T_{\mathrm{HP}}$ for Gr_{L^*}), g is the acceleration due to Earth's gravity, and β is the coefficient of thermal expansion.[6,8] Also, the (Sail Brand) glass slides used in the study were 1 in long × 1 in wide and had an average thickness $l = 1.1$ mm. Raithby and Hollands suggested a correction for thick boundary layers (i.e., $\overline{\mathrm{Nu}}_{L^*} < 10$):

$$\overline{\mathrm{Nu}}_{\mathrm{corrected}} = \frac{1.4}{\ln(1 + 1.4/\overline{\mathrm{Nu}}_{L^*})} \tag{10}$$

It must be noted that many of the aforementioned parameters are highly temperature dependent, and so $\overline{\mathrm{Nu}}_{L^*}$, h , and α (eq. 8) are ultimately functions of T_{HP}. We computed h using the definition of the Nusselt number shown below,

$$\overline{\mathrm{Nu}}_{\mathrm{corrected}} \equiv \frac{hL^*}{k} \Rightarrow h = \frac{\overline{\mathrm{Nu}}_{\mathrm{corrected}} \times k}{L^*} \tag{11}$$

Substituting h into eq. 8, we were able to compute α and thus T_s (eq. 12) as functions of T_{HP}:

$$T_\mathrm{s} = T(z = l) = \alpha l + T_{\mathrm{HP}} \tag{12}$$

Plotting T_s against T_{HP} over an appropriate temperature range (55 °C to 255 °C), we were able to obtain a simple, linear correction factor for any value of T_{HP} (**Figure A.2b**). As

mentioned in the full paper, the correction factor, although slight, was applied in the analysis of the UV-vis absorption spectra.

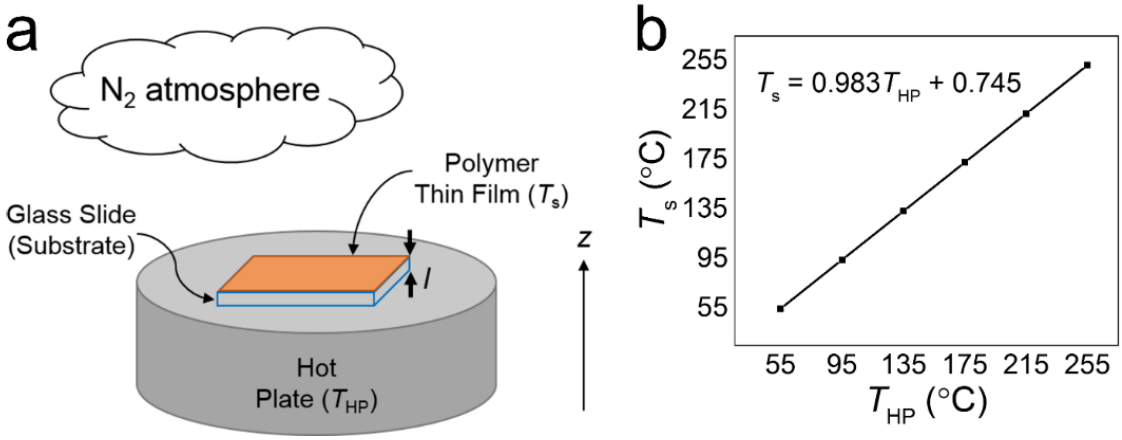

Figure A.2. Heat transfer corrections. (a) Conjugated polymer was spin-coated onto a glass slide (substrate) then placed onto a hot plate for annealing. (b) Heat transfer calculations produced a simple, linear relation between the polymer thin film temperature, T_s, and the hot plate temperature, T_{HP}.

A.3 Data Analysis

All data analysis was performed using the Python programming language. A script was developed to read in a list of .csv files containing the UV-vis absorption spectra after annealing at the film at various temperatures. The deviation metric was computed and plotted against annealing temperature. A bilinear regression algorithm was implemented to determine the temperature that the transition occurred. The algorithm works by sweeping through all possible bilinear regressions and finding the best fit. The quality of each bilinear fit is judged by the sum of the R^2 weighted by the number of data points (i, j) associated with each line (a, b): $i * R_a^2 + j * R_b^2$. An example is shown in **Figure A.3**. The code used to perform this analysis is openly available at https://github.com/seroot/UV_VIS_TG.

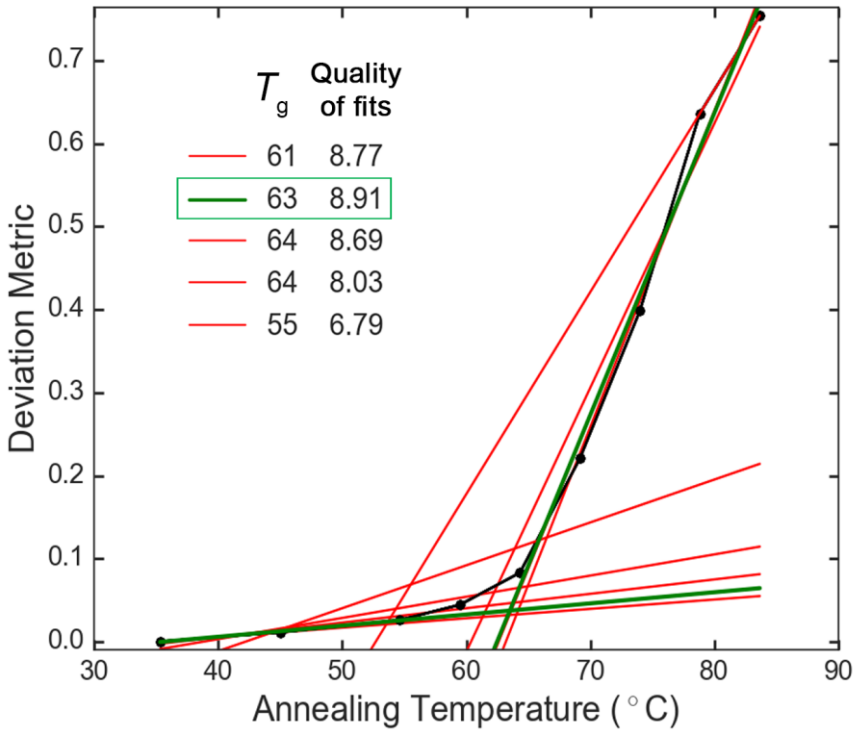

Figure A.3. Bilinear regression algorithm applied to P3BT. Plot showing various possible bilinear fits to the data, the green line indicates the best fit.

Although the T_g was obvious to determine from the deviation metric in almost all cases, PDTSTPD did not have as distinct of a transition as the other materials. In this case, it was important to use the algorithm to find the optimal bilinear regression. An example of the output is shown in **Figure A.4**.

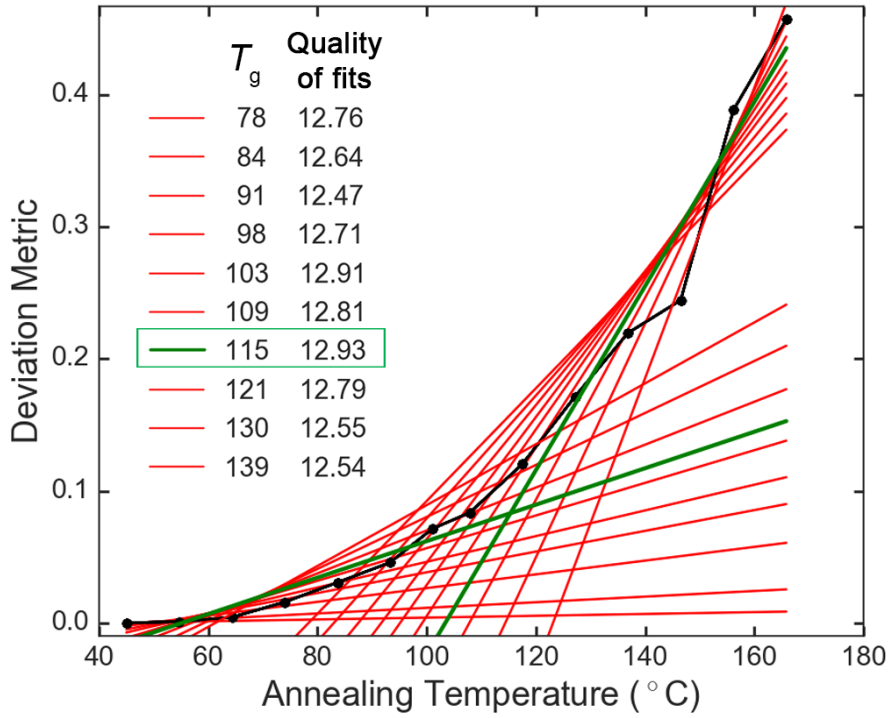

Figure A.4. Bilinear regression algorithm applied to PDTSTPD. Plot showing various possible bilinear fits to the data, the green line indicates the best fit.

A.4 Effect of Plasticizer

Solvent additives such as 1,8-diiodooctane (DIO) are ubiquitously used in the OPV literature as a facile processing strategy for controlling morphology and improving device performance.[9] DIO is expected to act as a plasticizer to reduce the T_g, and so we tested the ability of our technique to measure this plasticization effect. DIO (2% by volume) was added to the P3BT:PCBM bulk heterojunction. As shown in **Figure A.5**, the use of this additive resulted in a 20 ºC decrease in the T_g.

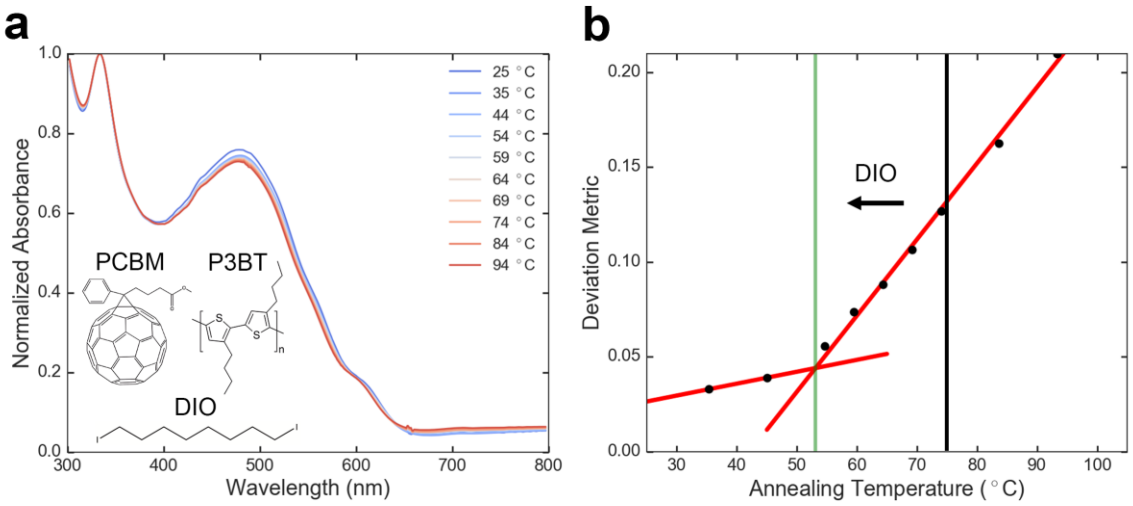

Figure A.5. Effect of processing additive, DIO, on the T_g of a P3BT:PCBM bulk heterojunction thin film. (a) Evolution of the thin-film absorption with thermal annealing. (b) Deviation metric as a function of annealing temperature. The addition of DIO to the bulk heterojunction results in a 20 ºC decrease in the T_g.

A.5 References

(1) Hsiao, Y. C.; Wu, T.; Li, M.; Qin, W.; Yu, L.; Hu, B. Revealing Optically Induced Dipole-Dipole Interaction Effects on Charge Dissociation at Donor: Acceptor Interfaces in Organic Solar Cells under Device-Operating Condition. *Nano Energy* **2016**, *26*, 595–602.

(2) Cho, S.; Seo, J. H.; Park, S. H.; Beaupré, S.; Leclerc, M.; Heeger, A. J. A Thermally Stable Semiconducting Polymer. *Adv. Mater.* **2010**, *22*, 1253–1257.

(3) Wang, E.; Hou, L.; Wang, Z.; Hellström, S.; Zhang, F.; Inganäs, O.; Andersson, M. R. An Easily Synthesized Blue Polymer for High-Performance Polymer Solar Cells. *Adv. Mater.* **2010**, *22*, 5240–5244.

(4) Yang, C. Y.; Heeger, A. J. Morphology of Composites of Semiconducting Polymers Mixed with C60. *Synth. Met.* **1996**, *83*, 85–88.

(5) Lu, X.; Hlaing, H.; Germack, D. S.; Peet, J.; Jo, W. H.; Andrienko, D.; Kremer, K.; Ocko, B. M. Bilayer Order in a Polycarbazole-Conjugated Polymer. *Nat. Commun.* **2012**, *3*, 795.

(6) Welty, J. R.; Wicks, C. E.; Wilson, R. E.; Rorrer, G. L. *Fundamentals of Momentum, Heat, and Mass Transfer*; 2008.

(7) Spalding, D. B. *Handbook of Heat Transfer*; 1975; Vol. 18.

(8) Iv, J. H. L.; Lienhard, J. H. A Heat Transfer Textbook. *J. Heat Transfer* **1986**, *108*, 198.

(9) Shao, M.; Keum, J. K.; Kumar, R.; Chen, J.; Browning, J. F.; Das, S.; Chen, W.; Hou, J.; Do, C.; Littrell, K. C.; Rondinone, A.; Geohegan, D. B.; Sumpter, B. G.; Xiao, K. Understanding How Processing Additives Tune the Nanoscale Morphology of High Efficiency Organic Photovoltaic Blends: From Casting Solution to Spun-Cast Thin Film. *Adv. Funct. Mater.* **2014**, *24*, 6647–6657.